Title
BCL6 maintains thermogenic capacity of brown adipose tissue during dormancy

Author
Kutyavin, Vassily Igor

Publication Date
2019

Peer reviewed|Thesis/dissertation

BCL6 maintains thermogenic capacity of brown adipose tissue during dormancy

by
Vassily Kutyavin

DISSERTATION
Submitted in partial satisfaction of the requirements for degree of
DOCTOR OF PHILOSOPHY

in

Biomedical Sciences

in the

GRADUATE DIVISION
of the
UNIVERSITY OF CALIFORNIA, SAN FRANCISCO

Approved:

DocuSigned by:
Eric Verdin
1874DD863CBA45D...

Eric Verdin
Chair

DocuSigned by:
Ajay Chawla

Ajay Chawla

DocuSigned by:
Ethan Weiss
7508BE9540AA44B...

Ethan Weiss

Committee Members

Dedicated to everyone who has supported me during my scientific education

Acknowledgements

I'm very grateful to my thesis adviser, Ajay Chawla, for his mentorship and support during my dissertation work over the past five years. Throughout my time in his lab, I was always able to rely on his guidance, and his enthusiasm for science was a great source of motivation. Even when he was traveling, he could easily be reached for advice by phone or e-mail. I am particularly grateful for his help with writing the manuscript, which was probably the most challenging aspect of graduate school for me. I am also very grateful to him for helping me find a postdoctoral fellowship position.

Ajay's inquisitive and fearless approach to science have been a great inspiration to me. In contrast to the majority of scientists who focus narrowly on a specific topic, Ajay pursued fundamental questions across a broad range of topics and was able to make tremendous contributions. My experience in his lab instilled in me a deep appreciation for thinking about the entire organism from an evolutionary perspective and focusing on the key questions that escape the attention of the larger scientific community. As I move forward in my scientific career, there is no doubt that I will rely on him as a role model.

I am very grateful to the other members of Ajay's lab who supported me during my thesis work. I am especially grateful to José Barreto Campello Carvalheira who worked directly with me during my first few months in the lab and helped to make the transition a smooth one. I am also grateful to Yifu Qiu, Min Woo Lee, and Yoshitaka Sogawa for teaching me many of the experimental approaches that proved to be very useful during my thesis work. I am also grateful to Xiaojin Cui for taking care of the lab, ordering all of the reagents that I needed, and helping to assemble the mouse lines that I used during my thesis work. I am grateful to fellow graduate students Yixuan Wu and Nyasha Chagwedera for their camaraderie and support.

I also would like to thank my thesis committee members, Eric Verdin and Ethan Weiss, for their excellent advice and support. In particular I appreciate Eric's willingness to continue his role on the committee even when he relocated to the Buck Institute halfway through my thesis and consequently had to drive a long distance to attend the committee meetings. I also want to thank De'Broski Herbert, Emin Maltepe, Jayanta Debnath, and Jeffrey Cox for serving on my qualifying exam committee. In addition, I am grateful to Art Weiss and Jason Cyster for granting me the opportunity to work in their labs as a rotation student. They were fantastic mentors and role models during my first year of graduate school.

I would also like to thank Judy Shigenega, the manager of the Molecular Core Facility at San Francisco VA Medical Center who provided invaluable assistance with next generation sequencing. In addition, I would like to thank Reena Zalpuri from the UC Berkeley Electron Microscope Lab for her assistance with electron microscopy.

Finally, I would like to thank my family for their great support during the past five years.

Contributions to the presented work

Chapter 2 is adapted from a manuscript (in preparation) with the following citation:

Kutyavin, V., Chawla, A. (2019). BCL6 regulates thermogenic capacity and survival of brown adipocytes during dormancy. Proc Natl Acad Sci U S A. *Manuscript in preparation.*

Vassily Kutyavin designed, performed, and analyzed all experiments. Vassily Kutyavin and Ajay Chawla wrote and edited the manuscript. Ajay Chawla supervised the study. Vassily Kutyavin's contributions to the work in Chapter 2 were equivalent in scope to the corresponding section of a standard doctoral thesis.

BCL6 maintains thermogenic capacity of brown adipose tissue during dormancy

by

Vassily Kutyavin

Abstract

During exposure to environmental cold, brown adipocytes protect against hypothermia by generating heat (thermogenesis). In warm environments, brown adipocytes become inactive or dormant, but still maintain their identity and thermogenic capacity, allowing rapid reactivation of thermogenesis upon subsequent cold exposure. Our understanding of the dormant state and its regulation is very limited. Here, we show that the transcription factor B cell leukemia/lymphoma 6 (BCL6) is specifically required for maintenance of thermogenic capacity during dormancy in mouse brown adipocytes. By a combination of both direct and indirect transcriptional mechanisms, BCL6 promotes uncoupled respiration, fatty acid oxidation, and survival in dormant brown adipocytes. In part, BCL6 achieves this by remodeling the epigenome of brown adipocytes to enforce brown and oppose white adipocyte cellular identity. Thus, unlike other transcription factors that regulate cold-induced thermogenesis, BCL6 is specifically required for maintenance of thermogenic fitness during adaptation to environmental warmth.

TABLE OF CONTENTS

LIST OF FIGURES

LIST OF TABLES

CHAPTER 1: INTRODUCTION

The importance of temperature for living organisms

Temperature exerts a profound influence on living organisms. The rates of biochemical reactions (Cannon and Nedergaard, 2011; Clarke and Fraser, 2004), the dynamics of protein folding (Guo et al., 2012), and the fluidity and permeability of lipid membranes (Brown and London, 1998) are all examples of fundamentally important parameters that depend on temperature. It is therefore not surprising that changes in an organism's temperature affect its survival, growth, and reproduction. For example, the growth of the bacterium *Escherichia coli*, which is optimal at approximately 37º C, the core temperature of its human host, gradually slows and eventually ceases as the temperature deviates from this optimal value (Than, 2011). In goldfish, a reduction in body temperature from 35º C to 15º C results in approximately 4-fold lower metabolic rate (Fry and Hart, 1948). In humans, an increase in core temperature to 40.5º C or higher can cause permanent brain damage (White et al., 2007). These examples demonstrate that temperature is a key determinant of biological fitness.

Diverse strategies of thermoregulation in the animal kingdom

The dependence of fitness on temperature implies the existence of an optimal body temperature at which fitness is maximal. Furthermore, one would expect that adaptations which promote maintenance of this optimal body temperature would benefit survival and reproduction, and therefore would be selected during evolution. In accordance with this postulate, many animal species possess behavioral or physiological mechanisms, collectively known as *thermoregulation*, that dynamically regulate body heat gain or loss and appear to target a specific body temperature value (Angilletta et al., 2010). These mechanisms buffer the impact of environmental temperature fluctuations resulting from uneven thermal conductivity, diurnal and

seasonal cycles, and dynamic weather, enabling the core body temperature to be more stable than the environmental temperature (Angilletta et al., 2010). On the basis of these adaptations, organisms can be divided into two distinct categories: *ectotherms* and *endotherms.*

Ectotherms

Organisms that lack or have very limited thermoregulation, and primarily rely on external sources of heat, like sunlight, are called *ectotherms* (Angilletta et al., 2010). These organisms, which include most species of invertebrates, reptiles, amphibians, and fish, exhibit a variable body temperature that is chiefly determined by the temperature of their immediate environment (Figure 1.1). The implications of this dependence are relatively insignificant in environments with low thermal variation, such as the deep ocean. On the other hand, high thermal variation, as seen for example in the Sahara desert (where daily fluctuation as large as 38º C has been recorded), represents a major obstacle to resident ectotherms (Berrahmouni and Burgess, 2019). These organisms limit the overall variation in their body temperature by seeking out environmental niches with a preferred temperature, such as sunlit areas when additional heat is needed, or shaded areas when the organism needs to cool down (Kiefer et al., 2007). Since these behaviors are typically insufficient to maintain a constant body temperature, physiological adaptations are required to tolerate large shifts in body temperature. Many ectotherms exhibit *bradymetabolism,* a state of very low metabolic rate during periods when their body temperature is low (Tzschentke and Rumpf, 2011). This represents a temporary sacrifice of biological functions (which depend on metabolic rate) and energy conservation during suboptimal conditions (low temperature), with recovery of function during optimal conditions (warm temperature). In addition, ectotherms rely on adaptations at the molecular level to limit the

impact of body temperature on metabolic rate. For example, many enzymes found in ectotherms have an enzyme-substrate affinity that declines in response to increasing temperature, which offsets the increase in reaction rate due to higher molecular energies, to reduce the dependence of overall reaction rate on temperature (Somero and Hochachka, 1969). In addition, certain enzymes in ectotherms have different variants that perform optimally at different temperatures, and the selective expression of each variant at the appropriate temperature serves to stabilize the overall enzyme activity across temperatures (Moon and Hochlachka, 1971). Changes in lipid membrane dynamics due to altered temperature are buffered by changes in membrane composition, such as altered proportion of unsaturated fatty acids (Wodtke, 1981). Collectively, these behavioral and physiological adaptations allow ectotherms to survive in spite of a variable body temperature.

Endotherms

The opposite of an ectotherm is an *endotherm*. Endotherms rely on internal heat production (thermogenesis) to maintain a near-constant core body temperature across a wide range of environmental temperatures (Angilletta et al., 2010). Most mammals, including humans, and most birds are endotherms. A constant body temperature provides several key benefits. For example, it allows physiological processes to sacrifice flexibility and instead become highly optimized for operation at a single temperature. It also enables the organism to maintain relatively consistent performance in many functions as it transitions between different environmental temperatures. Endotherms are also able to survive in cold environments where most ectotherms would struggle. However, these benefits come at a significant cost. In order sustain the target body temperature at environmental temperatures that are substantially lower or

higher than the preferred range, endotherms must expend a lot of extra energy (Cannon and Nedergaard, 2011). This extra energy is required for heat production (thermogenesis) in a cold environment, and heat dissipation in a hot environment. Thus, endothermy is a strategy that enables higher performance at the cost of greater energy expenditure.

The amount of energy expenditure required to maintain a constant body temperature in an endotherm is related to the environmental temperature. This relationship is observed in a plot of oxygen consumption rate (VO_2) over a range of environmental temperatures (Figure 1.2) (Cannon and Nedergaard, 2011). VO_2 is an indicator of energy expenditure because it is proportional to the rate of respiration in mitochondria. For an adult wild type mouse under standard laboratory conditions, reduction of environmental temperature below approximately 28º C results in proportional increase in VO_2, reflecting the upregulation of thermogenesis to maintain normal body temperature. Similarly, increase of environmental temperature above approximately 34º C results in proportional increase in VO_2, reflecting greater energy spent on mechanisms of heat loss. These two temperatures, 28º C and 34º C, are called the lower and upper critical temperatures, respectively, and the range of temperatures between them is called the *thermoneutral zone* (TNZ) (Cannon and Nedergaard, 2011). The TNZ is the range of environmental temperatures at which energy devoted to thermoregulation is minimal. Within the TNZ, the metabolic rate of a resting mouse is equal to its basal metabolic rate, and this level of energy expenditure is sufficient to maintain the body temperature. This means that the standard housing temperature of 20-22º C ("room temperature") is actually cold for a mouse and requires significant energy expenditure for thermogenesis.

The thermoregulatory circuit in mammals

Thermoregulation in mammals functions as a homeostatic circuit (Figure 1.3). This type of circuit has been previously described in terms of control theory and systems dynamics theory (Kotas and Medzhitov, 2015). According to this framework, body temperature is the regulated variable. Body temperature and environmental temperature are sensed by specialized nerves that innervate core tissues and the skin, respectively (Morrison and Nakamura, 2018). This temperature information is transmitted to the preoptic area (POA) of the hypothalamus. The POA functions as the controller, which is the circuit component that monitors the regulated variable (body temperature) and modulates the activity of effector mechanisms, called plants, which influence the value of the regulated variable (Kotas and Medzhitov, 2015). In the thermoregulatory circuit, the effector mechanisms include physiological and behavioral mechanisms which affect body heat loss or production (thermogenesis) to achieve a specific body temperature value (Morrison and Nakamura, 2018).

Physiological mechanisms that increase body temperature in response to cold

Blood is an important conduit of heat throughout the body. The amount of heat exchange between the blood and the environment at the skin surface is a major variable controlled by the autonomic nervous system to influence overall body temperature (Tansey and Johnson, 2015). The skin is richly innervated by sympathetic nerves, which secrete norepinephrine to activate vasoconstriction in local arterioles. In response to cold temperature, sympathetic tone is increased, resulting in greater vasoconstriction and reduced blood flow to the skin, thereby reducing the loss of heat from the blood to the environment. In mice, the tail skin is a particularly important site of heat exchange. In addition, non-glabrous (hairy) skin limits heat loss by

activating piloerection (Tansey and Johnson, 2015). Piloerection is the repositioning of hairs to an upright posture that is driven by arrector pili muscles. These small bands of smooth muscle contract in response to increased sympathetic tone, applying pressure to associated hair follicles. The extended hairs more effectively impede the circulation of air at the skin surface, thereby reducing heat loss to the environment.

Thermogenesis is the production of heat by metabolic processes. As the environmental temperature decreases, the body upregulates thermogenesis in order to counter the increased loss of heat to the environment (Cannon and Nedergaard, 2011). There are two categories of thermogenesis: shivering and non-shivering thermogenesis. Shivering thermogenesis, as the name indicates, derives from muscle shivering, which is an involuntary rhythmic contraction of skeletal muscles that is controlled by α-motoneurons (Periasamy et al., 2017). This mechanism is activated very quickly after exposure to cold temperature. The source of heat in shivering muscle is ATP hydrolysis by Na+/K+ ATPase, myosin ATPase, and the ATP-dependent calcium pump SERCA (Periasamy et al., 2017). Shivering is a particularly important source of thermogenesis in humans and other large mammals. Non-shivering thermogenesis comprises multiple mechanisms. It includes UCP1-dependent uncoupled respiration, as well as UCP1-independent futile cycles, in brown and beige adipocytes, which will be discussed in more detail in later sections (Cannon and Nedergaard, 2011). Evidence also exists for non-shivering thermogenesis in muscle, owing to uncoupling of SERCA by sarcolipin, resulting in greater ATP hydrolysis and thermogenesis (Periasamy et al., 2017).

Behavioral mechanisms that increase body temperature in response to cold

Both endotherms and ectotherms use behavioral mechanisms to regulate their body temperature. In response to cold temperature, organisms will modify their body posture to reduce heat loss to the environment (Terrien et al., 2011). In many organisms, including mice and humans, this has the appearance of a curled or hunched posture. In addition, organisms will navigate their environment in search of a zone of warmer temperature. In experiments designed to test thermal preference, mice are placed in an artificial environment with a temperature gradient (Dhaka et al., 2007). Healthy, wild type adult mice will move to a temperature within their thermoneutral zone (28-34º C). In the natural environment, a small mammal may seek shelter in a nest or a burrow. It may also huddle with other members of its social group to share body heat. In mammals, this cold avoidance behavior depends on sensory nerves in the skin that express the cold-activated ion channel TRPM8 (Dhaka et al., 2007). Among humans, the use of numerous technologies that provide protection from the cold, ranging from clothing to indoor heating, may also be considered forms of behavioral thermoregulation.

Physiological mechanisms that decrease body temperature in response to heat

In response to hot environmental temperature, the vasoconstriction and piloerection mechanisms described earlier are diminished, favoring vasodilation and greater blood flow to the skin (Tansey and Johnson, 2015). This facilitates the flow of heat from the blood to the surrounding air. In addition, non-glabrous skin contains sympathetic cholinergic nerves which mediate active vasodilation to further promote blood flow (Tansey and Johnson, 2015). This mechanism is incompletely understood, and is hypothesized to involve a combination of

acetylcholine and other neurotransmitters, possibly secreted from the same nerves that control sweating.

Evaporative heat loss facilitates the cooling of body temperature when exposed to a high environmental temperature. In some endotherms, including humans, sweating is a major component of evaporative heat loss. Sweat is a complex aqueous fluid secreted from eccrine and apocrine glands in the skin in response to warm temperature or physical activity (Bovell, 2015). The evaporation of sweat at the skin surface transfers heat from the body to the external air. Sweat secretion is controlled by the activity of sympathetic cholinergic nerves (Tansey and Johnson, 2015). Some endotherms, such as dogs, don't have many sweat glands and instead rely on panting, which is a mechanism of heat loss involving evaporation and subsequent exhalation of water from the respiratory tract (Goldberg et al., 1981). Mice are unable to sweat or pant, and therefore are particularly vulnerable to high environmental temperatures (Harkness, 1997).

Behavioral mechanisms that decrease body temperature in response to heat

Not surprisingly, behavioral responses to hot temperatures are typically the opposite of those observed in response to cold temperatures. Organisms will adopt open body postures that facilitate air movement across their bodies (Terrien et al., 2011). They will search for environmental niches with cooler temperature, such as shade or a body of water. In mammals, the sensation of environmental heat by peripheral sensory nerves is thought to be mediated by members of the TRP channel family, including TRPV1, TRPV2, TRPV3, and TRPV4, which are known to be activated by temperatures above 43º C, 52º C, 31º C, and 25º C, respectively (Tansey and Johnson, 2015). It is plausible that the combination of these receptors, each with a

distinct activation threshold, is key to enabling discrimination across a wide range of temperatures.

Roles of adipocytes in energy homeostasis and thermoregulation

Adipocytes play important roles in energy homeostasis in mammals. For a long time, only two types of adipocytes were recognized: white and brown. The primary function of white adipocytes is energy storage, which takes the form of a gigantic lipid droplet that occupies almost the entire volume of the cell (Saely et al., 2012). In contrast, brown adipocytes are specialized for thermogenesis. They contain a large quantity of mitochondria which are a key component of the thermogenic mechanism. In cold-adapted organisms, brown adipocytes have a distinctive multilocular appearance due to the presence of many small lipid droplets. White and brown adipocytes are the primary constituents of white and brown adipose tissue depots, respectively.

Upon cold exposure in an adult mouse, brown adipocyte-like cells appear in the subcutaneous white adipose tissue (sWAT). Only recently, these cells, called "beige" or "brite", were recognized as a distinct type of adipocyte (Sidossis and Kajimura, 2015). While very similar to brown adipocytes in their activated state, beige adipocytes are much more dependent on cold exposure for their thermogenic characteristics, employ distinct thermogenic mechanisms, and have a distinct developmental origin (Ikeda et al., 2018).

UCP1-dependent thermogenesis in brown and beige adipocytes

The major mechanism of non-shivering thermogenesis in mammals depends on uncoupling protein 1 (UCP1), a transmembrane protein located in the inner mitochondrial

membrane in brown and beige adipocytes (Cannon and Nedergaard, 2011). UCP1-dependent thermogenesis is a complex mechanism that is initiated upon exposure to environmental cold (Figure 1.4). Sensation of cold leads to increased activity of sympathetic nerves that innervate adipose tissue. These nerves secrete norepinephrine, which activates β3-adrenergic receptors on the surfaces of brown and beige adipocytes. This activation results in cyclic AMP production and stimulation of Protein Kinase A (PKA) activity. Phosphorylation of target proteins by PKA drives many key components of the thermogenic program. For example, phosphorylation of hormone sensitive lipase (HSL) by PKA promotes lipolysis (Carmen and Víctor, 2006). HSL hydrolyzes the triglycerides stored within the cell's lipid droplets, generating free fatty acids (FFAs), and this activity is positively regulated by PKA phosphorylation. PKA also phosphorylates proteins called perilipins, which normally associate with the lipid droplet and block lipolysis. Phosphorylation of perilipins disrupts their ability to block lipolysis, increasing the release of FFAs (Carmen and Víctor, 2006). The FFAs are converted to acyl-CoAs by enzymes called fatty acyl-CoA synthetases, a step that activates the fatty acid for utilization in many downstream metabolic pathways (Ellis et al., 2015). The reverse reaction, conversion of acyl-CoAs to FFAs, is catalyzed by enzymes called acyl-CoA thioesterases (ACOTs) (Ellis et al., 2015). Long chain acyl-CoAs are transported into mitochondria via the carnitine shuttle, which involves conversion of the acyl-CoA into acylcarnitine, transport into the mitochondria, and then conversion back into acyl-CoA once inside the mitochondria (Sharma and Black, 2009).

Once inside the mitochondria, acyl-CoAs are oxidized in a series of reactions called β-oxidation (Figure 1.5) (Houten and Wanders, 2010). This process consumes acyl-CoA and generates the electron carriers NADH, $FADH_2$, and acetyl-CoA. Acetyl-CoA is further oxidized in the tricarboxylic acid cycle to generate additional NADH, $FADH_2$, and ATP. The reducing

power of NADH and $FADH_2$ is harnessed by the electron transport chain, which uses it to generate a proton gradient across the inner mitochondrial membrane (Wilson, 2017). In most cell types, the main purpose of this proton gradient is to drive production of ATP by ATP synthase (also known as Complex V of the electron transport chain). This process of oxidative phosphorylation, also known as coupled respiration, is a major source of ATP and is particularly important for tissues that consume a lot of energy, like skeletal muscle, heart, and the brain.

The unique presence of uncoupling protein 1 (UCP1) in the inner mitochondrial membrane of brown and beige adipocytes fundamentally changes the process of mitochondrial respiration, transforming it into a pathway of heat production (Figure 1.5) (Cannon and Nedergaard, 2004). UCP1 acts as a proton transporter, facilitating the movement of protons from the intermembrane space into the mitochondrial matrix. In this way, UCP1 dissipates the proton gradient without concomitant synthesis of ATP. Since availability of ADP is no longer a limiting factor for mitochondrial respiration, the brown/beige adipocyte can achieve a very high rate of catabolism, and the vast majority of energy released by these catabolic reactions does not end up stored as chemical energy in the form of ATP, but instead is released to the rest of the body as thermal energy, or heat. This heat is carried to the rest of the body via the bloodstream. UCP1-dependent respiration is often called "uncoupled respiration" to distinguish it from respiration that is coupled to ATP synthesis.

The activity of UCP1 is regulated by physiological signals. In particular, the ability of UCP1 to transport protons is positively regulated by binding of fatty acids (Fedorenko et al., 2012). This allows the activity of UCP1 to be coordinated with the release of fatty acids due to lipolysis after activation of the adrenergic signaling pathway. On the other hand, UCP1 is negatively regulated by purine nucleotides, including ATP, ADP, GTP, and GDP (Macher et al.,

2018). The activity of UCP1 is also modulated by reactive oxygen species, in part due to sulfenylation of a key cysteine residue (Chouchani et al., 2016).

Alternative, UCP1-independent pathways of thermogenesis in brown and beige adipocytes

UCP1-dependent thermogenesis is considered to be the major component of non-shivering thermogenesis in adipocytes. However, it has been shown that lipid mobilization and turnover in brown adipose tissue after noradrenergic stimulation occurs independently of UCP1, suggesting the existence of alternative thermogenic pathways (Grimpo et al., 2014). Indeed, a recent study discovered that brown and beige adipocytes engage creatine-driven substrate cycling, a mechanism that converts mitochondrial ATP into ADP and promotes a higher rate of coupled respiration (Kazak et al., 2015). Interestingly, this pathway is upregulated in the setting of UCP1 deficiency, suggesting a compensatory relationship. Another alternative thermogenic pathway in beige adipocytes involves ATP-dependent calcium cycling by sarco/endoplasmic reticulum Ca2+-ATPase2b (SERCA2b) (Ikeda et al., 2017). Both of these pathways promote futile ATP consumption, in essence converting the stored chemical energy of ATP into heat. Another UCP1-independent pathway involves the secreted enzyme PM20D1, which catalyzes the formation of N-acyl amino acids (Long et al., 2016). These molecules bind to mitochondria and promote uncoupling in a UCP1-independent manner (Long et al., 2016).

Short- and long-term adaptation of brown and beige adipocytes to environmental temperature

The thermogenic activity of brown and beige adipocytes is tightly controlled by environmental temperature. A sudden change in temperature elicits a corresponding change in thermogenic activity within minutes. This acute regulation depends on control of metabolic

enzymes, such as those involved in lipolysis and fatty acid oxidation, by signaling pathways downstream of the β3-adrenergic receptor (Cannon and Nedergaard, 2011). It ensures an appropriate rate of thermogenesis that protects against hypothermia but does not contribute to hyperthermia and waste energy.

Over longer periods of time, such as days or weeks, environmental temperature remodels the thermogenic capacity of brown and beige adipocytes (Figure 1.6). Chronic exposure to cold results in greater thermogenic capacity in brown and beige adipocytes, a phenomenon called "recruitment" (Cannon and Nedergaard, 2011). Recruitment is a consequence of the cumulative effect of elevated adrenergic signaling on multiple variables, including adipocyte survival, proliferation of adipocyte precursors, differentiation, and the expression of many key components of the thermogenic pathway, such as UCP1 and various metabolic enzymes (Cannon and Nedergaard, 2004). Together, these changes contribute to a greater abundance of thermogenic adipocytes with higher thermogenic capacity, reinforcing the organism's ability to maintain core body temperature in the cold environment.

In contrast, long-term adaptation to warmth (thermoneutrality) causes brown and beige adipocytes to become dormant. Dormancy is a state of energy conservation, characterized by inactive thermogenesis, reduced thermogenic capacity, and elevated lipid storage (Jespersen et al., 2019). Dormancy occurs differently in brown and beige adipocytes. During dormancy, beige adipocytes undergo a dramatic transformation, losing virtually all of their thermogenic characteristics and becoming almost indistinguishable from white adipocytes (Figure 1.6) (Roh et al., 2018). In contrast, brown adipocytes undergo fewer changes during dormancy and mostly retain their thermogenic characteristics, including a high mitochondrial density (Roh et al., 2018; Shabalina et al., 2013). As a result, brown adipocytes can quickly reactivate thermogenesis

during a sudden transition from warmth to cold, whereas beige adipocytes can only do so after a significant delay. Thus, brown adipocytes are more dedicated to thermogenesis and are particularly important for acute cold adaptation, whereas beige adipocytes are more plastic, and only contribute to thermogenesis in the setting of chronic cold adaptation.

The role of thermogenic adipocytes in diet-induced thermogenesis

In addition to their key role in cold-induced thermogenesis, thermogenic adipocytes have been linked to diet-induced thermogenesis (Rothwell and Stock, 1979). As the name suggests, diet-induced thermogenesis is the increase in an organism's energy expenditure in response to feeding. Through this mechanism, it is proposed that thermogenic adipocytes protect against obesity. In particular, much attention has been devoted to the contribution of UCP1 to diet-induced thermogenesis. A previous study showed that *Ucp1* global knockout mice, when housed at thermoneutrality (to rule out the influence of cold), failed to engage diet-induced thermogenesis and accumulated more weight as a result (Feldmann et al., 2009). However, the significance of these findings has been questioned. Another study did not observe increased weight gain in *Ucp1* global knockout mice (Anunciado-Koza et al., 2008). In addition, several other mouse models with large reduction of UCP1 in brown adipocytes, such as mice with adipocyte-specific deletion of *Prdm16, ERRα/γ, Cpt2*, and *Hdac3*, do not exhibit increased weight gain (Brown et al., 2018; Emmett et al., 2017; Harms et al., 2014; Lee et al., 2016; Lee et al., 2015a). Therefore there is concern that the metabolic characteristics of the *Ucp1* global knockout mouse do not accurately reflect the contribution of UCP1 to diet-induced thermogenesis, and perhaps may be a consequence of secondary defects observed in the brown adipocytes of these mice, such as depletion of respiratory chain complexes and reduced calcium

buffering capacity (Kazak et al., 2017). More generally, the idea of brown adipocyte involvement in diet-induced thermogenesis has been questioned, based on studies that failed to observe evidence for this connection, and alternative explanations for data originally thought to be supporting (Kozak, 2010). However, there is no question that, at least in principle, activation of thermogenic adipocytes by cold exposure or synthetic agonists can ameliorate obesity.

Brown adipose tissue in humans

The abundance of brown adipose tissue (BAT) in humans peaks during infancy, and gradually declines with age (Betz and Enerbäck, 2015). Due to the difficulty of reliably detecting BAT in human adults, the contribution of BAT to thermogenesis and energy homeostasis in adults was questioned. This perception changed in the late 2000s when BAT in adults was "rediscovered" by means of 2-deoxy-2-[fluorine-18]fluoro-d-glucose integrated with computed tomography (18F-FDG PET/CT) scanning (Cypess et al., 2009) (van Marken Lichtenbelt et al., 2009). Increased glucose uptake in the supraclavicular region, corresponding to functional BAT, was observed during cold exposure and was correlated with increased thermogenesis, as measured by indirect calorimetry (van Marken Lichtenbelt et al., 2009). These regions were found to contain UCP1+ multilocular adipocytes (Cypess et al., 2009). Interestingly, both cold- and insulin-stimulated uptake of glucose into adult supraclavicular BAT is lower in obese patients, suggesting that reduced BAT activity may contribute to the development of obesity (Orava et al., 2013).

The relationship between adult human brown adipocytes and the much more extensively studied rodent brown adipocytes is not entirely clear but the current evidence indicates that the adult human "brown" adipocytes of the supraclavicular region are actually closer to rodent beige

adipocytes than to rodent brown adipocytes (Sharp et al., 2012). This idea is bolstered by the observation of a high degree of cold-dependent plasticity in the adult supraclavicular BAT depots (Blondin et al., 2014). In contrast, the brown adipocytes in the interscapular region of human infants are thought to more closely resemble the brown adipocytes of rodents (Lidell et al., 2013).

Brown adipose tissue in humans has attracted a great deal of attention due to its potential therapeutic value for the treatment of obesity and associated metabolic disorders. Increasing BAT abundance and/or activating existing BAT could increase energy expenditure and accelerate weight loss. However, these strategies have not yet proven successful (Marlatt et al., 2018). For example, attempts to pharmacologically activate BAT with β3-adrenergic agonists are complicated by side effects on the cardiovascular system, including increased heart rate and systolic blood pressure due to activation of β1- and β2-adrenoreceptors (Arch, 2011). Pharmacological activation of PPARγ with thiazolididiones has also been explored for stimulation of BAT thermogenesis, but serious side effects have limited the potential of these drugs (Lee and Greenfield, 2015). There is hope that transplantation of BAT into humans will be an effective strategy for obese individuals who lack BAT (Tharp and Stahl, 2015). More work is necessary to establish the viability of these approaches.

Transcriptional regulation of brown adipocyte thermogenesis

The thermogenic pathway in brown and beige adipocytes is regulated at the level of gene transcription. The transcriptional regulation of *Ucp1* in particular has been studied extensively and illustrates key principles that apply to the regulation of many other genes involved in thermogenesis (Seale, 2015). Appropriate expression of thermogenic genes requires both proper

differentiation, to establish the necessary chromatin architecture of a brown adipocyte, and proper control of gene expression in the differentiated cell, particularly in response to cold and other external signals. The transcriptional mechanisms governing brown adipocyte differentiation and thermogenic gene expression in differentiated brown adipocytes will be discussed in sequence.

Transcriptional mechanisms governing brown adipocyte differentiation

Brown adipocytes in mice arise from Myf5-expressing precursors which can also give rise to skeletal muscle cells or white adipocytes (Sanchez-Gurmaches and Guertin, 2014). Certain components of the differentiation programs of white and brown adipocytes are shared; these correspond to the "general" adipogenesis program (Figure 1.7). This program is coordinated by the nuclear receptor PPARγ and members of the c/EBP family of transcription factors (Rosen and MacDougald, 2006). Early during adipogenesis, c/EBPβ is expressed and promotes expression of PPARγ. Then, PPARγ and c/EBPα collaboratively drive expression of adipocyte-specific genes. The Krüppel-like factor (KLF) transcription factors also play important roles, both positive and negative, in the general adipogenesis program, in part by interacting with PPARγ and c/EBP transcription factors (Rosen and MacDougald, 2006).

Brown adipocyte differentiation requires the action of additional transcription factors and co-activators beyond the general adipogenesis program (Figure 1.7). The transcription factor EBF2 is selectively expressed in brown and beige adipocyte precursors and is required for commitment to these lineages (Rajakumari et al., 2013; Wang et al., 2014). EBF2 binds to brown adipocyte-specific enhancers and facilitates the recruitment of PPARγ to these sites, which drives expression of thermogenic genes like *Ucp1*. The long noncoding RNA *Blnc1* is also

critically important brown adipocyte differentiation, and it acts in part by binding and enhancing the function of EBF2 (Zhao et al., 2014).

PRDM16, a histone methyltransferase and zinc-finger–containing protein, plays an important role in brown adipocyte differentiation by binding near brown adipocyte-specific genes and positively regulating their expression (Seale et al., 2008). PRDM16 is believed to be recruited to these sites indirectly, through binding to c/EBPβ, PPARγ, and/or ZFP516. The mechanism by which PRDM16 promotes gene expression involves recruitment of the Mediator complex, which facilitates enhancer/promoter looping and RNA Pol II preinitiation complex assembly (Iida et al., 2015). PRDM16 also forms a complex with other factors that are important for repression of alternative cell fates. For example, PRDM16 and the histone demethylase LSD1 cooperatively repress white adipocyte-specific genes (Zeng et al., 2016). Similarly, PRDM16 forms a complex with the histone methyltransferase EHMT1, which stabilizes PRDM16 and represses muscle-specific genes (Ohno et al., 2013).

Transcriptional mechanisms controlling acute activation of thermogenesis in response to cold

Upon acute exposure to cold, thermogenic genes (for example *Ucp1*) in brown and beige adipocytes are upregulated to support the elevated thermogenic activity of these cells. These changes are driven by the signaling events downstream of β3-adrenergic receptor activation, including the cAMP/PKA signaling pathway (Cannon and Nedergaard, 2004). The mitogen-activated protein kinase p38 is activated by PKA and is required for cold-induced upregulation of *Ucp1* and other thermogenic genes (Cao et al., 2001). P38 phosphorylates and activates peroxisome proliferator-activated receptor gamma (PPAR gamma) coactivator 1 alpha (PGC-1alpha) and activating transcription factor 2 (ATF-2) (Figure 1.8) (Cao et al., 2004). PGC-1alpha

is an important co-activator for several different transcription factors that bind to the promoter and/or enhancers of *Ucp1* and other thermogenic genes, including IRF4 and members of the peroxisome proliferator-activated receptor (PPAR) and estrogen related receptor (ERR) nuclear receptor families (Seale, 2015). IRF4 is upregulated in response to adrenergic signaling and is required for cold-induced activation of thermogenic genes, including *Ucp1*, *Dio2*, and *Ppargc1a* (Kong et al., 2014). ATF-2 binds to a cAMP-responsive element (CRE) located in an enhancer upstream of *Ucp1* and positively regulates expression of this gene, as well as *Ppargc1a* (Cao et al., 2004). In addition, the transcription factor CREB is phosphorylated and activated by PKA, and positively regulates *Ucp1* expression by a mechanism involving direct binding to a CRE in the *Ucp1* promoter (Cao et al., 2004). Yet another transcription factor, ZFP516, is upregulated by the cAMP/ATF-2/CREB pathway (Dempersmier et al., 2015). ZFP516 binds to the promoters of *Ucp1* and *Ppargc1a* in association with PRDM16 and LSD1 and positively regulates their expression (Dempersmier et al., 2015; Sambeat et al., 2016) (Figure 1.8).

Thyroid hormone receptors

Thyroid hormones, which include thyroxine (T4) and triiodothyronine (T3), play a major role in cold-induced activation of thermogenesis (Mullur et al., 2014). T4 has little direct biological activity and serves as a precursor for T3, the active form of thyroid hormone. T4 is converted to T3 by enzymes called iodothyronine deiodinases. T3 regulates the expression of many metabolic genes by acting as a ligand for the nuclear receptors thyroid hormone receptor α and β (THRα/β). *Ucp1* expression in brown adipocytes is positively regulated by THRβ, which binds to two thyroid-hormone-responsive elements located about 2000 base pairs upstream of the *Ucp1* transcription start site (Rabelo et al., 1995)(Figure 1.8). In response to cold, iodothyronine

deiodinase 2 (DIO2) is upregulated in brown adipocytes, increasing the local amount of T3, which leads to greater activation of THRβ and resulting *Ucp1* expression (Mullur et al., 2014). DIO2-deficient mice have impaired cold-induced BAT thermogenesis and brown adipocytes from these mice exhibit impaired upregulation of *Ucp1* in response to norepinephrine (de Jesus et al., 2001).

Estrogen-related receptors

The estrogen-related receptors (ERRα, ERRγ, ERRβ) are a family of nuclear receptors that are key regulators of oxidative metabolism in many cell types. ERRs control the expression of genes involved in glucose uptake, glycolysis, fatty acid oxidation, TCA cycle, and oxidative phosphorylation (Audet-Walsh and Giguére, 2015). ERRs specifically bind to sequences called estrogen-related response elements (ERREs), often located near gene promoters (Figure 1.8). For many years, no natural ligands for these receptors were known, and these receptors were believed to be highly active in the absence of ligand. Recently, however, evidence emerged that cholesterol serves as a ligand for ERRα (Wei et al., 2016). As mentioned earlier, the activity of ERRs is also controlled by association with co-activators, such as PGC-1alpha, and co-repressor complexes such as NCOR1 (Pérez-Schindler et al., 2012). The ERRs are partially redundant in brown adipocytes: loss of only ERRα (the most abundant ERR), or only ERRβ and ERRγ, results in a smaller reduction of oxidative metabolic gene expression than loss of all three ERRs (Gantner et al., 2016). Another study reported that deletion of only ERRγ in brown adipocytes resulted in a milder thermogenic defect that only manifested upon prolonged housing at thermoneutrality, suggesting that ERRγ has a non-redundant contribution to maintenance of thermogenic gene expression in the dormant state (Ahmadian et al., 2018). ERRs are also critical

for cold-induced thermogenic activation. Mice with deletion of both ERRα and ERRγ in brown adipocytes have a severe defect in mitochondrial oxidative capacity and a dramatically blunted upregulation of thermogenic genes in response to adrenergic agonist (Brown et al., 2018). One of the key positive regulators of ERR activity at thermogenic genes like *Ucp1* is histone deacetylase 3 (HDAC3), which is recruited to the ERRα complex and deacetylates PGC-1alpha, thereby promoting its co-activation of ERRα (Emmett et al., 2017).

B cell leukemia/lymphoma 6 (BCL6)

BCL6 is a transcriptional repressor with important roles in multiple cell types. As its name suggests, BCL6 was first identified as an oncogene in B cell lymphoma, most notably diffuse large B cell lymphoma (Wagner et al., 2011). BCL6 normally functions as a key regulator of the germinal center stage of B cell development, and mutations that disrupt the normal regulation of BCL6 expression can lead to uncontrolled proliferation and resistance to apoptosis (Pasqualucci et al., 2003). Important roles for BCL6 have also been discovered in T follicular helper cells, macrophages, hepatocytes, adipocytes, and other cell types. In the following sections, the molecular mechanisms of transcriptional regulation by BCL6, the regulation of BCL6, and its functions in different cell types will be reviewed. Most of our knowledge about BCL6 comes from studies of B cells; unless mentioned otherwise, the following sections refer to BCL6 in the B cell setting.

<u>Molecular mechanisms of transcriptional regulation by BCL6</u>

The BCL6 protein contains six C-terminal zinc finger DNA-binding motifs, three central PEST domains, and an N-terminal BTB/POZ domain (Basso and Dalla-Favera, 2012) (Figure

1.9). The zinc finger DNA-binding motifs enable BCL6 to bind to a specific DNA sequence motif. However, the cistromes of BCL6 in different cell types, as determined by ChIP-seq, are quite distinct, indicating that cell type-specific features have a strong influence on BCL6 binding (Liu et al., 2016). In some cases, BCL6 can be recruited to a chromatin site not by direct binding to DNA, but by binding to another transcription factor, such as ZBTB17 (Miz1) (Saito et al., 2009). The PEST domains influence the activity and stability of the protein (Basso and Dalla-Favera, 2012). The BTB/POZ domain is important for BCL6 dimerization and also for interaction with co-repressors (Basso and Dalla-Favera, 2012). Most of the repressive activity of BCL6 is due to its binding near target genes and recruitment of co-repressor complexes that negatively regulate expression of the target gene (Figure 1.9). BCL6 can recruit many different co-repressors, including NCOR1, NCOR2, BCOR, CTBP1, and MTA3, as well as type 1 and type 2 histone deacetylases, either directly or indirectly (Basso and Dalla-Favera, 2012). Deacetylation of local histone residues by these enzymes negatively regulates the expression of the target gene by causing the chromatin to adopt a more compact state and limiting the access of other transcription factors that positively regulate expression of the target gene (Delcuve et al., 2012).

Transcriptional regulation of *Bcl6*

BCL6 represses the expression of its own gene by binding to a site within its first exon, a form of negative autoregulation (Pasqualucci et al., 2003). This mechanism is disrupted by mutations at the binding site, as observed in some cases of DLBCL leading to elevated BCL6 expression (Pasqualucci et al., 2003). *Bcl6* is also directly repressed by the transcription factors BLIMP-1 (Shaffer et al., 2002) and STAT5 (Walker et al., 2007). *Bcl6* is positively regulated by

the transcription factors IRF8 (Lee et al., 2006), FOXO1 and FOXO3A in Th1 T cells (Oestreich et al., 2012), STAT1 and STAT3 in multiple cell types (Choi et al., 2013; Nakayamada et al., 2014; Walker et al., 2013), and Aiolos and Ikaros in T follicular helper cells (Read et al., 2017).

Post-translational regulation of BCL6

In addition to its regulation at the transcriptional level, BCL6 is regulated post-translationally by multiple mechanisms. BCL6 is acetylated by P300, a transcriptional co-activator with histone acetyltransferase activity, at a KKYK motif in its PEST domain (Bereshchenko et al., 2002). This acetylation inactivates BCL6 by disrupting its ability to recruit HDACs. It is reversed by HDAC- and Sir2-dependent pathways. BCL6 also undergoes regulated proteasomal degradation. In response to DNA damage, the kinase ATM phosphorylates BCL6, which promotes its interaction with the peptidyl-prolyl isomerase Pin1 and subsequent proteasomal degradation (Phan et al., 2007). Similarly, antigen receptor activation leads to phosphorylation of BCL6 in its PEST domain by MAP kinase, triggering its proteasomal degradation (Niu et al., 1998). This involves the SKP1–CUL1–F-box protein (SCF) ubiquitin ligase complex, which contains the orphan F-box protein FBXO11 (Duan et al., 2012). *FBXO11* itself is often mutated or deleted in DLBCL, and this is correlated with elevated expression of BCL6. On the other hand, BCL6 is stabilized by interaction with molecular chaperone heat-shock protein 90 (HSP90) (Cerchietti et al., 2009).

Functions of BCL6 in germinal center B cells

BCL6 is specifically expressed during the germinal center stage of B cell development, when these cells are undergoing somatic hypermutation of their antibody genes in order to

achieve higher affinity for antigen. This high amount of DNA mutation would normally elicit DNA damage response and DNA damage-induced apoptosis programs, but these are inhibited by BCL6, which directly represses key genes in these pathways, including *TP53*, *ATR*, and *CHEK1* (Basso et al., 2010; Phan and Dalla-Favera, 2004; Ranuncolo et al., 2007). In addition, BCL6 represses some genes that inhibit apoptosis, such as *BCL2* (Ci et al., 2009), which potentially contributes to the greater sensitivity of germinal center B cells to apoptosis.

Another function of BCL6 in germinal center B cells is to dampen signaling pathways that promote B cell activation, thereby reducing the likelihood of the cell prematurely exiting the germinal center program. BCL6 achieves this by directly repressing genes involved in signal transduction downstream of the B cell receptor and CD40, including those involved in NF-kB signaling (*NFKB1*, *NFKB2*), MAPK signaling (*MAP3K5*, *MAPK1*), and calcium signaling (*INPP5D, CACNB1*) (Basso et al., 2010). Furthermore, BCL6 represses genes that are important for interactions between B and T cells, such as *CD274* and *CD80* (Niu et al., 2003).

BCL6 also maintains the germinal center program by directly repressing *Prdm1* and *Irf4*, genes that encode transcription factors that promote differentiation to the plasma cell stage (Basso et al., 2010; Shaffer et al., 2000; Tunyaplin et al., 2004). After receiving sustained antigen receptor signaling, BCL6 is degraded (as described above), resulting in upregulation of IRF4 and PRDM1, which together promote transition from the germinal center stage to the plasma cell stage.

BCL6 as an oncogene

While these functions of BCL6 enable normal germinal center B cells to develop their antigen specificities, unfortunately they can also support the survival of cancerous B cells that

have lost control of BCL6 expression. This typically occurs as a result of mutations in proximal regulatory regions or chromosomal translocations involving the *BCL6* gene, which juxtapose the 5'-end of the *BCL6* gene to a different promoter, leading to excessive expression of BCL6 (Basso and Dalla-Favera, 2012). These genetic lesions are found in a subset of diffuse large B cell lymphoma (DLBCL), primary mediastinal B cell lymphoma (PMBL), follicular lymphoma (FL), and in nodular lymphocyte predominant Hodgkin lymphoma (NLPHL) (Wagner et al., 2011). In addition, BCL6 has been implicated in the progression of several other types of cancer, including B cell acute lymphoblastic leukemia (B-ALL), chronic myeloid leukemia (CML), acute lymphoblastic leukemia (ALL), breast cancer, non–small cell lung cancer (NSCLC), and glioblastoma (Cardenas et al., 2017; Duy et al., 2011; Xu et al., 2017). In breast cancer, BCL6 is frequently amplified and supports cell survival (Walker et al., 2015). In glioblastoma, BCL6 supports cell survival by several mechanisms, including repression of the TP53 pathway (Xu et al., 2017). Thus, a common function of BCL6 across diverse cancer types is reinforcement of cell survival.

Functions of BCL6 in T follicular helper cells

T follicular helper cells (Tfh cells) provide help to B cells in the germinal center (GC) reaction. Like GC B cells, Tfh cells are characterized by high expression of BCL6, and BCL6 is essential for their differentiation, as demonstrated by overexpression and knockout experiments (Johnston et al., 2009; Nurieva et al., 2009). As in GC B cells, BCL6 in Tfh cells represses PRDM1, which opposes Tfh differentiation (Johnston et al., 2009). BCL6 binds near thousands of genes in Tfh cells, many of which are involved in diverse T cell-related programs, including T cell receptor signaling and T cell differentiation (Hatzi et al., 2015). Interestingly, BCL6-

mediated repression of many Tfh genes occurs in the absence of a consensus BCL6 binding site and involves interaction with the transcription factor AP1, suggesting that AP1 facilitates recruitment of BCL6 to these sites (Hatzi et al., 2015).

Functions of BCL6 in memory and effector T cells

BCL6 also plays a role in other populations of T cells. BCL6 was found to be necessary for the generation and maintenance of memory CD8+ T cells and long-term memory CD4+ T cells by regulating their expansion and/or survival (Ichii et al., 2007; Ichii et al., 2002; Ichii et al., 2004). BCL6 also negatively regulates the cytotoxicity of effector CD8+ T cells by directly repressing *Gzmb*, the gene that encodes granzyme B (Yoshida et al., 2006). In addition, in the context of chronic viral infection, BCL6 was shown to promote a progenitor-like state in CD8+ T cells, which aided the antiviral response (Wu et al., 2016).

Functions of BCL6 in macrophages

One of the most striking characteristics of mice with global deletion of *Bcl6* is extensive type 2 inflammation (Ye et al., 1997). This is at least partially attributable to repression of macrophage activation by BCL6. In macrophages, BCL6 represses expression of the chemokines MCP-1, MCP-3 and MRP-1 (Toney et al., 2000). Furthermore, genome-wide analysis revealed that BCL6 represses a large proportion of NF-κB target genes, and that deletion of BCL6 sensitizes macrophages to activation by LPS (Barish et al., 2010). In the setting of atherosclerosis, BCL6 protects against lesion development by repressing pro-atherogenic genes in macrophages (Barish et al., 2012). BCL6-deficient macrophages also have enhanced proliferation as a result of elevated secretion of IL-6, which is normally repressed by BCL6 in

these cells (Yu et al., 2005). BCL6 also regulates macrophage morphology and motility by suppressing RhoA activity via a mechanism involving upregulation of CSF1R (Pixley et al., 2005).

Functions of BCL6 in hepatocytes

In mice with global *Bcl6* deletion, there is a dramatic reduction in total body fat content, including in the liver (LaPensee et al., 2014). This is accompanied by downregulation of genes involved in lipogenesis, including *Fasn*, *Scd1*, and *Chrebp*. While these observations suggest that BCL6 regulates lipid metabolism in hepatocytes, they should be interpreted with caution, since the effects observed in a global knock-out may be the indirect consequence of BCL6 action in a different cell type.

Interestingly, liver BCL6 expression is dramatically higher in male mice. This is due to negative regulation of BCL6 by growth hormone, which has a pulsatile secretion pattern in males and a near-continuous pattern in females (Meyer et al., 2009). Furthermore, BCL6 has a mutually antagonistic interaction with STAT5, which is activated by growth hormone. Many growth hormone-regulated, sex-biased genes in liver are directly bound by both BCL6 and STAT5, and correlational analysis suggests that BCL6 represses, while STAT5 induces these genes (Zhang et al., 2012). In particular, genes related to lipid and drug metabolism are enriched among BCL6/STAT5 direct targets, suggesting that BCL6 is important for maintaining sex-biased expression of these pathways.

BCL6 expression in hepatocytes is influenced by feeding, being upregulated during the fed state. Hepatocyte-specific deletion of *Bcl6* results in elevated lipid catabolism and protects mice from high-fat diet-induced hepatitis steatosis (Sommars et al., 2019). Mechanistically,

BCL6 co-localizes with PPARα near genes involved in lipid metabolism and opposes the action of PPARα at these sites by recruitment of co-repressors SMRT, NCOR, and HDAC3. While the involvement of growth hormone was not examined in this study, it is quite likely that the feeding-dependent changes in BCL6 abundance are driven by changes in growth hormone secretion, which is elevated during fasting (Ho et al., 1988). Thus, BCL6 may constitute an important link between growth hormone and the hepatic fasting response.

Functions of BCL6 in adipocytes

The observation of dramatically reduced adipose tissue mass in mice with global deletion of *Bcl6* suggested a possible role of BCL6 in adipocytes (LaPensee et al., 2014). One study found that BCL6 positively regulates adipogenesis *in vitro*, although this function was not tested *in vivo* (Hu et al., 2016). Recently, a study by Senagolage and colleagues found that deletion of BCL6 in mature adipocytes led to selective hypertrophy of subcutaneous adipose tissue, improved insulin sensitivity, and reduced hepatic steatosis during high-fat diet. This was linked to repression of genes involved in unsaturated fatty acid synthesis (e.g. *Fads1* and *Elovl6*) and growth (e.g. *Igf2* and *Akt1*) by BCL6. In brown adipose tissue, the authors observed reduced glucose uptake and modestly reduced thermogenic gene expression (e.g. *Ucp1*, *Prdm16*, and *Cidea*) in the mutant mice, but did not identify a requirement for BCL6 in brown adipose tissue thermogenesis.

General remarks about the role of BCL6 across cell types

It is clear that the precise functions of BCL6 are highly cell-type dependent (Table 1.1). This diversity of function is accompanied by tremendous variation in BCL6 binding sites across

cell types (Liu et al., 2016), despite the fact that the zinc finger domain of BCL6 binds to DNA in a sequence-dependent manner. A likely explanation for this unexpected observation is that in some cases, BCL6 is recruited to chromatin through cooperation with other transcription factors (Wei et al., 2009), underscoring the importance of cellular context for the actions of BCL6. Furthermore, regulation of a particular gene by BCL6 may occur in some cell types and not others due to differences in abundance or recruitment of particular co-repressors or other components that are required for gene regulation. Despite these differences, the general theme that emerges from the comparison of BCL6 functions is that it opposes transitions between cellular states. For example, it opposes apoptosis, activation, and plasma cell differentiation in germinal center B cells; it opposes inflammatory activation in macrophages; and it opposes the fasting response in hepatocytes (Table 1.1). Thus, it appears that BCL6 has been co-opted by different cell types over the course of evolution to restrict plasticity, enforcing the maintenance of specific cellular states.

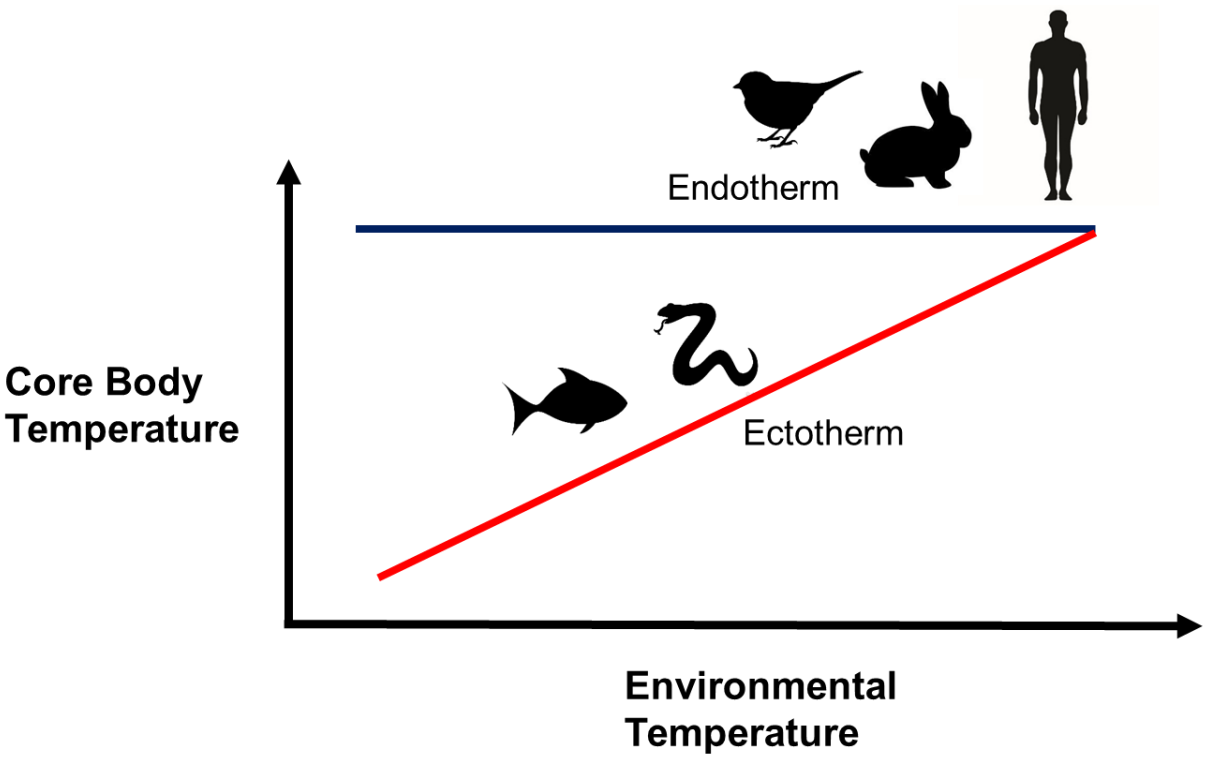
Endotherm
Ectotherm
Core Body Temperature
Environmental Temperature

Figure 1.1. The relationship between core body temperature and environmental temperature in endotherms and ectotherms.
Unlike ectotherms, endotherms possess powerful mechanisms of internal heat production that enable them to maintain a relatively constant core body temperature across a wide range of environmental temperatures. Endotherms include most species of mammals and birds, whereas ectotherms include most species of reptiles, amphibians, fish, and invertebrates.

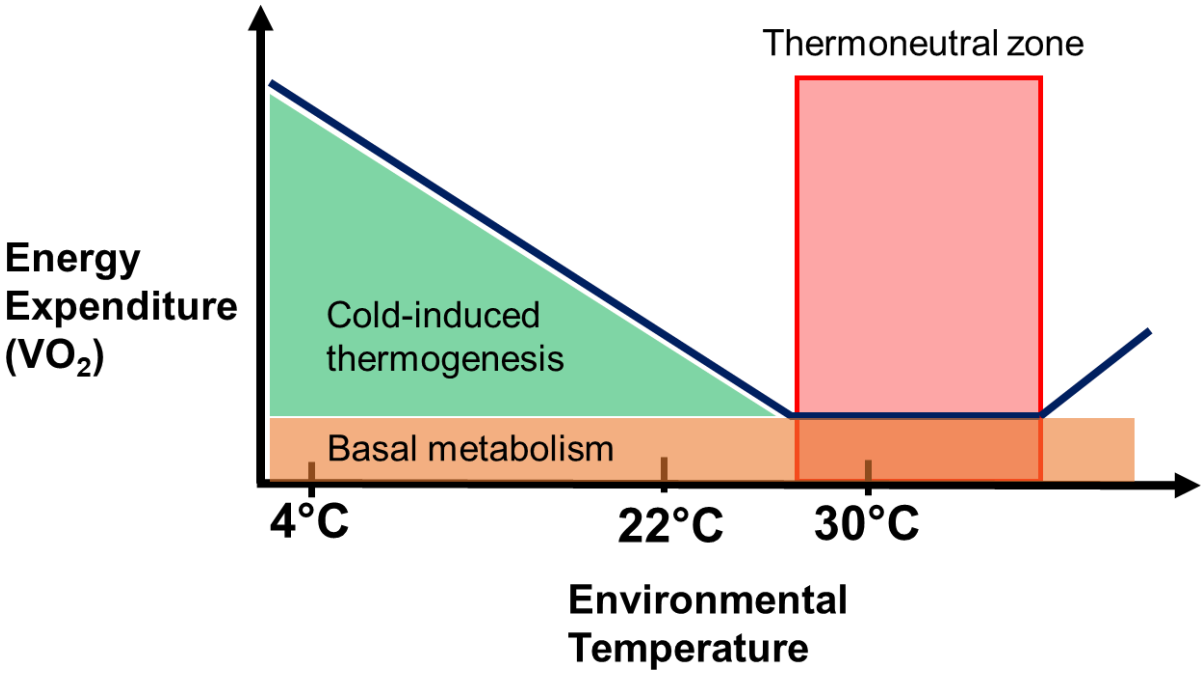
Thermoneutral zone
Energy Expenditure (VO_2)
Cold-induced thermogenesis
Basal metabolism
4°C
22°C
30°C
Environmental Temperature

Figure 1.2. Thermogenesis as a function of environmental temperature in mice.
The plot depicts the relationship between total energy expenditure (often measured as oxygen consumption, VO_2) and environmental temperature in mice. As the environmental temperature decreases below approximately 28º C, the energy dedicated to thermogenesis increases in order to maintain the normal body temperature. In the thermoneutral zone, which is above approximately 28º C, the basal metabolic rate is sufficient for maintenance of the normal body temperature without any extra energy dedicated to thermogenesis. Therefore, the thermoneutral zone is the most energy-efficient range of temperature for the mouse. This plot is modeled after Figure 1 in (Cannon and Nedergaard, 2011).

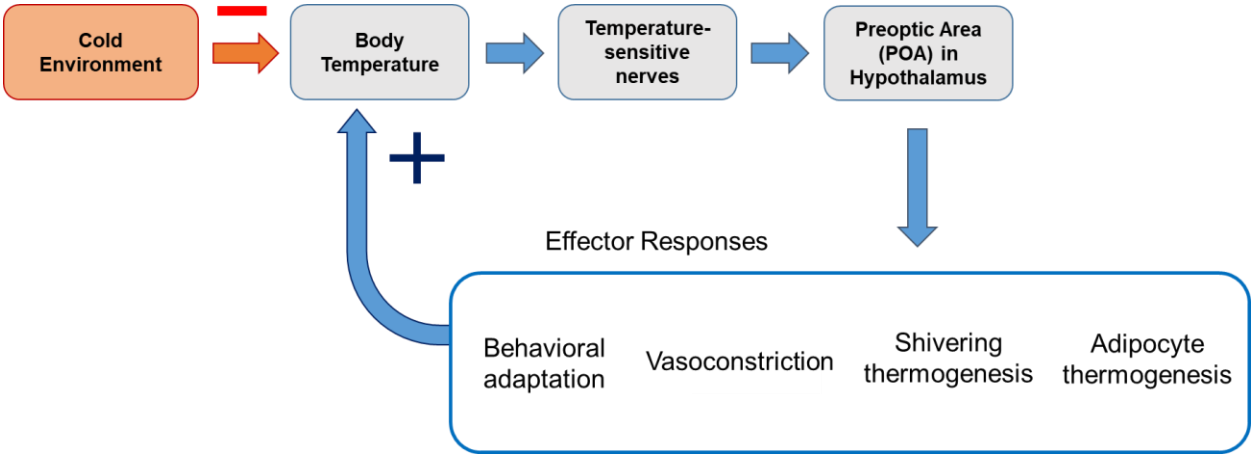
Cold Environment
Body Temperature
Temperature-sensitive nerves
Preoptic Area (POA) in Hypothalamus
Effector Responses
Behavioral adaptation
Vasoconstriction
Shivering thermogenesis
Adipocyte thermogenesis

Figure 1.3. Defense of core body temperature by homeostatic mechanisms in mammals. When the environmental temperature decreases, the rate of body heat loss to the environment increases. In order to maintain its normal body temperature, the mammal relies on homeostatic thermoregulation to oppose the influence of environmental temperature. The decrease in environmental temperature is sensed by specialized temperature-sensitive nerves in the skin, which relay this information to the preoptic area of the hypothalamus. The hypothalamus then activates multiple mechanisms that reduce heat loss or increase heat production (thermogenesis). These include behavioral mechanisms (adopting a hunched body posture, huddling, burrowing), vasoconstriction at the body surface (to reduce heat loss from the blood to the environment), shivering thermogenesis (in skeletal muscle), and adipocyte thermogenesis (in brown and beige adipocytes). Collectively, these mechanisms oppose the increased heat loss to the cold environment in order to stabilize the core body temperature.

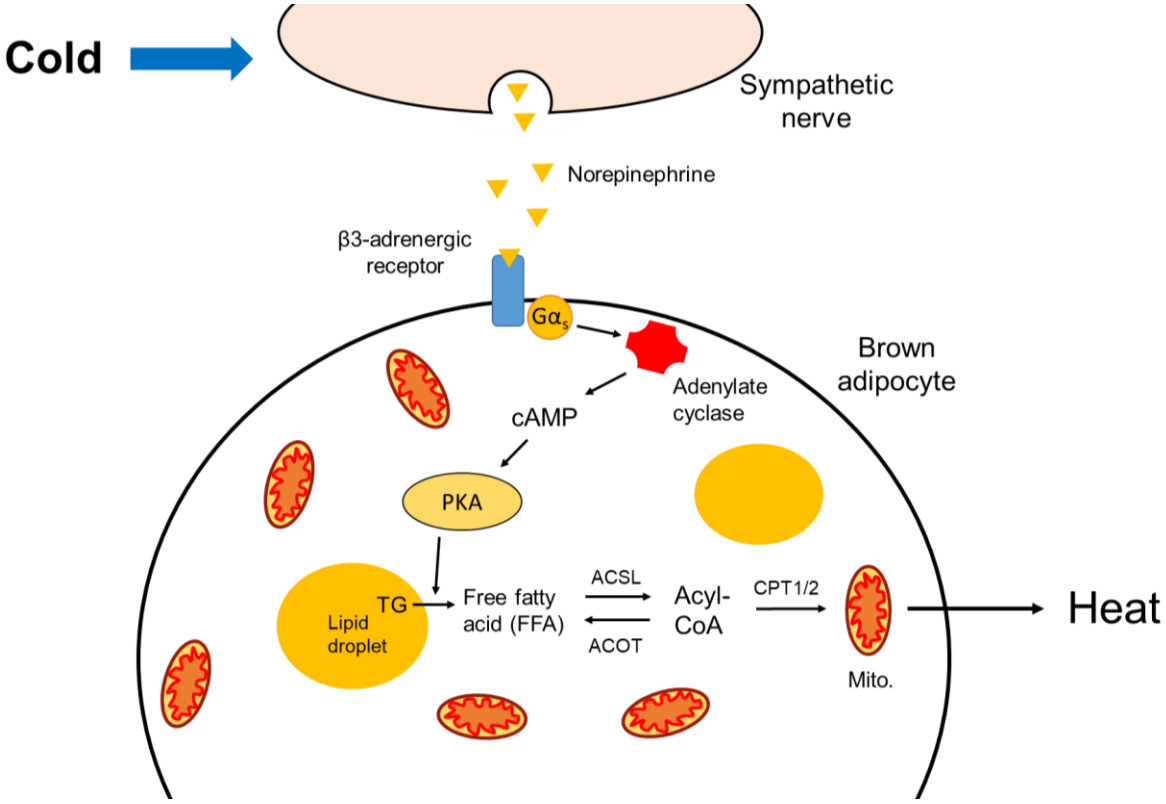
Cold
Sympathetic nerve
Norepinephrine
β3-adrenergic receptor
Gαs
Adenylate cyclase
Brown adipocyte
cAMP
PKA
TG
Lipid droplet
Free fatty acid (FFA)
ACSL
ACOT
Acyl-CoA
CPT1/2
Mito.
Heat

Figure 1.4. Sympathetic nerves control activation of brown adipocyte thermogenesis. As depicted in the model, sensation of cold leads to activation of sympathetic nerves that innervate brown adipose tissue. These nerves secrete norepinephrine, which acts on β3-adrenergic receptors (β3ARs) located on the surface of brown adipocytes. β3ARs are G protein-coupled receptors that signal via Gαs to trigger cyclic AMP (cAMP) production by adenylyl cyclase. Protein kinase A (PKA), which is activated by cAMP, phosphorylates various proteins involved in thermogenesis. For example, it phosphorylates hormone-sensitive lipase (HSL), which stimulates HSL's conversion of triglycerides (TGs) to free fatty acids (FFAs). FFAs are then converted to acyl-CoAs by acyl-CoA synthetases (ACSLs), and the acyl-CoAs are imported into mitochondria via the carnitine shuttle (involving the enzymes CPT1 and CPT2), where they undergo oxidation, a key step in the thermogenic pathway.

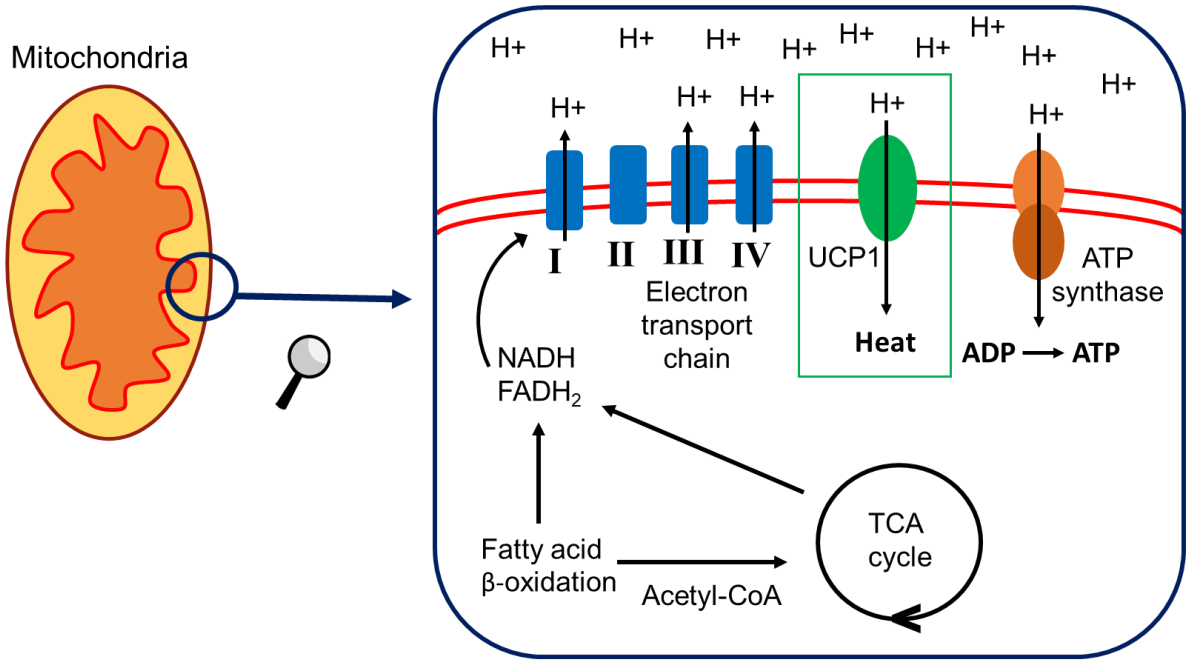
Mitochondria
H+
I
II
III
IV
Electron transport chain
UCP1
Heat
ATP synthase
ADP → ATP
NADH
FADH2
Fatty acid β-oxidation
Acetyl-CoA
TCA cycle

Figure 1.5. Brown adipocyte thermogenesis depends on uncoupled mitochondrial respiration.
After being imported into the mitochondrial matrix, acyl-CoAs undergo β-oxidation to generate acetyl-CoA, NADH, and $FADH_2$. Acetyl-CoA is further oxidized in the tricarboxylic acid (TCA) cycle to generate additional NADH and $FADH_2$, which provide electrons to the electron transport chain, resulting in the generation of a proton gradient at the inner mitochondrial membrane. In most cell types, the primary purpose of the proton gradient is to drive ATP production by ATP synthase, which is called *coupled respiration*. In brown adipocytes, the primary purpose is *uncoupled respiration*, which depends on a unique mitochondrial protein called uncoupling protein 1 (UCP1). UCP1 acts as a proton transporter, dissipating the proton gradient *without* concomitant synthesis of ATP. In this way, UCP1 allows mitochondrial respiration to proceed without being limited by the cell's ATP demand. During active thermogenesis, uncoupled respiration can reach a very high rate, and the resulting energy is released as heat to the rest of the body.

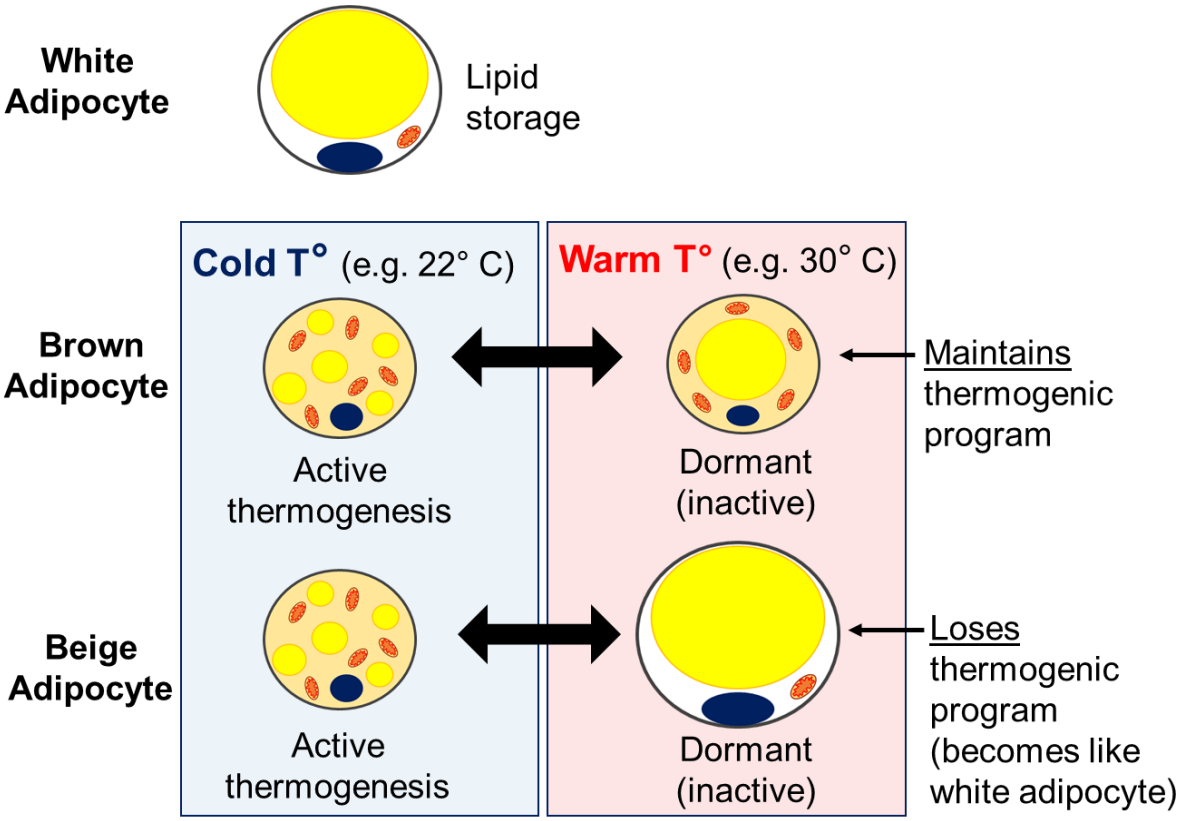
White Adipocyte
Lipid storage
Cold T° (e.g. 22° C)
Warm T° (e.g. 30° C)
Brown Adipocyte
Active thermogenesis
Dormant (inactive)
Maintains thermogenic program
Beige Adipocyte
Active thermogenesis
Dormant (inactive)
Loses thermogenic program (becomes like white adipocyte)

Figure 1.6. Brown adipocytes, unlike beige, maintain thermogenic program during dormancy. Three different types of adipocytes are found in mammals. White adipocytes are specialized for lipid storage. Brown and beige adipocytes contribute to thermogenesis during cold exposure, and become dormant (inactive) during adaptation to warm temperature. While brown adipocytes mostly maintain their thermogenic characteristics during dormancy, beige adipocytes lose virtually all thermogenic characteristics and become almost indistinguishable from white adipocytes.

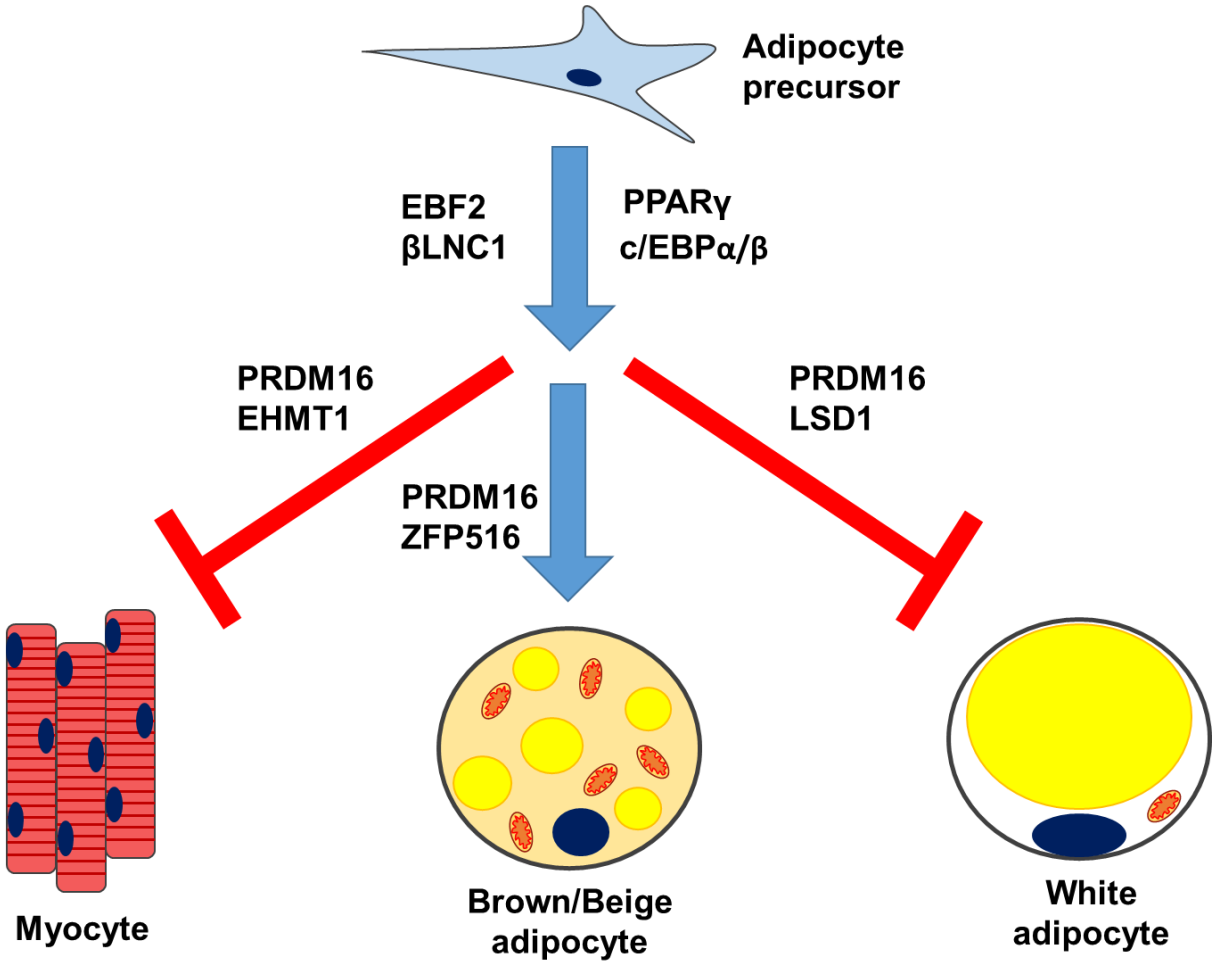
Adipocyte
precursor
EBF2
βLNC1
PPARγ
c/EBPα/β
PRDM16
EHMT1
PRDM16
ZFP516
PRDM16
LSD1
Myocyte
Brown/Beige
adipocyte
White
adipocyte

Figure 1.7. Transcriptional regulators that influence brown/beige adipocyte differentiation. PPARγ and CEBPα/β and are important drivers of the "general" adipocyte differentiation pathway. EBF2, βLNC1, PRDM16, and ZFP516 are important for directing differentiation towards the brown/beige adipocyte fate. In collaboration with EHMT1, PRDM16 opposes differentiation to the myocyte fate. Similarly, in collaboration with LSD1, PRDM16 opposes differentiation to the white adipocyte fate.

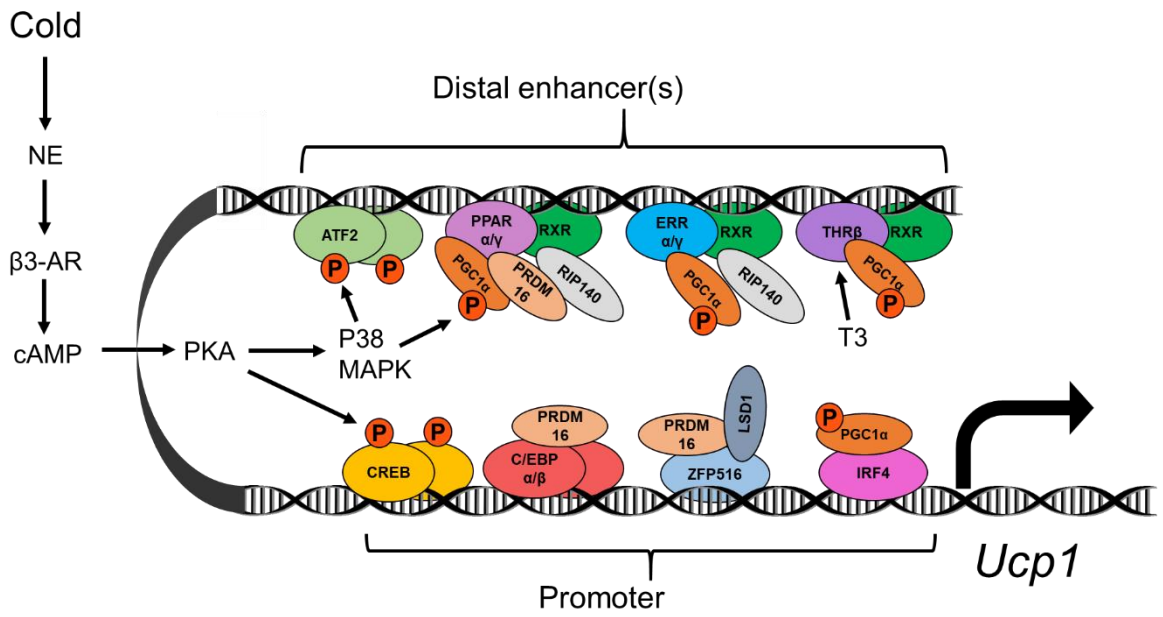
Cold
NE
β3-AR
cAMP
PKA
P38
MAPK
Distal enhancer(s)
ATF2
PPAR
α/γ
RXR
PGC1α
PRDM
16
RIP140
ERR
α/γ
RXR
PGC1α
RIP140
THRβ
RXR
PGC1α
T3
CREB
PRDM
16
C/EBP
α/β
PRDM
16
LSD1
ZFP516
PGC1α
IRF4
Promoter
Ucp1

Figure 1.8. Regulation of *Ucp1* transcription.
Transcription of *Ucp1* is controlled by transcription factors and associated co-activators that are recruited to the promoter and upstream enhancer(s). Some of these, including PPARα/γ and PRDM16, are particularly important in the context of differentiation. Others, such as ERRα/γ, CREB, ATF2, IRF4, and PGC-1α, are particularly important for cold-induced upregulation of *Ucp1*. Phosphorylation of CREB, ATF2, and PGC-1α by PKA/p38 plays a key role in linking adrenergic signaling to *Ucp1* expression during cold exposure.

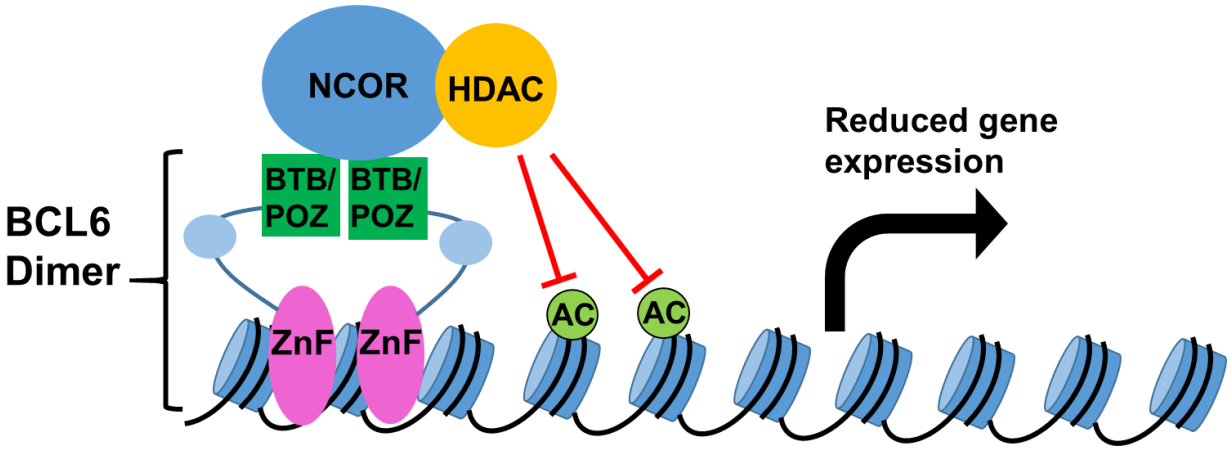
NCOR
HDAC
BTB/
POZ
BTB/
POZ
BCL6
Dimer
ZnF
ZnF
AC
AC
Reduced gene
expression

Figure 1.9. BCL6 represses target gene expression via recruitment of histone deacetylases. BCL6 binds to DNA as a homodimer in a sequence-specific manner via its zinc finger (ZnF) domains. One of the mechanisms by which BCL6 represses target gene expression involves recruitment of a co-repressor complex, such as NCOR, through interaction with its BTB/POZ domain, which in turn facilitates recruitment of histone deacetylases (HDACs). Histone deacetylation causes chromatin to adopt a more compact or closed conformation and limits recruitment of other transcription factors that positively regulate expression of the target gene, resulting in reduced gene expression.

Table 1.1. Reported function(s) of BCL6 in different cell types.
Previous studies have reported diverse functions of BCL6 in germinal center B cells, T follicular helper cells, memory T cells, macrophages, hepatocytes, white adipocytes, and multiple types of cancer. While the specific functions of BCL6 are very cell type-dependent, a general feature of BCL6 is that it opposes transitions to alternative cell states.

Cell Type	Reported Function(s) of BCL6
Germinal Center B cell	Inhibits differentiation to plasma cell, apoptosis, and antigen-induced activation (Basso and Dalla-Favera, 2012)
T Follicular Helper (TFH) cell, Memory T cell	Essential for generation and maintenance of these populations (Hatzi et al., 2015; Ichii et al., 2007; Ichii et al., 2004)
Macrophage	Inhibits inflammatory activation (represses NF-κB target genes) (Barish et al., 2010)
Hepatocyte	Inhibits fasting response (represses PPARα target genes) (Sommars et al., 2019)
White Adipocyte	Inhibits insulin signaling and lipogenesis (Senagolage et al., 2018)
Multiple Forms of Cancer	Promotes proliferation and inhibits apoptosis (Cardenas et al., 2017)

CHAPTER 2: BCL6 MAINTAINS THERMOGENIC CAPACITY OF BROWN ADIPOSE TISSUE DURING DORMANCY

Abstract

Brown adipocytes provide a metabolic defense against environmental cold, but become inactive or dormant as mammals habituate to warm environments. Although dormant brown adipocytes maintain their cellular identity and thermogenic capacity, the mechanisms that support dormancy in brown adipocytes are not well understood. Here, we identify B cell leukemia/lymphoma 6 (BCL6) as a critical regulator of dormancy in mouse brown adipocytes, but not for their commitment, differentiation, or cold-induced activation. By a combination of both direct and indirect transcriptional mechanisms, BCL6 promotes uncoupled respiration, fatty acid oxidation, and survival in dormant brown adipocytes. In part, BCL6 achieves this by remodeling the epigenome of brown adipocytes to enforce brown and oppose white adipocyte cellular identity. Thus, unlike other transcription factors that regulate cold-induced thermogenesis, BCL6 is specifically required for maintaining thermogenic fitness during adaptation to environmental warmth.

Introduction

In mammals, thermogenic adipocytes generate heat through fuel oxidation and uncoupled respiration to defend core temperature in cold environments (Cannon and Nedergaard, 2004, 2011; Harms and Seale, 2013; Lowell and Spiegelman, 2000). Thermogenic adipocytes include brown adipocytes, which are located in brown adipose tissue (BAT), and beige adipocytes, which develop in white adipose tissue (WAT). Thermogenesis in brown and beige adipocytes is strongly influenced by environmental temperature. In response to acute cold exposure, sympathetic nerves secrete norepinephrine to activate β3-adrenergic receptors on thermogenic adipocytes, resulting in activation of cyclic AMP-dependent signaling pathways to enhance thermogenesis. Prolonged exposure to cold not only increases the thermogenic capacity of individual adipocytes, but also enhances their differentiation and survival, allowing for metabolic adaptation of mammals to the cold environment.

In contrast, as mammals acclimate to warm environments, their need for thermogenesis decreases, resulting in the entry of brown and beige adipocytes into an inactive dormant state, which conserves energy and prevents hyperthermia (Cannon and Nedergaard, 2004, 2011). Dormancy is characterized by reduced thermogenic capacity, including downregulation of key mitochondrial proteins required for fuel oxidation and uncoupled respiration, such as uncoupling protein 1 (UCP1). While beige adipocytes lose virtually all of their thermogenic capacity during acclimation to environmental warmth, brown adipocytes retain a significant portion of their thermogenic capacity even after remaining dormant for many weeks (Roh et al., 2018; Sanchez-Gurmaches et al., 2016). This distinction between beige and brown adipocytes is also observed at the level of the epigenome. For example, the enhancer landscape of beige adipocytes undergoes profound remodeling during adaptation to warmth, becoming almost indistinguishable from that

of white adipocytes (Roh et al., 2018). In contrast, brown adipocytes largely maintain their chromatin state during dormancy (Roh et al., 2018). This epigenetic stability of dormant brown adipocytes contributes to maintenance of their thermogenic capacity, which is essential for rapid adaptation of mammals to changes in environmental temperature. Furthermore, because thermogenic adipocytes in humans are largely dormant (Lichtenbelt et al., 2014), a better understanding of this state will aid efforts to target brown adipocytes for the treatment of obesity and diabetes.

B cell leukemia/lymphoma 6 (BCL6), a sequence-specific transcriptional repressor, is expressed in many cell types but has been best studied in the immune system. In germinal center B cells, it plays an essential role in the germinal center reaction by repressing genes involved in DNA damage response, apoptosis, cell activation, and plasma cell differentiation (Dent et al., 1997; Ye et al., 1997). BCL6 is also required for the differentiation of T follicular helper cells and modulates the inflammatory activation of macrophages (Barish et al., 2010; Johnston et al., 2009; Lee et al., 2003; Nurieva et al., 2009). Outside the immune system, BCL6 is expressed in metabolic tissues, such as adipocytes and liver, where its functions are just beginning to be investigated (Basse et al., 2015; Hu et al., 2016; LaPensee et al., 2014; Senagolage et al., 2018). For example, a recent report found that deletion of *Bcl6* in all adipocytes increased *de novo* lipogenesis, resulting in selective expansion of subcutaneous WAT and protection from obesity-induced insulin resistance (Senagolage et al., 2018). Although these studies suggest a potential role for BCL6 in fatty acid metabolism, the role of BCL6 in brown adipocytes has not been explored.

Here, we investigated the regulatory functions of BCL6 in both metabolically active and dormant brown adipocytes. We found that loss of BCL6 did not impair the commitment,

differentiation, or adrenergic activation of brown adipocytes, but it selectively impaired their survival and maintenance of thermogenic capacity during dormancy. Thus, unlike other thermogenic regulators that act downstream of the sympathetic nervous system, our data suggest that BCL6 acts in parallel with the sympathetic nervous system to reinforce brown adipocyte cellular identity when sympathetic activation of BAT is reduced.

Results

BCL6 is required for maintenance of thermogenic capacity in dormant BAT

BCL6 is expressed in mature BAT and differentiating brown adipocytes (Figure 2.2A-C), where its functions are not well understood. To investigate the role of BCL6 in brown adipocyte development and function, we crossed *Bcl6*$^{f/f}$ mice on C57BL6/J background with *Ucp1*^{Cre}, *Adipoq*^{Cre}, and *Myf5*^{Cre} to generate conditional knockouts of BCL6 in BAT (*Bcl6*$^{f/f}$*Ucp1*^{Cre}), pan-adipose (*Bcl6*$^{f/f}$*Adipoq*^{Cre}), and Myf5^{+} somitic brown adipocyte precursors (*Bcl6*$^{f/f}$*Myf5*^{Cre}), respectively (Figure 2.1A). In all three conditional knockout models, adult BAT remained intact when mice were adapted to cold (raised at the normal vivarium temperature of 22ºC) (Figure 2.1B). In contrast to a previous study that had implicated BCL6 in commitment and differentiation of adipocyte precursors (Hu et al., 2016), we found that BCL6 was not required in Myf5^{+} precursors for the development of the brown adipocyte lineage (Figure 2.1B). Furthermore, in cold-adapted mice, BCL6 was not required for BAT thermogenesis elicited by extreme environmental cold, as evidenced by normal core body temperature and survival of *Bcl6*$^{f/f}$*Ucp1*^{Cre} and *Bcl6*$^{f/f}$*Adipoq*^{Cre} mice upon acute exposure to 4º C (Figure 2.1C-D, 2.2D). Since BCL6 was not required for BAT thermogenesis in cold-adapted mice, we considered the alternative hypothesis that BCL6 is important for maintenance of thermogenic capacity in dormant BAT.

To investigate the role of BCL6 in BAT dormancy, we bred and reared mice at thermoneutrality (30º C), a warm environment that minimizes thermogenesis and promotes entry of BAT into its dormant state. Although thermoneutral housing did not alter expression of BCL6 protein in BAT (Figure 2.2E), loss of BCL6 had a profound effect on the thermogenic competence of dormant BAT. For example, during a cold challenge from 30º C to 10º C, core

temperature rapidly declined in *Bcl6*$^{f/f}$*Ucp1*^{Cre} and *Bcl6*$^{f/f}$*Myf5*^{Cre} mice, resulting in severe hypothermia (Figure 2.1E and 2.2F). In both conditional knockouts, the inability to maintain core temperature was uniformly lethal, whereas the majority of the control animals were able to survive the cold challenge after adaptation to thermoneutrality (Figure 2.1F and 2.2G).

We next asked whether a decrease in thermogenic capacity of dormant (30º C) BAT led to cold intolerance in *Bcl6*$^{f/f}$*Ucp1*^{Cre} mice. Increase in oxygen consumption in response to norepinephrine injection, which reflects the organism's thermogenic capacity (Golozoubova et al., 2006; Granneman et al., 2003), was blunted in *Bcl6*$^{f/f}$*Ucp1*^{Cre} mice when they were bred or adapted at 30º C, but not when they were bred at 22º C (Figure 2.1G-I). In agreement with these data, thermographic imaging revealed lower surface temperature over interscapular BAT (iBAT) in 30º C-adapted *Bcl6*$^{f/f}$*Ucp1*^{Cre} and *Bcl6*$^{f/f}$*Adipoq*^{Cre} mice during an acute cold challenge (Figure 2.1J-K, 2.2H), which contributed to lethal hypothermia and impaired survival in 30º C-adapted *Bcl6*$^{f/f}$*Adipoq*^{Cre} mice (Figure 2.2I-J). This decrease in iBAT thermogenesis was not the result of changes in adrenergic signaling, as evidenced by normal expression of β3-adrenergic receptor and PKA-dependent phosphorylation in iBAT of *Bcl6*$^{f/f}$*Ucp1*^{Cre} mice after injection of the β3-adrenergic agonist CL-316,243 (Figure 2.1L). Together, these findings demonstrate that BCL6 is required for the maintenance of thermogenic capacity in dormant iBAT of mice adapted to thermoneutrality (30º C), but not in active iBAT of mice adapted to cold (22º C).

BCL6 regulates survival of dormant brown adipocytes

To further investigate how BCL6 regulates thermogenic capacity in dormant (30º C) BAT, we examined the size and morphology of BAT from *Bcl6*$^{f/f}$ and *Bcl6*$^{f/f}$*Ucp1*^{Cre} mice that

were adapted to cold (22º C) or thermoneutrality (30º C). Whereas BAT mass was slightly increased in *Bcl6*$^{f/f}$*Ucp1*^{Cre} mice in the cold-adapted state (22º C), it was considerably reduced during dormancy (30º C) (Figure 2.3A). This reduction was observed despite elevated lipid accumulation in the *Bcl6*$^{f/f}$*Ucp1*^{Cre} BAT at both temperatures (Figure 2.4), suggesting that the quantity of brown adipocytes was reduced. Indeed, total DNA content in the adipocyte fraction of BAT was lower in *Bcl6*$^{f/f}$*Ucp1*^{Cre} mice during dormancy (30º C) (Figure 2.3B). To understand why loss of *Bcl6* led to loss of cellularity in dormant (30º C) BAT, we analyzed the iBAT transcriptome of *Bcl6*$^{f/f}$ and *Bcl6*$^{f/f}$*Ucp1*^{Cre} mice during cold adaptation and dormancy using RNA-seq. This analysis revealed that BCL6 regulates the iBAT transcriptome in a temperature-dependent manner. For example, ~65-68% of differentially expressed genes (induced or repressed) were specifically regulated by BCL6 during BAT dormancy (30º C) (Figure 2.3C). Because BCL6 functions as a transcriptional repressor in other contexts, we first focused on genes induced in iBAT of *Bcl6*$^{f/f}$*Ucp1*^{Cre} mice. Gene ontology enrichment analysis revealed significant enrichment of genes involved in immune, inflammatory, and apoptotic processes (Figure 2.3D). Among these were genes linked to extrinsic and intrinsic pathways of apoptosis, including *Bcl10, Bmf, Traf1*, *Dlc1*, *Litaf, Tnfrsf10b, Wdr92, Dapk1*, and *Egln3* (Table 2.1). Although a gene signature of tissue inflammation was also induced in iBAT of *Bcl6*$^{f/f}$*Ucp1*^{Cre} mice adapted to thermoneutrality (30º C) (Figure 2.3D and Table 2.2), flow cytometric analysis did not reveal increased recruitment of immune cells into iBAT, indicating the absence of an overt inflammatory response (Figure 2.5).

Previous studies have demonstrated that, in addition to activating thermogenesis, adrenergic stimuli promote survival of brown adipocytes (Lindquist and Rehnmark, 1998; Nedergaard et al., 2018). These findings, together with the observed upregulation of apoptotic

genes in dormant (30º C) iBAT of *Bcl6*$^{f/f}$*Ucp1*^{Cre} mice, led us to ask whether BCL6 might function in parallel with sympathetic signaling to promote survival of brown adipocytes during dormancy. To assess cell survival, we performed terminal deoxynucleotidyl transferase dUTP nick end labeling (TUNEL), which marks apoptotic cells. We observed an increased frequency of TUNEL^{+} apoptotic cells in dormant (30º C) iBAT of *Bcl6*$^{f/f}$*Ucp1*^{Cre} mice (Figure 2.3E-F). In contrast, during cold adaptation (22º C), the frequency of TUNEL^{+} apoptotic cells was not increased in iBAT of *Bcl6*$^{f/f}$*Ucp1*^{Cre} mice (Figure 2.3F). Because the frequency of Ki67^{+} proliferating cells was not significantly different between the genotypes (Figure 2.3G-H), these findings collectively suggest that BCL6 promotes survival of brown adipocytes specifically during dormancy, when sympathetic activation of BAT is minimal.

The upregulation of apoptotic genes in dormant (30º C) iBAT of *Bcl6*$^{f/f}$*Ucp1*^{Cre} mice suggested that BCL6 might directly repress these genes. To test this possibility, we performed chromatin immunoprecipitation followed by sequencing (ChIP-seq) for BCL6 in dormant (30º C) BAT. We found over 3000 binding sites for BCL6 in BAT, which localized primarily to intronic, intergenic, and promoter regions (Figure 2.6A). *De novo* motif analysis revealed enrichment for the consensus BCL6 binding motif amongst the identified peaks (Figure 2.6B), confirming the specificity of the ChIP-seq. To identify genes that are likely to be directly regulated by BCL6, we searched for genes that are both differentially expressed in dormant (30º C) iBAT of *Bcl6*$^{f/f}$*Ucp1*^{Cre} mice (fold change > 1.5) and which are nearest to a BCL6 binding site. This approach revealed 226 and 112 genes that are negatively and positively regulated by BCL6, respectively (Table 2.3). Amongst these genes, we found specific binding of BCL6 near pro-apoptotic genes *Bmf* and *Egln3* (Figure 2.6D), as well as *Dapk1* and *Wdr92* (Table 2.3). Quantitative RT-PCR confirmed that *Bmf* and *Egln3* were upregulated in dormant (30º C) iBAT

of *Bcl6*$^{f/f}$*Ucp1*^{Cre} mice (Figure 2.6C). Taken together, these data indicate that BCL6 directly represses pro-apoptotic genes in brown adipocytes, which likely enhances their survival during dormancy.

BCL6 maintains uncoupled respiration in dormant BAT

We next asked whether BCL6 also regulates the respiratory capacity of the surviving cells in dormant BAT of *Bcl6*$^{f/f}$*Ucp1*^{Cre} mice. We found that, after an acute cold challenge, respiration in isolated iBAT was reduced by ~40-50% in *Bcl6*$^{f/f}$*Ucp1*^{Cre} and *Bcl6*$^{f/f}$*Adipoq*^{Cre} mice during dormancy (30º C) (Figure 2.7A and 2.9A). A similar respiration defect was observed in mitochondria isolated from dormant (30º C) iBAT of *Bcl6*$^{f/f}$*Ucp1*^{Cre} mice (Figure 2.7B). This decrease in mitochondrial respiration was associated with near complete absence of UCP1 mRNA and protein in dormant (30º C), but not cold-adapted (22º C) iBAT of *Bcl6*$^{f/f}$*Ucp1*^{Cre} mice (Figure 2.7C and 2.9B). Consistent with this observation, addition of guanosine diphosphate (GDP), which inhibits UCP1, had no effect on the respiration rate of mitochondria isolated from dormant (30º C) iBAT of *Bcl6*$^{f/f}$*Ucp1*^{Cre} mice (Figure 2.7B). A similar decrease in UCP1 protein expression was also observed when *Bcl6*$^{f/f}$*Ucp1*^{Cre} mice that were bred at 22º C were adapted to 30º C for 6 weeks, independently verifying the importance of BCL6 in regulation of BAT dormancy (Figure 2.9C). In contrast, mitochondrial abundance, cristae density, and expression of respiratory chain complexes I to IV were not significantly perturbed in dormant (30º C) iBAT of *Bcl6*$^{f/f}$*Ucp1*^{Cre} mice (Figure 2.7D and 2.9D-G).

Because we observed that abundance of ATP5A, an F_0 subunit of ATP synthase, was increased in iBAT of *Bcl6*$^{f/f}$*Ucp1*^{Cre} mice (Figure 2.7D), we hypothesized that BCL6 regulates

switching between uncoupled (UCP1-mediated) and coupled (ATP synthase-mediated) respiration. ChIP-seq analysis revealed BCL6 binding sites near the promoter region of the *Atp5g1* gene (Figure 2.7E), which encodes the rate-limiting component in the assembly of ATP synthase in brown adipocytes (Houstek et al., 1995; Kramarova et al., 2008). Consistent with our hypothesis, loss of BCL6 resulted in increased expression of *Atp5g1* mRNA, resulting in higher ATP synthase activity in dormant (30º C) iBAT of $Bcl6^{f/f}Ucp1^{Cre}$ mice (Figure 2.7F-G). These findings suggest that BCL6 suppresses coupled respiration while maintaining uncoupled respiration in BAT during dormancy.

In addition to its role in cold-induced thermogenesis, UCP1 has been implicated in diet-induced thermogenesis, which can mitigate the deleterious effects of high fat diet (HFD) feeding (Feldmann et al., 2009). These observations prompted us to ask whether BCL6 in brown adipocytes might also regulate diet-induced thermogenesis. To test this hypothesis, we housed $Bcl6^{f/f}$ and $Bcl6^{f/f}Ucp1^{Cre}$ mice at thermoneutrality (30º C) and fed them HFD for 13 weeks. We found that body mass, body composition, glucose tolerance, and insulin sensitivity were not significantly different between the two genotypes after HFD feeding (Figure 2.8). In aggregate, these results suggest that while BCL6 is required for the maintenance of thermogenic capacity in BAT during dormancy, it is dispensable for diet-induced thermogenesis.

BCL6 regulates fatty acid metabolism in dormant BAT

We then asked whether BCL6 is required for maintenance of catabolic pathways in dormant BAT. Gene ontology enrichment analysis of downregulated genes in dormant (30º C) iBAT of $Bcl6^{f/f}Ucp1^{Cre}$ mice revealed significant enrichment of genes involved in fatty acid β-

oxidation, TCA cycle, and carbohydrate metabolism (Figure 2.10A). For example, we observed that almost the entire program for β-oxidation of fatty acids was suppressed in dormant (30º C) iBAT of *Bcl6*$^{f/f}$*Ucp1*^{Cre} mice (Figure 2.10B). This decrease in catabolism of fatty acids was accompanied by altered expression of acyl-CoA thioesterases (ACOTs), enzymes that hydrolyze fatty acyl-CoAs to the metabolically inactive fatty acids (Tillander et al., 2017). In particular, we observed that many of the cytosolic and peroxisomal ACOTs (*Acot1, Acot3, Acot4, Acot7, and Acot 8*) were induced in iBAT of *Bcl6*$^{f/f}$*Ucp1*^{Cre} mice during dormancy, whereas expression of mitochondrial ACOTs (*Acot2, Acot9, Acot13, and Them4*) was more variable (Figure 2.10C). The expression of acyl-CoA synthetases, which catalyze the reverse reaction of synthesizing acyl-CoAs from fatty acids, was mostly unchanged (Figure 2.10H).

The importance of ACOTs in fatty acid metabolism prompted us to take a closer look at the regulation of these genes by BCL6. ChIP-seq revealed that BCL6 bound near the promoter region of *Acot1* (Figure 2.10D), and the expression of *Acot1*, as well as the neighboring *Acot3* and *Acot4* genes was increased in dormant iBAT of *Bcl6*$^{f/f}$*Ucp1*^{Cre} mice (Figure 2.10E), indicating potential co-regulation of these ACOT genes by BCL6. Because shifts in ACOT activity can alter the balance between oxidation and storage of fatty acids (Okada et al., 2016; Tillander et al., 2017), we next quantified ACOT activity in iBAT. We found that ACOT activity was increased by ~40% in the cytosolic, but not the mitochondrial, fraction of dormant (30º C) iBAT of *Bcl6*$^{f/f}$*Ucp1*^{Cre} mice (Figure 2.10F, G). These data together suggest a model in which BCL6 determines how fatty acids are apportioned between storage and oxidation in brown adipocytes. In the absence of BCL6, activation and oxidation of fatty acids is decreased, favoring their storage into cytosolic lipid droplets (Figure 2.4)

BCL6 reinforces brown- and opposes white-specific enhancers to maintain cellular identity

Because genes involved in thermogenic metabolism were downregulated in dormant BAT of *Bcl6*$^{f/f}$*Ucp1*^{Cre} mice, we asked whether this represented a shift in adipocyte cellular identity from brown to white. Analysis of the BATLAS gene set, which can robustly differentiate between brown and white adipocytes (Perdikari et al., 2018), revealed that loss of BCL6 led to upregulation of white adipocyte (such as *Lep*, *Nnat*, *Igf1*, *Ccdc80*, and *Gadd45a*) and downregulation of brown adipocyte (such as *Acads*, *Cpt1b*, *Ech1*, *Hadha*, *Idh3a*, *Ndufs1*, *Sdha*, *Suclg1*, and *Ucp1*) markers in dormant (30º C) iBAT of *Bcl6*$^{f/f}$*Ucp1*^{Cre} mice (Figure 2.11A and Table 2.4). These changes in gene expression suggested that BCL6 might be necessary to maintain a stable chromatin state in brown adipocytes during dormancy. To test this hypothesis, we used ChIP-seq to measure the genome-wide abundance of acetylated histone 3 lysine 27 (H3K27ac), which marks active enhancers and promoters. We found that deletion of *Bcl6* altered the chromatin state of brown adipocytes in a temperature-dependent manner. For example, H3K27 acetylation was increased at 224 sites and reduced at 1,011 sites in iBAT of *Bcl6*$^{f/f}$*Ucp1*^{Cre} mice during dormancy (30º C) (Figure 2.11B and 2.12A), whereas acetylation was increased at 303 sites but reduced at only 228 sites during cold adaptation (22º C) (Figure 2.12A-B).

We next asked whether these global changes in the chromatin state of *Bcl6*$^{f/f}$*Ucp1*^{Cre} mice reflected a shift in adipocyte lineage-specific enhancers. For this analysis, we first constructed a list of brown and white adipocyte-specific enhancers (enriched >4-fold in either brown or white adipocytes) from the previously identified group of adipocyte enhancers (Roh et al., 2018). We then asked how loss of BCL6 affected the activation of these enhancers in dormant iBAT. We found that approximately half (~55%) of BCL6-dependent enhancers were brown or white

adipocyte-specific enhancers (Figure 2.11C). Importantly, the direction of BCL6 regulation at these enhancers clearly indicated a reinforcement of brown adipocyte cellular identity. For instance, amongst the BCL6-regulated brown adipocyte-specific enhancers, 99% exhibited decreased acetylation in *Bcl6*$^{f/f}$*Ucp1*^{Cre} dormant (30º C) iBAT (Figure 2.11D). In contrast, 100% of the BCL6-regulated white adipocyte-specific enhancers exhibited increased acetylation in the *Bcl6*$^{f/f}$*Ucp1*^{Cre} dormant (30º C) iBAT (Figure 2.11E). Although the number of BCL6-dependent active enhancers was ~2-fold lower in iBAT of cold-adapted mice (Figure 2.12C), BCL6 acted in a similar manner at these enhancers (Figure 2.12D, E). In particular, we found that H3K27 acetylation was reduced at brown adipocyte-specific enhancers associated with *Ucp1*, *Elovl3*, *Acaa1b*, *Cidea*, *Slc27a2*, *Gdf*, and *Ptk2b* (Figure 2.11F and 2.12F). In contrast, we found that H3K27 acetylation was increased at white adipocyte-specific enhancers associated with *Ccdc80*, *Lep*, and *Nnat* in iBAT of *Bcl6*$^{f/f}$*Ucp1*^{Cre} mice (Figure 2.11G and 2.12G). Similar enrichment of H3K27 acetylation was observed near BCL6 target genes in iBAT of *Bcl6*$^{f/f}$*Ucp1*^{Cre} mice, including *Atp5g1*, acyl-CoA thioesterases (*Acot1*, *3*, and *4*) and *Bmf* (Figure 2.11F-G, and 2.12H), consistent with their direct repression by BCL6. In aggregate, these results indicate that BCL6 maintains thermogenic capacity of dormant BAT in part by reinforcing brown adipocyte-specific enhancers while concurrently suppressing white adipocyte-specific enhancers.

BCL6 regulates brown adipocyte enhancers by direct and indirect mechanisms

Because BCL6 binding sites were not identified near the majority of altered enhancers in the iBAT of *Bcl6*$^{f/f}$*Ucp1*^{Cre} mice, we postulated that BCL6 regulates brown adipocyte enhancers by both direct and indirect mechanisms. *De novo* sequence motif analysis revealed enrichment of the consensus binding motifs for hepatic leukemia factor (HLF) and BCL6 amongst the sites

with increased H3K27 acetylation (Figure 2.13A), whereas a nuclear receptor half-site recognized by NR4A family members and estrogen-related receptors (ERRs) was enriched amongst the sites with reduced H3K27 acetylation in dormant (30º C) iBAT of *Bcl6*$^{f/f}$*Ucp1*^{Cre} mice (Figure 2.13B). This suggested that while BCL6 directly represses a subset of enhancers and promoters, such as those associated with the metabolic genes *Atp5g1* and *Acot1*, and the white adipocyte-specific genes *Lep*, *Ccdc80*, and *Nnat* (Figure 2.13C, Table 2.3), it indirectly activates other regulatory sites, possibly by a mechanism involving ERRs, which are known to regulate fatty acid and oxidative metabolism in brown adipocytes (Giguere, 2008; Villena and Kralli, 2008). Indeed, analysis of previously published ChIP-seq data for ERRα and ERRγ in BAT (Ahmadian et al., 2018; Emmett et al., 2017), revealed that the hypoacetylated H3K27 sites in dormant (30º C) iBAT of *Bcl6*$^{f/f}$*Ucp1*^{Cre} mice were highly enriched for ERRα and ERRγ binding (Figure 2.13D). For example, we observed decreased H3K27 acetylation near *Ucp1* and genes involved in fatty acid oxidation, including *Slc27a2*, *Hadha*, *Hadhb*, and *Acaa2*, in iBAT of *Bcl6*$^{f/f}$*Ucp1*^{Cre} mice housed at 30ºC, and these regions contained ERRα and ERRγ binding sites (Figure 2.13E). These results suggest that BCL6 might regulate the expression of these key metabolic genes indirectly by promoting the activity of ERRs at their nearby enhancers and promoters.

To investigate this possibility further, we analyzed the expression and recruitment of ERRs to their binding sites in dormant (30º C) BAT of *Bcl6*$^{f/f}$*Ucp1*^{Cre} mice. We observed that expression of the three ERR subtypes was unchanged in dormant (30º C) iBAT of *Bcl6*$^{f/f}$*Ucp1*^{Cre} mice (Figure 2.13F). To determine if BCL6 modulated recruitment of ERRs to their binding sites near thermogenic genes, we performed ChIP-seq for ERRα (the most abundant ERR in BAT) in dormant (30º C) iBAT of *Bcl6*$^{f/f}$ and *Bcl6*$^{f/f}$*Ucp1*^{Cre} mice housed at 30ºC. Contrary to our

expectations, we found that recruitment of ERRα to the vast majority of its target genes was not significantly reduced in the absence of BCL6 (Figure 2.13G). Surprisingly, there actually was increased recruitment to a binding site in an upstream *Ucp1* enhancer (Figure 2.13H). Thus, it remains unclear if and how BCL6 regulates the activity of ERRs in dormant BAT. Additional studies are necessary to conclusively answer these questions.

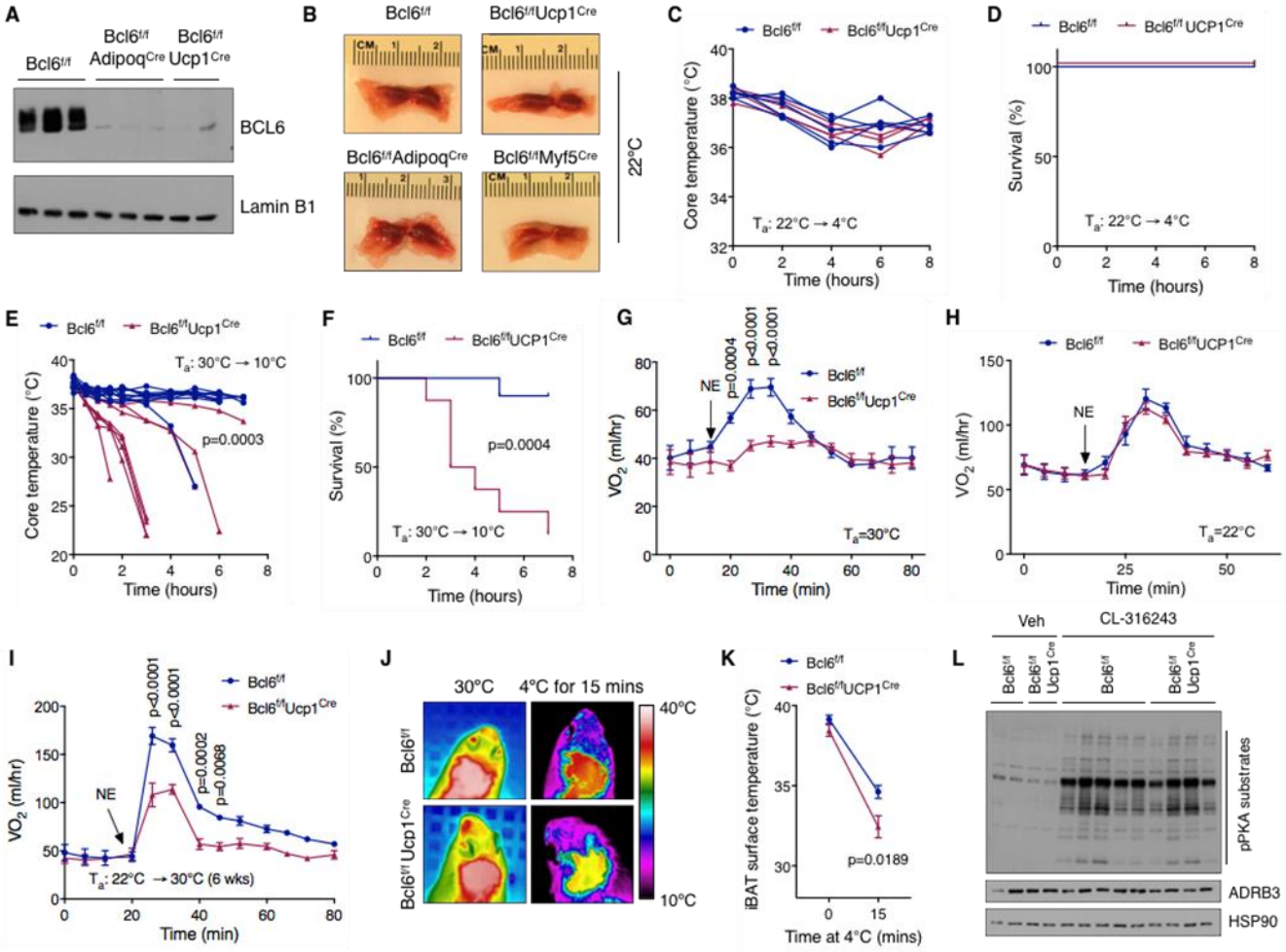
A
Bcl6f/f
Bcl6f/f AdipoqCre
Bcl6f/f Ucp1Cre
BCL6
Lamin B1
B
Bcl6f/f
Bcl6f/fUcp1Cre
Bcl6f/fAdipoqCre
Bcl6f/fMyf5Cre
22°C
C
Bcl6f/f
Bcl6f/fUcp1Cre
Core temperature (°C)
Ta: 22°C → 4°C
Time (hours)
D
Bcl6f/f
Bcl6f/f UCP1Cre
Survival (%)
Ta: 22°C → 4°C
Time (hours)
E
Bcl6f/f
Bcl6f/fUcp1Cre
Ta: 30°C → 10°C
p=0.0003
Core temperature (°C)
Time (hours)
F
Bcl6f/f
Bcl6f/fUCP1Cre
p=0.0004
Ta: 30°C → 10°C
Survival (%)
Time (hours)
G
NE
p=0.0004
p<0.0001
p<0.0001
Bcl6f/f
Bcl6f/fUcp1Cre
VO2 (ml/hr)
Ta=30°C
Time (min)
H
Bcl6f/f
Bcl6f/fUCP1Cre
NE
VO2 (ml/hr)
Ta=22°C
Time (min)
I
Bcl6f/f
Bcl6f/fUcp1Cre
p<0.0001
p<0.0001
p=0.0002
p=0.0068
NE
Ta: 22°C → 30°C (6 wks)
VO2 (ml/hr)
Time (min)
J
30°C
4°C for 15 mins
Bcl6f/f
Bcl6f/f Ucp1Cre
40°C
10°C
K
Bcl6f/f
Bcl6f/fUCP1Cre
iBAT surface temperature (°C)
p=0.0189
Time at 4°C (mins)
L
Veh
CL-316243
Bcl6f/f
Bcl6f/f Ucp1Cre
Bcl6f/f
Bcl6f/f Ucp1Cre
pPKA substrates
ADRB3
HSP90

Figure 2.1. BCL6 is required to maintain thermogenic capacity of dormant BAT.
(A) Immunoblotting for BCL6 and Lamin B1 protein in nuclear extracts of iBAT of *Bcl6*$^{f/f}$, *Bcl6*$^{f/f}$*Ucp1*^{Cre}, and *Bcl6*$^{f/f}$*Adipoq*^{Cre} mice (n=2-3 per genotype). (B) Gross morphology of iBAT isolated from *Bcl6*$^{f/f}$, *Bcl6*$^{f/f}$*Ucp1*^{Cre}, *Bcl6*$^{f/f}$*Adipoq*^{Cre}, and *Bcl6*$^{f/f}$*Myf5*^{Cre} mice bred and housed at 22ºC. (C, D) Core temperature measurements (C) and survival curves (D) of *Bcl6*$^{f/f}$ and *Bcl6*$^{f/f}$*Ucp1*^{Cre} female mice bred at 22ºC and subjected to 4ºC cold challenge (n=4-5 per genotype). (E, F) Core temperature measurements (E) and survival curves (F) of *Bcl6*$^{f/f}$ and *Bcl6*$^{f/f}$*Ucp1*^{Cre} female mice bred at 30ºC and subjected to 10ºC cold challenge (n=8-10 per genotype). The p-value for (E) were calculated using Mann-Whitney U test at the 3 hr timepoint. (G, H) Norepinephrine-stimulated changes in oxygen consumption rate (VO_2) in *Bcl6*$^{f/f}$ and *Bcl6*$^{f/f}$*Ucp1*^{Cre} female mice housed at 30ºC (G, n=6 per genotype) or 22ºC (H, n=4-6 per genotype). Arrow indicates the time of norepinephrine injection. (I) Norepinephrine-stimulated changes in oxygen consumption rate (VO_2) in *Bcl6*$^{f/f}$ and *Bcl6*$^{f/f}$*Ucp1*^{Cre} male mice initially housed at 22ºC (until 5 weeks of age) followed by housing at 30ºC for 6 weeks (n=3-5 per genotype). (J, K) Representative infrared images (J) and quantified thermographic measurements of interscapular surface temperature (K) for *Bcl6*$^{f/f}$ and *Bcl6*$^{f/f}$*Ucp1*^{Cre} male mice subjected to 4ºC cold challenge from 30ºC (n=5-6 per genotype). (L) Immunoblotting for phosphorylated PKA substrates, β3-adrenergic receptor (ADRB3), and HSP90 in whole cell extracts of iBAT of *Bcl6*$^{f/f}$ and *Bcl6*$^{f/f}$ *Ucp1*^{Cre} male mice that were housed at 30ºC and injected with CL-316,243 (1mg/kg) or vehicle (Veh) for 30 mins. Data are presented as mean ± SEM.

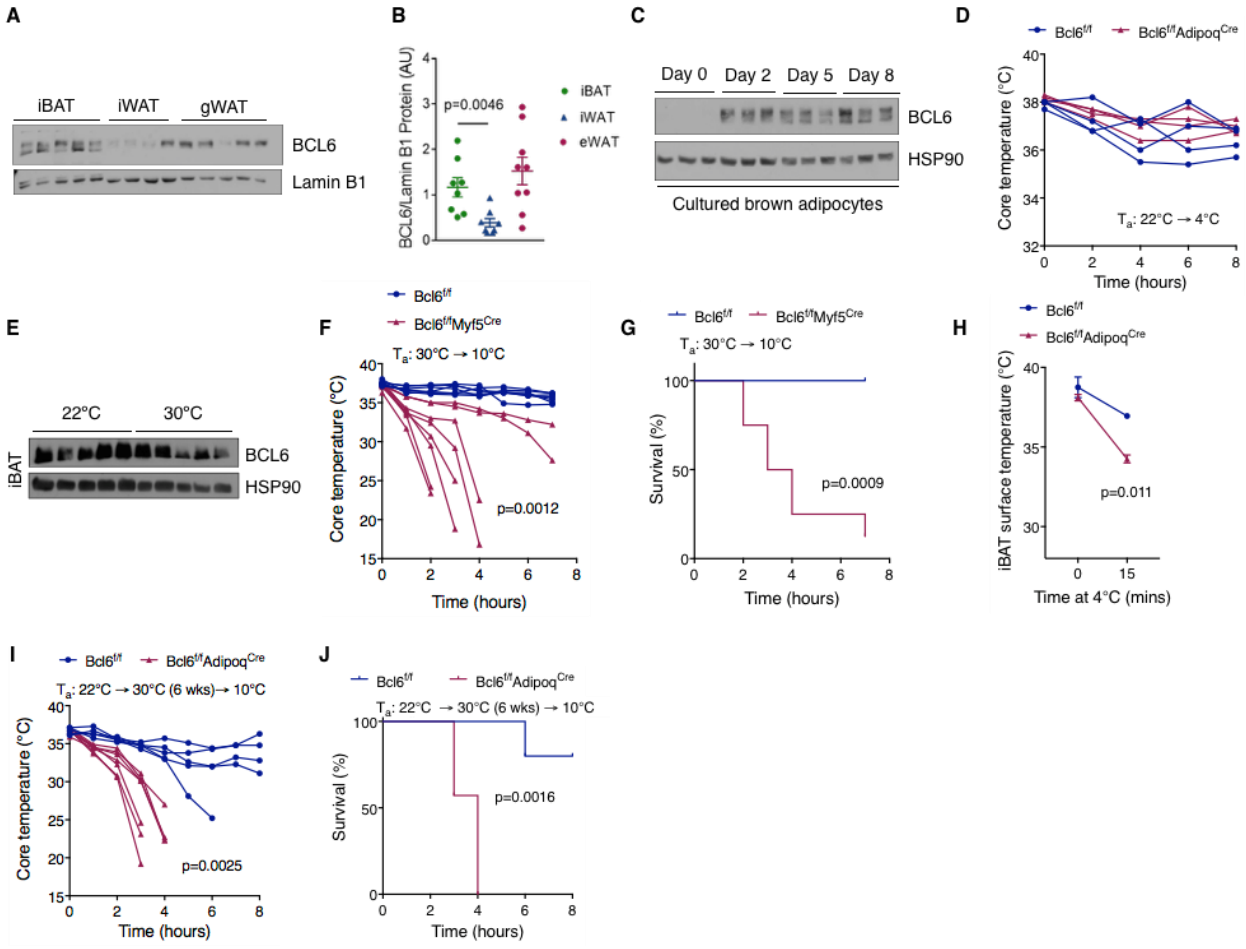
A
iBAT
iWAT
gWAT
BCL6
Lamin B1
B
BCL6/Lamin B1 Protein (AU)
p=0.0046
iBAT
iWAT
eWAT
C
Day 0
Day 2
Day 5
Day 8
BCL6
HSP90
Cultured brown adipocytes
D
Bcl6f/f
Bcl6f/fAdipoqCre
Core temperature (°C)
Ta: 22°C → 4°C
Time (hours)
E
22°C
30°C
iBAT
BCL6
HSP90
F
Bcl6f/f
Bcl6f/fMyf5Cre
Ta: 30°C → 10°C
Core temperature (°C)
p=0.0012
Time (hours)
G
Bcl6f/f
Bcl6f/fMyf5Cre
Ta: 30°C → 10°C
Survival (%)
p=0.0009
Time (hours)
H
Bcl6f/f
Bcl6f/fAdipoqCre
iBAT surface temperature (°C)
p=0.011
Time at 4°C (mins)
I
Bcl6f/f
Bcl6f/fAdipoqCre
Ta: 22°C → 30°C (6 wks)→ 10°C
Core temperature (°C)
p=0.0025
Time (hours)
J
Bcl6f/f
Bcl6f/fAdipoqCre
Ta: 22°C → 30°C (6 wks) → 10°C
Survival (%)
p=0.0016
Time (hours)

Figure 2.2. Characterization of BCL6 expression and function in brown adipocytes.
(A) Immunoblotting for BCL6 and Lamin B1 protein in nuclear extracts of interscapular brown adipose tissue (iBAT), inguinal white adipose tissue (iWAT), and gonadal white adipose tissue (gWAT) of C57BL/6J mice (n=4-5 per tissue). (B) Quantification of BCL6 protein band density (relative to Lamin B1 protein band density) in (A) and additional replicates (n=8 per tissue). Only the top BCL6 protein band was quantified. (C) Immunoblotting for BCL6 and HSP90 protein in whole cell extracts of cultured brown adipocytes at different time points after start of *in vitro* differentiation. (D) Core temperature measurements of 8-week-old $Bcl6^{f/f}$ and $Bcl6^{f/f}Adipoq^{Cre}$ female mice bred at 22ºC and subjected to 4ºC cold challenge (n=4 per genotype). (E) Immunoblotting for BCL6 and HSP90 in whole cell extracts of iBAT of 11-week old C57BL/6J mice housed at 22ºC or 30ºC for 6 weeks. (F, G) Core temperature measurements (F) and survival (G) of 8-week old female $Bcl6^{f/f}$ and $Bcl6^{f/f}Myf5^{Cre}$ bred at 30ºC and subjected to 10ºC cold challenge (n=7-8 per genotype). (H) Quantification of thermographic measurements of interscapular surface temperature for $Bcl6^{f/f}$ and $Bcl6^{f/f}Adipoq^{Cre}$ female mice subjected to 4ºC cold challenge from 30ºC (n=2 per genotype). (I, J) Core temperature measurements (I) and survival (J) of 11-week old male $Bcl6^{f/f}$ and $Bcl6^{f/f}Adipoq^{Cre}$ mice housed at 30°C for 6 weeks and subjected to 10ºC cold challenge (n=5-7 per genotype). The p-values for (F) and (I) were calculated using Mann-Whitney U test at the 3 hr timepoint. Data are presented as mean ± SEM.

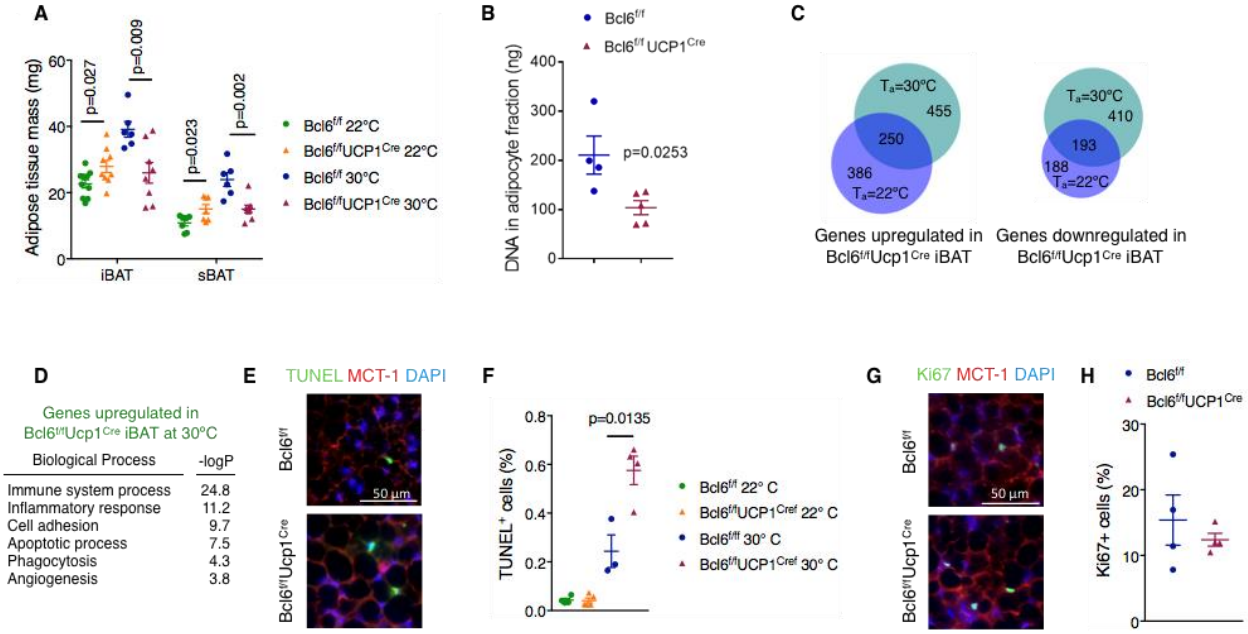
A
Adipose tissue mass (mg)
p=0.027
p=0.009
p=0.023
p=0.002
iBAT
sBAT
Bcl6f/f 22°C
Bcl6f/fUCP1Cre 22°C
Bcl6f/f 30°C
Bcl6f/fUCP1Cre 30°C
B
Bcl6f/f
Bcl6f/f UCP1Cre
DNA in adipocyte fraction (ng)
p=0.0253
C
Ta=30°C
455
250
386
Ta=22°C
Ta=30°C
410
193
188
Ta=22°C
Genes upregulated in Bcl6f/fUcp1Cre iBAT
Genes downregulated in Bcl6f/fUcp1Cre iBAT
D
Genes upregulated in Bcl6f/fUcp1Cre iBAT at 30°C
Biological Process | -logP
Immune system process | 24.8
Inflammatory response | 11.2
Cell adhesion | 9.7
Apoptotic process | 7.5
Phagocytosis | 4.3
Angiogenesis | 3.8
E
TUNEL MCT-1 DAPI
Bcl6f/f
Bcl6f/fUcp1Cre
50 µm
F
TUNEL+ cells (%)
p=0.0135
Bcl6f/f 22° C
Bcl6f/fUCP1Cref 22° C
Bcl6f/f 30° C
Bcl6f/fUCP1Cref 30° C
G
Ki67 MCT-1 DAPI
Bcl6f/f
Bcl6f/fUcp1Cre
50 µm
H
Bcl6f/f
Bcl6f/fUCP1Cre
Ki67+ cells (%)

Figure 2.3. BCL6 promotes survival of dormant brown adipocytes.
(A) BAT mass in 8-week-old *Bcl6*$^{f/f}$ and *Bcl6*$^{f/f}$*Ucp1*^{Cre} male mice bred at 22ºC or 30ºC (n=6-10 per genotype and condition). Interscapular BAT (iBAT), subscapular BAT (sBAT). (B) DNA content in adipocyte fraction of iBAT from *Bcl6*$^{f/f}$ and *Bcl6*$^{f/f}$*Ucp1*^{Cre} mice bred at 30ºC (n=4-5 per genotype). (C) Venn diagrams showing differentially expressed genes in iBAT of *Bcl6*$^{f/f}$*Ucp1*^{Cre} mice (fold change ≥1.5, adjusted P value <0.05). Genes upregulated (left) and downregulated (right) in iBAT of *Bcl6*$^{f/f}$*Ucp1*^{Cre} mice that were housed at different ambient temperatures. (D) Gene ontology enrichment analysis of upregulated genes in iBAT of *Bcl6*$^{f/f}$*Ucp1*^{Cre} mice housed at 30ºC. Enriched biological processes and corresponding P values are shown. (E) Terminal deoxynucleotidyl transferase dUTP nick end labeling (TUNEL, green), immunofluorescent staining for MCT-1 (red), and nuclear staining with DAPI (blue) in representative iBAT sections from *Bcl6*$^{f/f}$ and *Bcl6*$^{f/f}$*Ucp1*^{Cre} mice housed at 30ºC for 1 week. (F) Quantification of TUNEL^{+} apoptotic cells in iBAT of *Bcl6*$^{f/f}$ and *Bcl6*$^{f/f}$*Ucp1*^{Cre} male mice housed at 22ºC or 30ºC for 1 week (n=3-5 per genotype). (G) Immunofluorescent staining for Ki67 (green) and MCT-1 (red), and nuclear staining with DAPI (blue) in representative iBAT sections from *Bcl6*$^{f/f}$ and *Bcl6*$^{f/f}$*Ucp1*^{Cre} mice housed at 30ºC for 1 week. (H) Quantification of Ki67+ proliferating cells in iBAT of *Bcl6*$^{f/f}$ and *Bcl6*$^{f/f}$*Ucp1*^{Cre} mice housed at 30ºC for 1 week (n=4 per genotype). Data are presented as mean ± SEM.

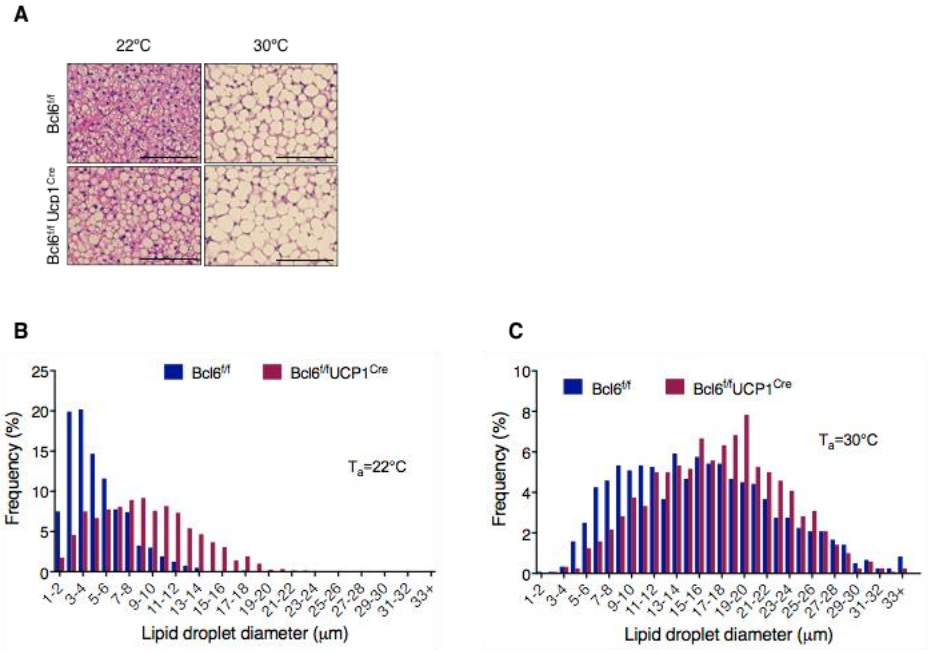
A
22°C
30°C
Bcl6f/f
Bcl6f/f Ucp1Cre
B
Bcl6f/f
Bcl6f/fUCP1Cre
Ta=22°C
Frequency (%)
Lipid droplet diameter (μm)
C
Bcl6f/f
Bcl6f/fUCP1Cre
Ta=30°C
Frequency (%)
Lipid droplet diameter (μm)

Figure 2.4. BCL6 regulates lipid metabolism in brown adipocytes.
(A) Hematoxylin and eosin staining of representative iBAT sections from *Bcl6*$^{f/f}$*Ucp1*^{Cre} mice bred and housed at 22ºC or 30ºC. Scale bar is 100 μm. (B, C) Quantification of lipid droplet diameter in brown adipocytes of *Bcl6*$^{f/f}$ and *Bcl6*$^{f/f}$*Ucp1*^{Cre} mice bred and housed at 22ºC (B) or 30ºC (C).

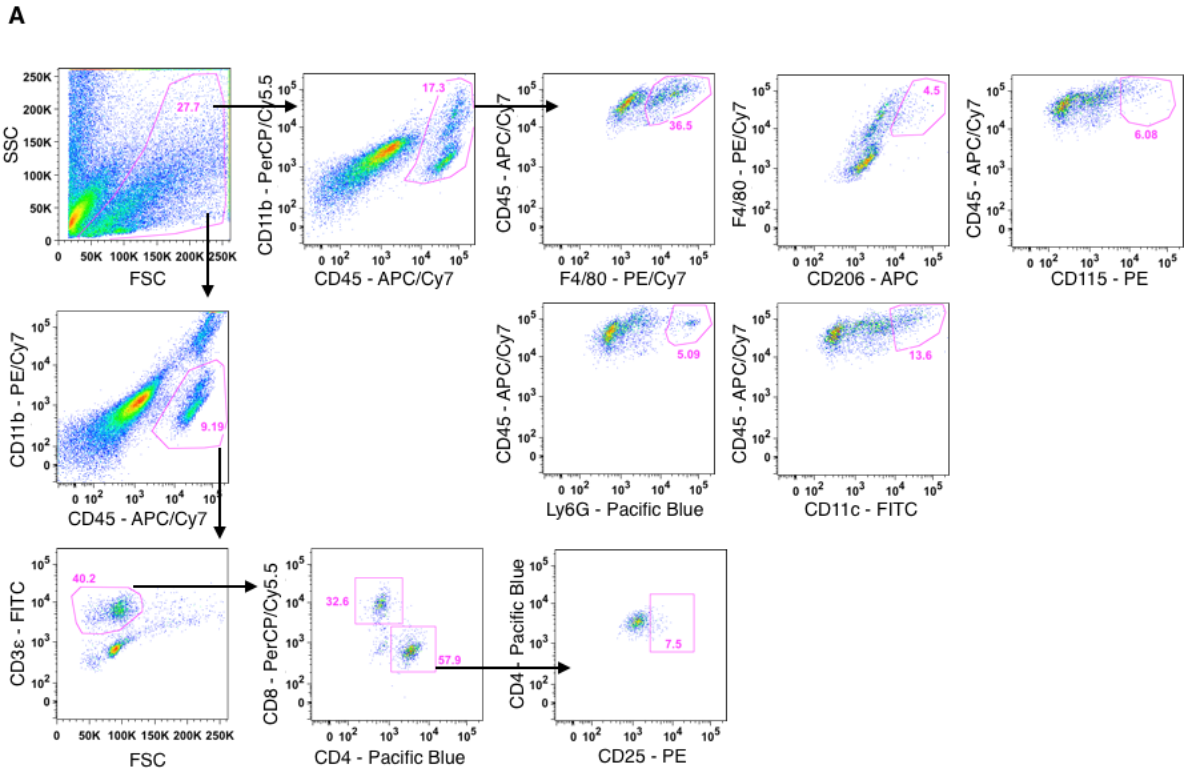
A
SSC
FSC
27.7
CD11b - PerCP/Cy5.5
CD45 - APC/Cy7
17.3
CD45 - APC/Cy7
F4/80 - PE/Cy7
36.5
F4/80 - PE/Cy7
CD206 - APC
4.5
CD45 - APC/Cy7
CD115 - PE
6.08
CD11b - PE/Cy7
CD45 - APC/Cy7
9.19
CD45 - APC/Cy7
Ly6G - Pacific Blue
5.09
CD45 - APC/Cy7
CD11c - FITC
13.6
CD3ε - FITC
FSC
40.2
CD8 - PerCP/Cy5.5
CD4 - Pacific Blue
32.6
57.9
CD4 - Pacific Blue
CD25 - PE
7.5

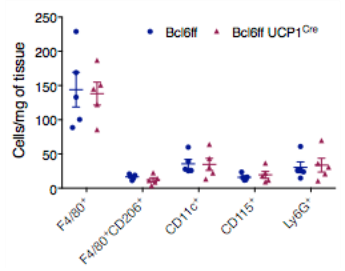
B
Bcl6ff
Bcl6ff UCP1Cre
Cells/mg of tissue
F4/80+
F4/80+CD206+
CD11c+
CD115+
Ly6G+

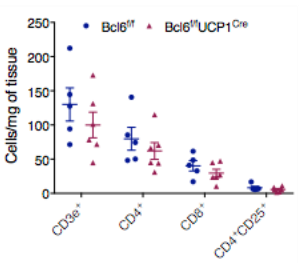
C
Bcl6f/f
Bcl6f/fUCP1Cre
Cells/mg of tissue
CD3ε+
CD4+
CD8+
CD4+CD25+

Figure 2.5. Loss of BCL6 does not alter immune cell infiltration in brown adipose tissue. (A) Gating strategy for flow cytometric quantification of myeloid and lymphoid cell subsets in iBAT of *Bcl6*$^{f/f}$ and *Bcl6*$^{f/f}$*Ucp1*^{Cre} mice housed at 30ºC. (B, C) Quantification of myeloid (B) and lymphoid (C) cell density in iBAT of *Bcl6*$^{f/f}$ and *Bcl6*$^{f/f}$*Ucp1*^{Cre} mice housed at 30ºC (n=5-6 per genotype). Data are presented as mean ± SEM.

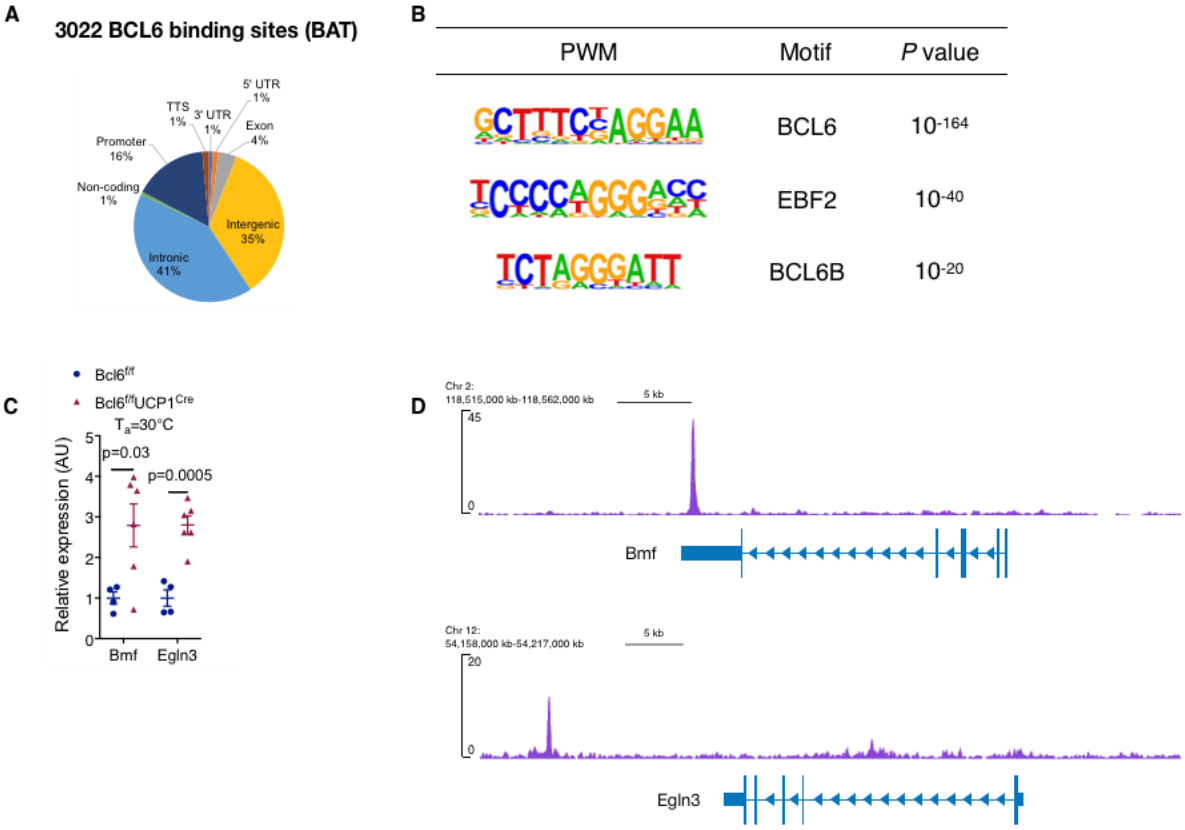
A
3022 BCL6 binding sites (BAT)
5' UTR 1%
TTS 1%
3' UTR 1%
Exon 4%
Promoter 16%
Non-coding 1%
Intergenic 35%
Intronic 41%
B
PWM
Motif
P value
BCL6
10-164
EBF2
10-40
BCL6B
10-20
C
Bcl6f/f
Bcl6f/fUCP1Cre
Ta=30°C
p=0.03
p=0.0005
Relative expression (AU)
Bmf
Egln3
D
Chr 2:
118,515,000 kb-118,562,000 kb
5 kb
45
0
Bmf
Chr 12:
54,158,000 kb-54,217,000 kb
5 kb
20
0
Egln3

Figure 2.6. Analysis of BCL6 cistrome in brown adipose tissue and identification of *Bcl6* binding sites near *Bmf* and *Egln3.*
(A) Pie chart showing the distribution of BCL6 binding sites across the genome of brown adipocytes from mice housed at 30ºC. (B) De novo sequence motif discovery within BCL6 ChIP-seq peaks in brown adipocytes; position weight matrix (PWM). (C) Quantitative RT-PCR measurement of *Bmf* and *Egln3* mRNAs in iBAT of $Bcl6^{f/f}$ and $Bcl6^{f/f}Ucp1^{Cre}$ mice housed at 30ºC (n=4-6 per genotype). (D) Genome browser tracks showing BCL6 binding sites near pro-apoptotic genes *Bmf* and *Egln3*. Data are presented as mean ± SEM.

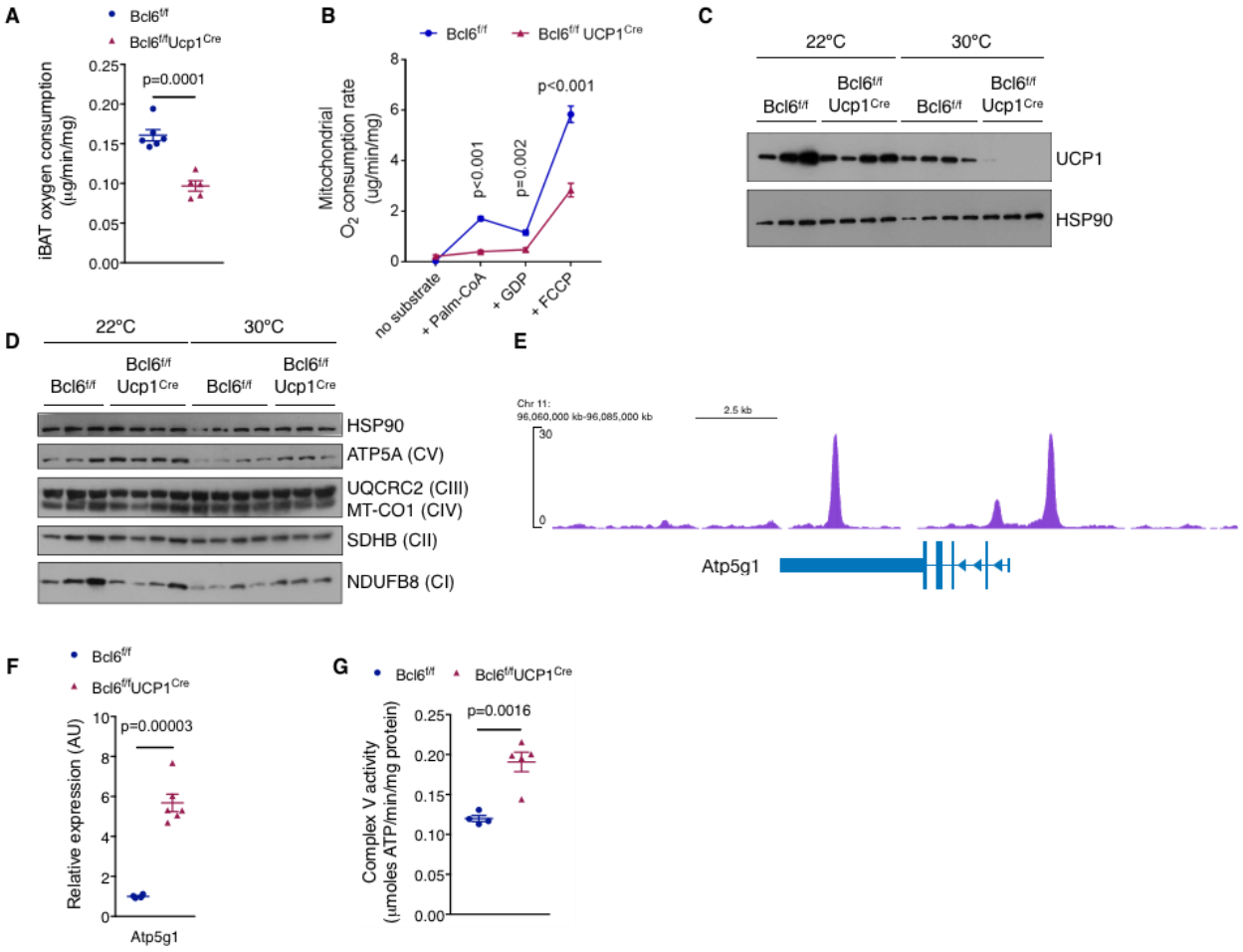
A
Bcl6f/f
Bcl6f/fUcp1Cre
iBAT oxygen consumption (µg/min/mg)
p=0.0001
B
Bcl6f/f
Bcl6f/f UCP1Cre
Mitochondrial O2 consumption rate (ug/min/mg)
p<0.001
p<0.001
p=0.002
no substrate
+ Palm-CoA
+ GDP
+ FCCP
C
22°C
30°C
Bcl6f/f
Bcl6f/f Ucp1Cre
UCP1
HSP90
D
HSP90
ATP5A (CV)
UQCRC2 (CIII)
MT-CO1 (CIV)
SDHB (CII)
NDUFB8 (CI)
E
Chr 11: 96,060,000 kb-96,085,000 kb
2.5 kb
Atp5g1
F
Relative expression (AU)
p=0.00003
Atp5g1
G
Complex V activity (µmoles ATP/min/mg protein)
p=0.0016

Figure 2.7 BCL6 maintains uncoupled respiration in dormant BAT.
(A) Oxygen consumption rate of iBAT isolated from *Bcl6*$^{f/f}$ and *Bcl6*$^{f/f}$*Ucp1*^{Cre} mice housed at 30ºC and exposed to 4ºC for 15 mins (n=5-6 per genotype). (B) Oxygen consumption rate of mitochondria isolated from iBAT of *Bcl6*$^{f/f}$ and *Bcl6*$^{f/f}$*Ucp1*^{Cre} mice housed at 30ºC. Rates are reported before and after addition of palmitoyl-CoA, guanosine diphosphate (GDP), and carbonyl cyanide-4-(trifluoromethoxy) phenylhydrazone (FCCP) (C) Immunoblotting for UCP1 and HSP90 in whole cell extracts of iBAT of male 8-week-old mice housed at 22ºC or 30ºC (n=3-4 per genotype and temperature). (D) Immunoblotting for subunits of mitochondrial complexes I-V and HSP90 in iBAT of *Bcl6*$^{f/f}$ and *Bcl6*$^{f/f}$*Ucp1*^{Cre} mice housed at 22ºC or 30ºC (n=3-4 per genotype and temperature). (E) Genome browser track showing BCL6 binding near the promoter of the *Atp5g1* gene. (F) Quantitative RT-PCR measurement of *Atp5g1* mRNA in iBAT of *Bcl6*$^{f/f}$ and *Bcl6*$^{f/f}$*Ucp1*^{Cre} mice housed at 30ºC (n=4-6 per genotype). (G) ATP synthase activity in mitochondria isolated from iBAT of *Bcl6*$^{f/f}$ and *Bcl6*$^{f/f}$*Ucp1*^{Cre} mice housed at 30ºC (n=4-5 per genotype). Data are presented as mean ± SEM.

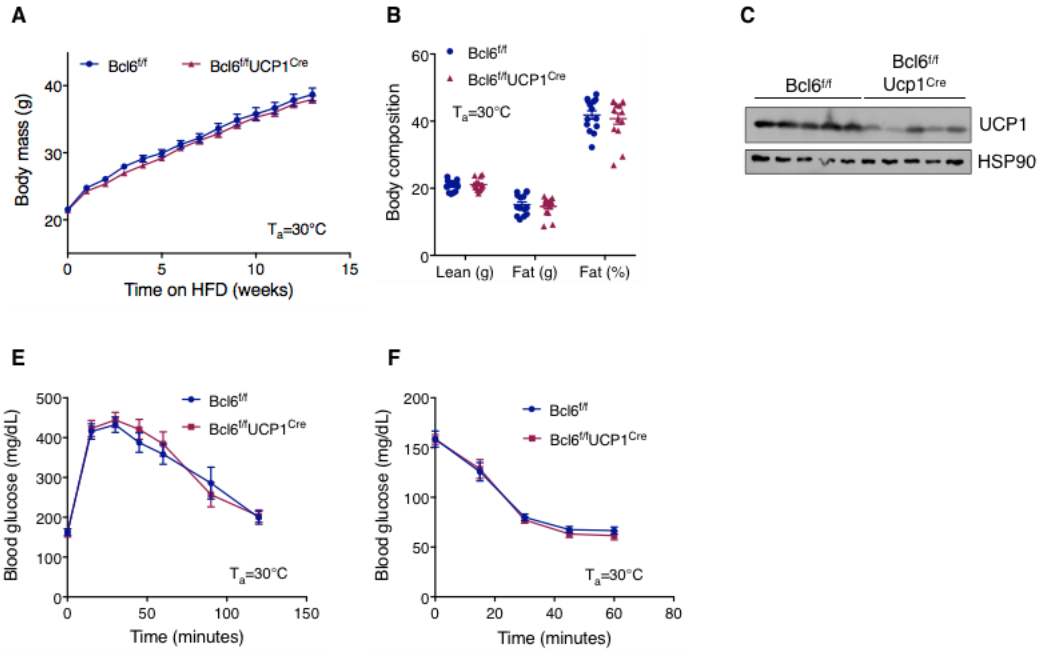
A
Bcl6f/f
Bcl6f/fUCP1Cre
Body mass (g)
Ta=30°C
Time on HFD (weeks)
B
Bcl6f/f
Bcl6f/fUCP1Cre
Ta=30°C
Body composition
Lean (g)
Fat (g)
Fat (%)
C
Bcl6f/f
Bcl6f/f
Ucp1Cre
UCP1
HSP90
E
Bcl6f/f
Bcl6f/fUCP1Cre
Blood glucose (mg/dL)
Ta=30°C
Time (minutes)
F
Bcl6f/f
Bcl6f/fUCP1Cre
Blood glucose (mg/dL)
Ta=30°C
Time (minutes)

Figure 2.8. BCL6 is not required for diet-induced thermogenesis in BAT.
(A) Body mass of male *Bcl6*$^{f/f}$ and *Bcl6*$^{f/f}$*Ucp1*^{Cre} mice fed high fat diet at 30ºC starting at the age of 10 weeks (n=13 per genotype, data pooled from multiple experiments). (B) Body composition analysis by Dual X-ray Absorptiometry of male *Bcl6*$^{f/f}$ and *Bcl6*$^{f/f}$*Ucp1*^{Cre} mice fed high fat diet at 30ºC (n=14 per genotype, data pooled from multiple experiments). (C) Immunoblotting for UCP1 and HSP90 in whole cell extracts of iBAT from male *Bcl6*$^{f/f}$, *Bcl6*$^{f/f}$*Ucp1*^{Cre}, and *Bcl6*$^{f/f}$*Adipoq*^{Cre} mice fed high fat diet at 30ºC (n=4-5 per genotype). (D, E) Glucose (D) and insulin (E) tolerance tests in male *Bcl6*$^{f/f}$ and *Bcl6*$^{f/f}$*Ucp1*^{Cre} mice fed high fat diet at 30ºC (n=14-15 per genotype, data pooled from multiple experiments). Data are presented as mean ± SEM.

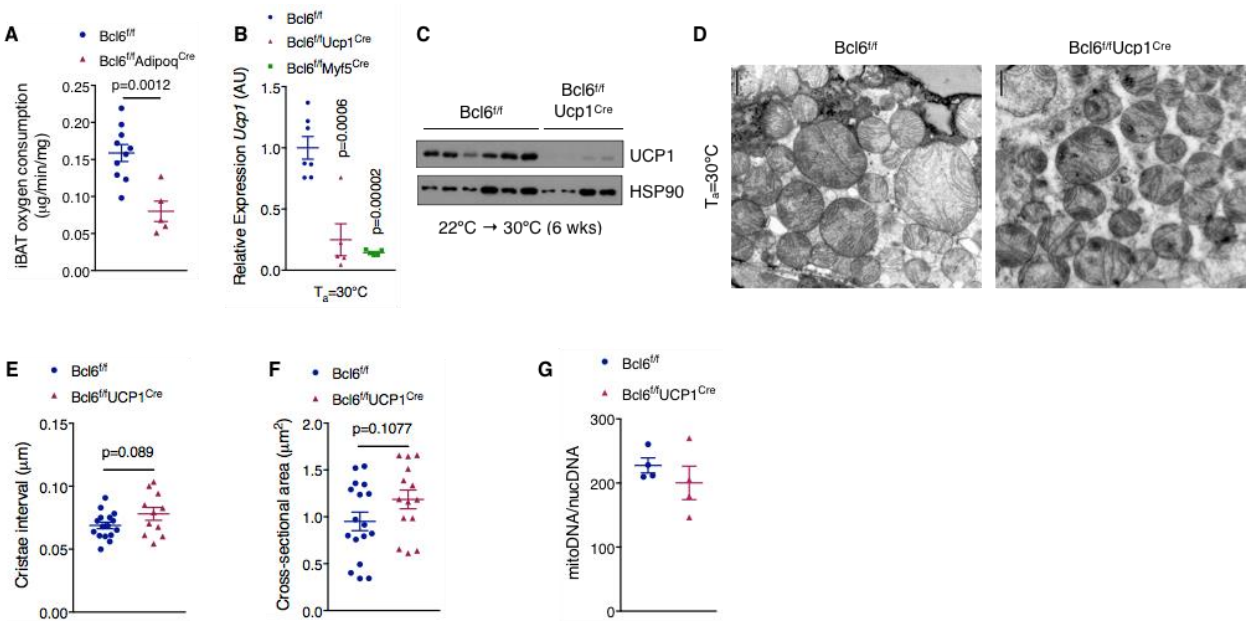
A
Bcl6f/f
Bcl6f/fAdipoqCre
p=0.0012
iBAT oxygen consumption (µg/min/mg)
B
Bcl6f/f
Bcl6f/fUcp1Cre
Bcl6f/fMyf5Cre
Relative Expression Ucp1 (AU)
p=0.0006
p=0.00002
Ta=30°C
C
Bcl6f/f
Bcl6f/f Ucp1Cre
UCP1
HSP90
22°C → 30°C (6 wks)
D
Bcl6f/f
Bcl6f/fUcp1Cre
Ta=30°C
E
Bcl6f/f
Bcl6f/fUCP1Cre
p=0.089
Cristae interval (µm)
F
Bcl6f/f
Bcl6f/fUCP1Cre
p=0.1077
Cross-sectional area (µm2)
G
Bcl6f/f
Bcl6f/fUCP1Cre
mitoDNA/nucDNA

Figure 2.9. BCL6 regulates mitochondrial uncoupled respiration in dormant brown adipocytes.
(A) Oxygen consumption rate of iBAT isolated from *Bcl6*$^{f/f}$ and *Bcl6*$^{f/f}$*Adipoq*^{Cre} female mice subjected to 15 minutes of 4ºC cold challenge from 30ºC (n=5-10 per genotype). (B) Quantitative RT-PCR measurement of *Ucp1* mRNA in iBAT of *Bcl6*$^{f/f}$, *Bcl6*$^{f/f}$*Ucp1*^{Cre}, and *Bcl6*$^{f/f}$*Myf5*^{Cre} male mice bred and housed at 30ºC (n=5-7 per genotype). (C) Immunoblotting for UCP1 and HSP90 in whole cell extracts of iBAT from female *Bcl6*$^{f/f}$ and *Bcl6*$^{f/f}$*Ucp1*^{Cre} mice bred at 22ºC and then housed at 30ºC for 6 weeks (n=4-6 per genotype). (D) Representative transmission electron microscopy images of iBAT from *Bcl6*$^{f/f}$ and *Bcl6*$^{f/f}$*Ucp1*^{Cre} mice housed at 30ºC. (E, F) Quantification of cristae interval (E) and cross-sectional area (F) in brown adipocyte mitochondria using representative transmission electron microscopy images taken of iBAT from *Bcl6*$^{f/f}$ and *Bcl6*$^{f/f}$*Ucp1*^{Cre} mice housed at 30ºC. (G) Measurement of mitochondrial DNA (mitoDNA) and nuclear DNA (nucDNA) ratio by quantitative PCR in iBAT isolated from *Bcl6*$^{f/f}$ and *Bcl6*$^{f/f}$*Ucp1*^{Cre} mice housed at 30ºC for 8 weeks (n=4 per genotype). Data are presented as mean ± SEM.

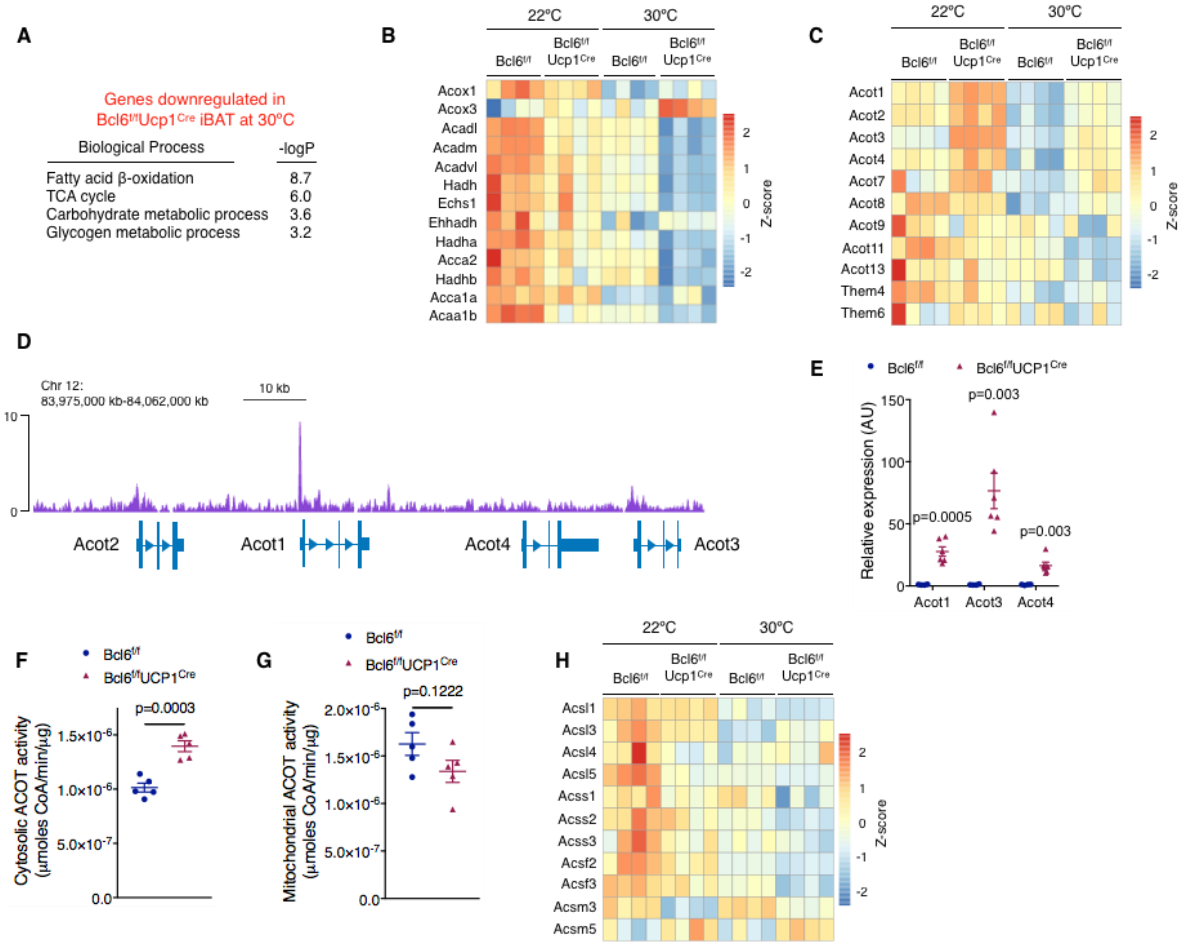
A
Genes downregulated in Bcl6f/fUcp1Cre iBAT at 30°C
Biological Process
-logP
Fatty acid β-oxidation 8.7
TCA cycle 6.0
Carbohydrate metabolic process 3.6
Glycogen metabolic process 3.2
B
22°C
30°C
Bcl6f/f
Bcl6f/f Ucp1Cre
Acox1
Acox3
Acadl
Acadm
Acadvl
Hadh
Echs1
Ehhadh
Hadha
Acca2
Hadhb
Acca1a
Acaa1b
Z-score
C
Acot1
Acot2
Acot3
Acot4
Acot7
Acot8
Acot9
Acot11
Acot13
Them4
Them6
D
Chr 12:
83,975,000 kb-84,062,000 kb
10 kb
Acot2
Acot1
Acot4
Acot3
E
Bcl6f/f
Bcl6f/fUCP1Cre
Relative expression (AU)
p=0.0005
p=0.003
p=0.003
Acot1
Acot3
Acot4
F
Cytosolic ACOT activity (μmoles CoA/min/μg)
p=0.0003
G
Mitochondrial ACOT activity (μmoles CoA/min/μg)
p=0.1222
H
Acsl1
Acsl3
Acsl4
Acsl5
Acss1
Acss2
Acss3
Acsf2
Acsf3
Acsm3
Acsm5

Figure 2.10. BCL6 regulates fatty acid metabolism in dormant BAT.
(A) Gene ontology enrichment analysis and corresponding P values for the downregulated genes in iBAT of *Bcl6*$^{f/f}$*Ucp1*^{Cre} mice housed at 30ºC. (B, C) Heatmaps showing expression of genes involved in β-oxidation of fatty acids (B) and acyl-CoA thioesterase (ACOT) genes (C) in iBAT of *Bcl6*$^{f/f}$ and *Bcl6*$^{f/f}$*Ucp1*^{Cre} mice housed at 22ºC and 30ºC (n=4 per genotype and temperature). (D) Genome browser track showing BCL6 binding site near the promoter of *Acot1* gene. (E) Quantitative RT-PCR measurement of *Acot1*, *Acot3*, and *Acot4* mRNAs in iBAT of *Bcl6*$^{f/f}$ and *Bcl6*$^{f/f}$*Ucp1*^{Cre} mice housed at 30ºC (n=4-6 per genotype). (F, G) Measurement of ACOT activity in cytosolic (F) and mitochondrial (G) fractions of isolated iBAT of *Bcl6*$^{f/f}$ and *Bcl6*$^{f/f}$*Ucp1*^{Cre} mice housed at 30ºC (n=5 per genotype). ACOT activity is expressed as micromoles of CoA produced per minute per microgram of protein. (H) Heatmap showing expression of acyl-CoA synthetase (ACSL) genes in iBAT of *Bcl6*$^{f/f}$ and *Bcl6*$^{f/f}$*Ucp1*^{Cre} mice housed at 22ºC and 30ºC (n=4 per genotype and temperature). Data are presented as mean ± SEM.

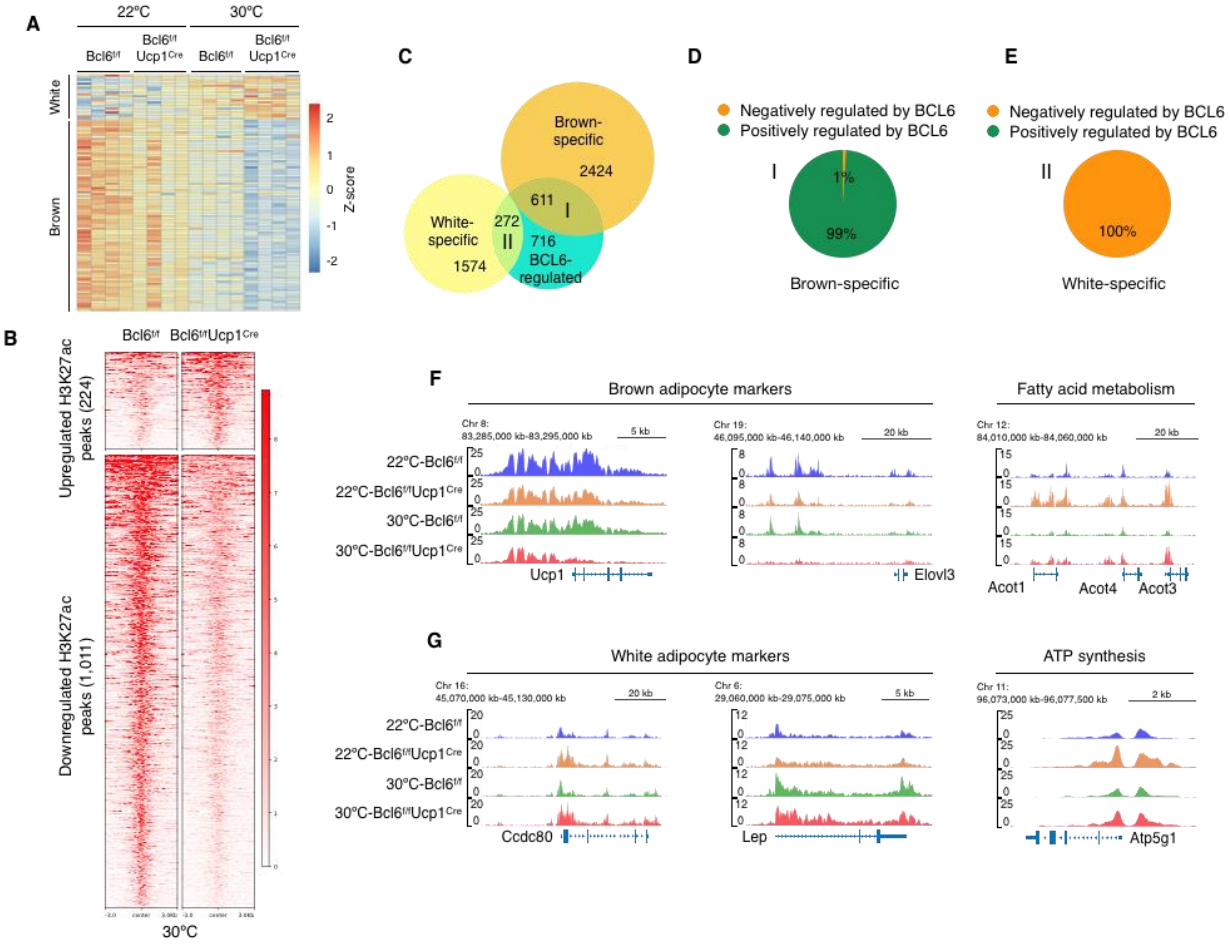
A
22°C
30°C
Bcl6f/f
Bcl6f/f Ucp1Cre
White
Brown
Z-score
B
Bcl6f/f
Bcl6f/fUcp1Cre
Upregulated H3K27ac peaks (224)
Downregulated H3K27ac peaks (1,011)
30°C
C
Brown-specific
2424
611
I
White-specific
1574
272
II
716
BCL6-regulated
D
Negatively regulated by BCL6
Positively regulated by BCL6
I
1%
99%
Brown-specific
E
Negatively regulated by BCL6
Positively regulated by BCL6
II
100%
White-specific
F
Brown adipocyte markers
Fatty acid metabolism
22°C-Bcl6f/f
22°C-Bcl6f/fUcp1Cre
30°C-Bcl6f/f
30°C-Bcl6f/fUcp1Cre
Ucp1
Elovl3
Acot1
Acot4
Acot3
G
White adipocyte markers
ATP synthesis
Ccdc80
Lep
Atp5g1

Figure 2.11. BCL6 reinforces brown and opposes white adipocyte-specific enhancers to maintain cellular identity.
(A) Heatmap of nuclear encoded brown and white adipocyte-specific genes (BATLAS) in iBAT of *Bcl6*$^{f/f}$ and *Bcl6*$^{f/f}$*Ucp1*^{Cre} mice at 22°C and 30°C. List of genes provided in Table 2.4. (B) Heatmaps showing H3K27ac peaks that are upregulated or downregulated in iBAT of *Bcl6*$^{f/f}$*Ucp1*^{Cre} mice housed at 30°C. H3K27ac peaks in heatmaps represent an average of three biological replicates and the amplitude of each peak center (±3 kb) is represented in color as indicated. (C) Venn diagram showing the overlap of BCL6-regulated enhancers at 30°C with brown and white adipocyte-specific enhancers. The numbers indicate the number of enhancers in each field. (D, E) Pie charts showing the % of BCL6-regulated brown (D) and white (E) adipocyte-specific enhancers that are positively or negatively regulated by BCL6 at 30°C. (F, G) Representative H3K27ac genome browser tracks for brown adipocyte-specific genes *Ucp1* and *Elovl3* (F), fatty acid metabolism genes *Acot1*, *Acot3*, and *Acot4* (F), white adipocyte-specific genes *Ccdc80* and *Lep* (G), and ATP synthesis gene *Atp5g1* (G). The effects of temperature and BCL6 are highlighted for each category. Data are presented as mean ± SEM.

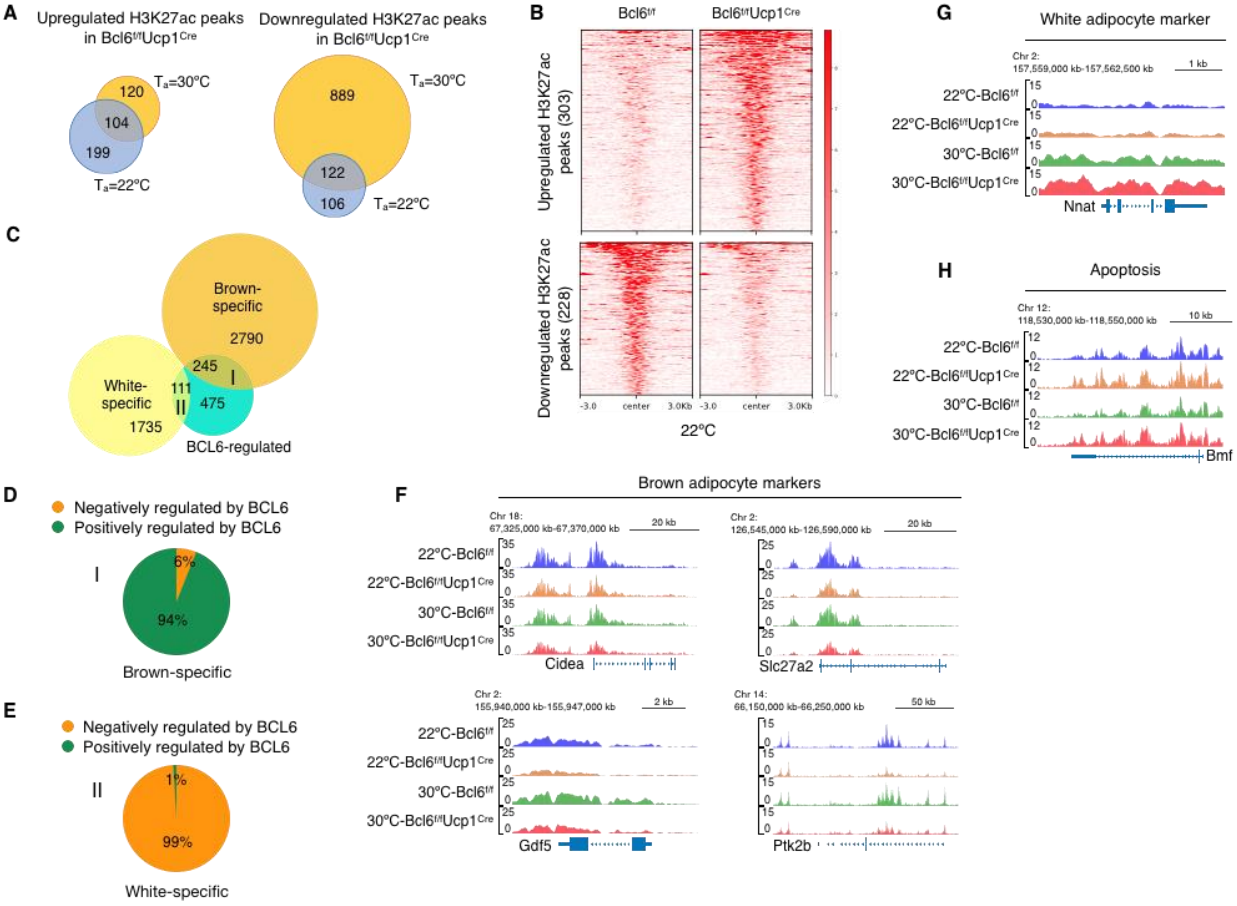
A
Upregulated H3K27ac peaks in Bcl6f/fUcp1Cre
120
104
199
Ta=30°C
Ta=22°C
Downregulated H3K27ac peaks in Bcl6f/fUcp1Cre
889
122
106
Ta=30°C
Ta=22°C
B
Bcl6f/f
Bcl6f/fUcp1Cre
Upregulated H3K27ac peaks (303)
Downregulated H3K27ac peaks (228)
-3.0
center
3.0Kb
22°C
C
Brown-specific
2790
245
I
White-specific
1735
111
II
475
BCL6-regulated
D
Negatively regulated by BCL6
Positively regulated by BCL6
I
6%
94%
Brown-specific
E
Negatively regulated by BCL6
Positively regulated by BCL6
II
1%
99%
White-specific
F
Brown adipocyte markers
Chr 18: 67,325,000 kb-67,370,000 kb
20 kb
22°C-Bcl6f/f
22°C-Bcl6f/fUcp1Cre
30°C-Bcl6f/f
30°C-Bcl6f/fUcp1Cre
Cidea
Chr 2: 126,545,000 kb-126,590,000 kb
20 kb
Slc27a2
Chr 2: 155,940,000 kb-155,947,000 kb
2 kb
Gdf5
Chr 14: 66,150,000 kb-66,250,000 kb
50 kb
Ptk2b
G
White adipocyte marker
Chr 2: 157,559,000 kb-157,562,500 kb
1 kb
22°C-Bcl6f/f
22°C-Bcl6f/fUcp1Cre
30°C-Bcl6f/f
30°C-Bcl6f/fUcp1Cre
Nnat
H
Apoptosis
Chr 12: 118,530,000 kb-118,550,000 kb
10 kb
22°C-Bcl6f/f
22°C-Bcl6f/fUcp1Cre
30°C-Bcl6f/f
30°C-Bcl6f/fUcp1Cre
Bmf

Figure 2.12. BCL6 reinforces brown and opposes white adipocyte-specific enhancers to maintain cellular identity (continued).
(A) Venn diagrams showing how ambient temperature modulates upregulated and downregulated H3K27ac peaks in iBAT of *Bcl6*$^{f/f}$*Ucp1*^{Cre} mice. (B) Heatmaps showing H3K27ac peaks that are upregulated and downregulated in iBAT of *Bcl6*$^{f/f}$*Ucp1*^{Cre} mice housed at 22°C. H3K27ac peaks in heatmaps represent an average of three biological replicates and the amplitude of each peak center (±3 kb) is represented in color as indicated. (C) Venn diagram showing the overlap of BCL6-regulated enhancers at 22°C with brown and white adipocyte-specific enhancers. The numbers indicate the number of enhancers in each field. (D, E) Pie charts showing the % of BCL6-regulated brown (D) and white (E) adipocyte-specific enhancers that are positively or negatively regulated by BCL6 at 22°C. (F) Genome browser tracks showing H3K27ac abundance at representative brown adipocyte-specific genes *Cidea*, *Slc27a2*, *Gdf5*, and *Ptk2b*. The effects of temperature and BCL6 are highlighted for each category. (G, H) Genome browser tracks showing H3K27ac abundance at representative white adipocyte-specific gene *Nnat* (G) and apoptosis promoting gene *Bmf* (H). The effects of temperature and BCL6 are highlighted for each category.

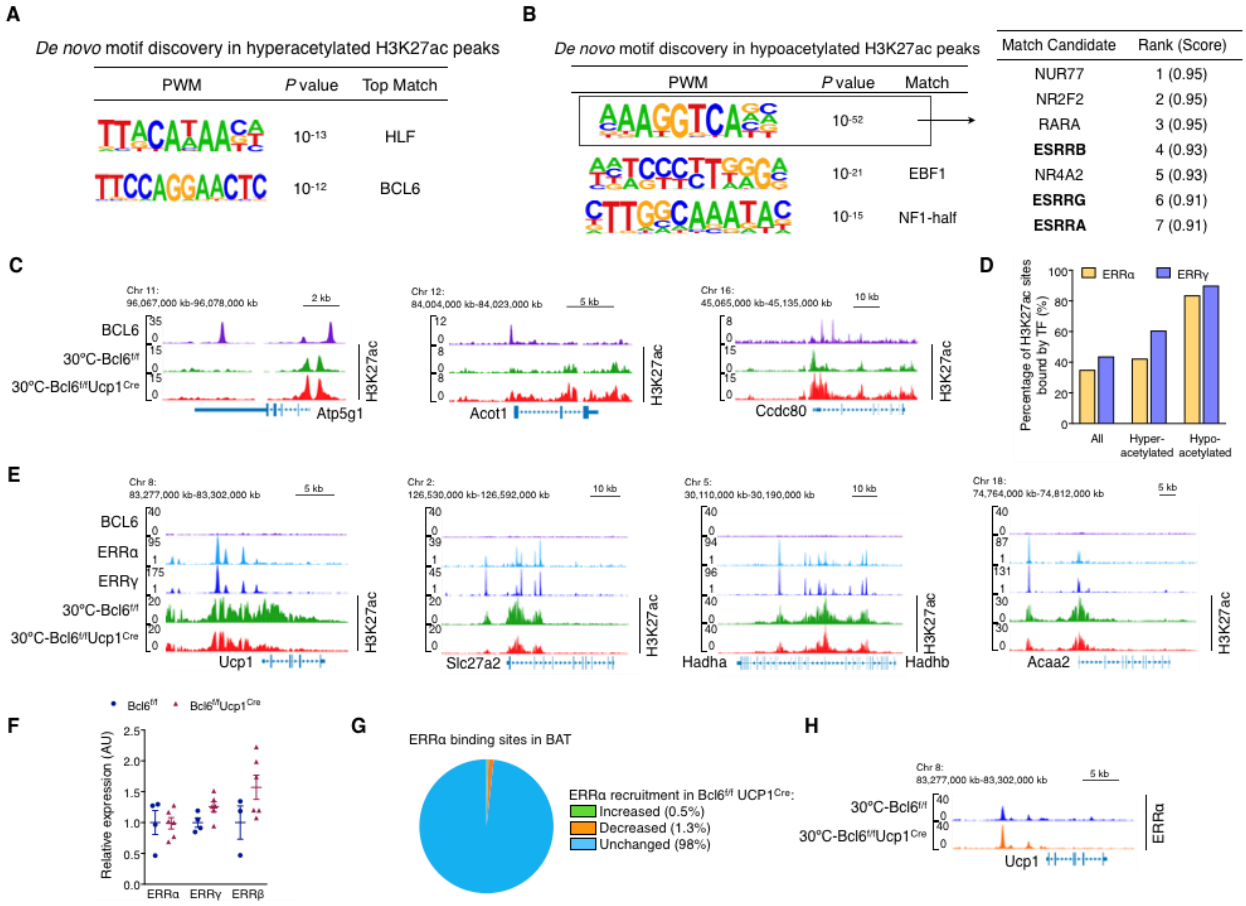
A
De novo motif discovery in hyperacetylated H3K27ac peaks
PWM
P value
Top Match
10-13
HLF
10-12
BCL6
B
De novo motif discovery in hypoacetylated H3K27ac peaks
PWM
P value
Match
10-52
10-21
EBF1
10-15
NF1-half
Match Candidate
Rank (Score)
NUR77
1 (0.95)
NR2F2
2 (0.95)
RARA
3 (0.95)
ESRRB
4 (0.93)
NR4A2
5 (0.93)
ESRRG
6 (0.91)
ESRRA
7 (0.91)
C
BCL6
30°C-Bcl6f/f
30°C-Bcl6f/fUcp1Cre
H3K27ac
Atp5g1
Acot1
Ccdc80
D
ERRα
ERRγ
Percentage of H3K27ac sites bound by TF (%)
All
Hyper-acetylated
Hypo-acetylated
E
BCL6
ERRα
ERRγ
30°C-Bcl6f/f
30°C-Bcl6f/fUcp1Cre
H3K27ac
Ucp1
Slc27a2
Hadha
Hadhb
Acaa2
F
Bcl6f/f
Bcl6f/fUcp1Cre
Relative expression (AU)
ERRα
ERRγ
ERRβ
G
ERRα binding sites in BAT
ERRα recruitment in Bcl6f/f UCP1Cre:
Increased (0.5%)
Decreased (1.3%)
Unchanged (98%)
H
30°C-Bcl6f/f
30°C-Bcl6f/fUcp1Cre
ERRα
Ucp1

Figure 2.13. BCL6 regulates brown adipocyte enhancers by direct and indirect mechanisms.

(A, B) *De novo* sequence motif discovery at hyperacetylated (A) and hypoacetylated (B) H3K27 sites in iBAT of *Bcl6*$^{f/f}$*Ucp1*^{Cre} mice housed at 30°C; position weight matrix (PWM). For the top enriched motif in (B), a list of the top 7 matches from a database of known transcription factor binding site motifs and corresponding match scores are listed. (C) Genome browser tracks for visualization of the *Atp5g1*, *Acot1*, and *Ccdc80* loci highlighting BCL6 and H3K27ac ChIP-Seq data. (D) Percentage of H3K27 acetylation sites in iBAT (all sites, or only sites that are hyperacetylated or hypoacetylated in *Bcl6*$^{f/f}$*Ucp1*^{Cre} mice at 30°C) that are bound by ERRγ or ERRα. (E) Genome browser tracks for visualization of the *Ucp1*, *Slc27a2*, *Hadha*, *Hadhb*, and *Acaa2* loci highlighting BCL6, ERRα, ERRγ, and H3K27ac ChIP-Seq data. (F) Quantitative RT-PCR measurement of *Esrra*, *Esrrg*, and *Esrrb* mRNA in iBAT of *Bcl6*$^{f/f}$ and *Bcl6*$^{f/f}$*Ucp1*^{Cre} mice housed at 30°C (n=4-6 per genotype). (G) ChIP-seq analysis of ERRα recruitment to binding sites in iBAT of *Bcl6*$^{f/f}$ and *Bcl6*$^{f/f}$*Ucp1*^{Cre} mice housed at 30°C (n=4 per genotype). Percentages of total binding sites with increased, decreased, or unchanged enrichment in *Bcl6*$^{f/f}$*Ucp1*^{Cre} mice are indicated. Data are presented as mean ± SEM.

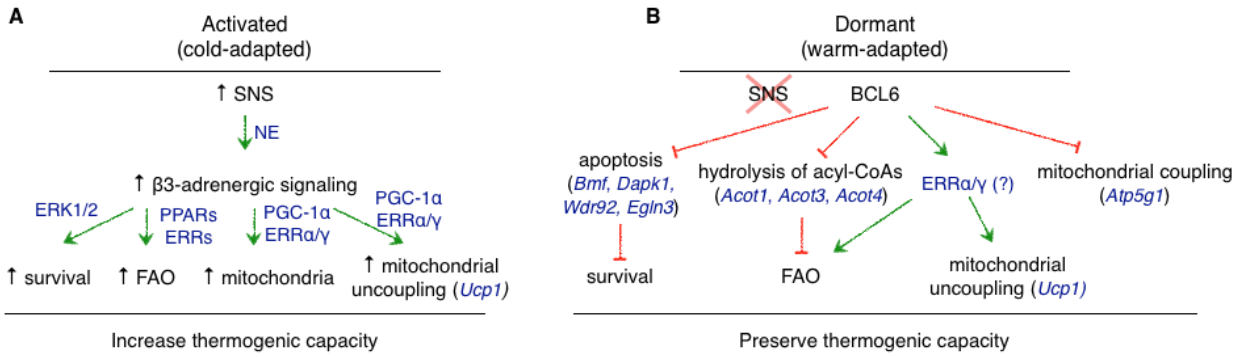
A
Activated
(cold-adapted)
↑ SNS
NE
↑ β3-adrenergic signaling
ERK1/2
PPARs
ERRs
PGC-1α
ERRα/γ
PGC-1α
ERRα/γ
↑ survival
↑ FAO
↑ mitochondria
↑ mitochondrial
uncoupling (Ucp1)
Increase thermogenic capacity
B
Dormant
(warm-adapted)
SNS
BCL6
apoptosis
(Bmf, Dapk1,
Wdr92, Egln3)
hydrolysis of acyl-CoAs
(Acot1, Acot3, Acot4)
ERRα/γ (?)
mitochondrial coupling
(Atp5g1)
survival
FAO
mitochondrial
uncoupling (Ucp1)
Preserve thermogenic capacity

Figure 2.14. A model depicting the distinct pathways controlling survival and thermogenic capacity in active and dormant brown adipocytes.
During adaptation to cold (A), norepinephrine (NE) released by the sympathetic nervous system (SNS) activates β3-adrenergic signaling in brown adipocytes, which supports their survival and increases their thermogenic capacity. Survival is mediated by the action of ERK1/2, while fatty acid oxidation (FAO), mitochondrial biogenesis, and mitochondrial uncoupling (UCP1) are stimulated at the transcriptional level by peroxisome-proliferator activated receptors (PPARs), estrogen-related receptors (ERRs), and the co-activator protein PGC-1α. In contrast, during adaptation to warmth (B), when sympathetic tone is minimal and brown adipocytes become dormant, BCL6 reinforces survival and preserves thermogenic capacity. BCL6 promotes survival by repressing pro-apoptotic genes, such as *Bmf*, *Egln3*, *Dapk1*, and *Wdr92*, and maintains reserve thermogenic capacity by repressing genes involved in hydrolysis of acyl-CoAs (*Acot1*, *Acot3*, *Acot4*) and mitochondrial coupling (*Atp5g1*), and potentially by indirectly stimulating the activity of ERRs to promote expression of genes involved in FAO and uncoupled respiration.

Table 2.1. List of genes in the "Apoptotic Process" category that were upregulated in iBAT of *Bcl6$^{f/f}$Ucp1^{Cre}* mice housed at 30ºC.

"Apoptotic Process" genes (Table 2.1)
B cell leukemia/lymphoma 10(Bcl10)
BCL2 modifying factor(Bmf)
Bruton agammaglobulinemia tyrosine kinase(Btk)
Eph receptor A2(Epha2)
G protein-coupled receptor kinase 5(Grk5)
G-protein coupled receptor 65(Gpr65)
LPS-induced TN factor(Litaf)
NLR family, apoptosis inhibitory protein 2(Naip2)
NLR family, apoptosis inhibitory protein 5(Naip5)
NUAK family, SNF1-like kinase, 2(Nuak2)
PRKC, apoptosis, WT1, regulator(Pawr)
Sp110 nuclear body protein(Sp110)
TNF receptor-associated factor 1(Traf1)
WD repeat domain 92(Wdr92)
absent in melanoma 2(Aim2)
caspase 1(Casp1)
cell adhesion molecule 1(Cadm1)
complement component 5a receptor 1(C5ar1)
cysteine-serine-rich nuclear protein 1(Csrnp1)
death associated protein kinase 1(Dapk1)
deleted in liver cancer 1(Dlc1)
egl-9 family hypoxia-inducible factor 3(Egln3)
growth arrest and DNA-damage-inducible 45 gamma(Gadd45g)
heme oxygenase 1(Hmox1)
lymphocyte specific 1(Lsp1)
microtubule-associated protein tau(Mapt)
myeloid cell leukemia sequence 1(Mcl1)
myeloid differentiation primary response gene 88(Myd88)
neutrophil cytosolic factor 1(Ncf1)
paternally expressed 3(Peg3)
peroxisome proliferator activator receptor delta(Ppard)
polo-like kinase 3(Plk3)
protein kinase C, beta(Prkcb)
protein kinase C, delta(Prkcd)
protein kinase D1(Prkd1)
protein phosphatase 1, regulatory (inhibitor) subunit 15A(Ppp1r15a)
proviral integration site 3(Pim3)
ras homolog family member B(Rhob)
serine (or cysteine) peptidase inhibitor, clade A, member 3G(Serpina3g)

"Apoptotic Process" genes (Table 2.1 continued)
serum/glucocorticoid regulated kinase 1(Sgk1)
seven in absentia 2(Siah2)
sulfatase 1(Sulf1)
transient receptor potential cation channel, subfamily V, member 2(Trpv2)
transmembrane protein 173(Tmem173)
tumor necrosis factor receptor superfamily, member 10b(Tnfrsf10b)
ubiquitin-conjugating enzyme E2Z(Ube2z)
zinc finger protein 385A(Zfp385a)

Table 2.2. List of genes in the "Inflammatory Response" category that were upregulated in iBAT of *Bcl6$^{f/f}$Ucp1^{Cre}* mice housed at 30ºC

"Inflammatory Response" genes (Table 2.2)
B cell leukemia/lymphoma 6(Bcl6)
C-type lectin domain family 7, member a(Clec7a)
CD180 antigen(Cd180)
Eph receptor A2(Epha2)
KDM1 lysine (K)-specific demethylase 6B(Kdm6b)
NLR family, apoptosis inhibitory protein 2(Naip2)
NLR family, apoptosis inhibitory protein 5(Naip5)
a disintegrin and metallopeptidase domain 8(Adam8)
absent in melanoma 2(Aim2)
allograft inflammatory factor 1(Aif1)
annexin A1(Anxa1)
atypical chemokine receptor 1 (Duffy blood group)(Ackr1)
carbohydrate (keratan sulfate Gal-6) sulfotransferase 1(Chst1)
chemokine (C-C motif) ligand 6(Ccl6)
chemokine (C-C motif) ligand 9(Ccl9)
chemokine (C-X-C motif) ligand 9(Cxcl9)
colony stimulating factor 1 receptor(Csf1r)
complement component 3a receptor 1(C3ar1)
complement component 5a receptor 1(C5ar1)
cytochrome b-245, alpha polypeptide(Cyba)
cytochrome b-245, beta polypeptide(Cybb)
hemopoietic cell kinase(Hck)
insulin-like growth factor binding protein 4(Igfbp4)
lymphocyte antigen 86(Ly86)
myeloid differentiation primary response gene 88(Myd88)
neutrophil cytosolic factor 1(Ncf1)
nuclear factor of kappa light polypeptide gene enhancer in B cells inhibitor, zeta(Nfkbiz)
platelet-activating factor receptor(Ptafr)

"Inflammatory Response" genes (Table 2.2 continued)
proline-serine-threonine phosphatase-interacting protein 1(Pstpip1)
protein kinase D1(Prkd1)
purinergic receptor P2X, ligand-gated ion channel, 7(P2rx7)
secreted phosphoprotein 1(Spp1)
selectin, platelet(Selp)
solute carrier family 11 (proton-coupled divalent metal ion transporters), member 1(Slc11a1)
thrombospondin 1(Thbs1)
thymocyte selection associated family member 2(Themis2)
toll-like receptor 13(Tlr13)
toll-like receptor 7(Tlr7)
toll-like receptor 8(Tlr8)
tumor necrosis factor receptor superfamily, member 10b(Tnfrsf10b)
tumor necrosis factor receptor superfamily, member 1b(Tnfrsf1b)

Table 2.3. List of genes that are likely to be directly regulated by BCL6 in brown adipocytes (nearest to BCL6 binding site, expression altered >1.5-fold in BAT of *Bcl6$^{f/f}$Ucp1^{Cre}* mice at 30° C)

Gene name	Regulation by BCL6
nucleoside-triphosphatase, cancer-related(Ntpcr)	Repressed
suppressor of cytokine signaling 2(Socs2)	Repressed
carboxypeptidase A2, pancreatic(Cpa2)	Repressed
BCL2 modifying factor(Bmf)	Repressed
nucleic acid binding protein 1(Nabp1)	Repressed
dipeptidylpeptidase 9(Dpp9)	Repressed
protein tyrosine phosphatase, non-receptor type 4(Ptpn4)	Repressed
ATP synthase, H+ transporting, mitochondrial F0 complex, subunit C1 (subunit 9)(Atp5g1)	Repressed
UHRF1 (ICBP90) binding protein 1-like(Uhrf1bp1l)	Repressed
tenascin C(Tnc)	Repressed
CD180 antigen(Cd180)	Repressed
leucine rich repeat neuronal 4(Lrrn4)	Repressed
nicotinamide nucleotide transhydrogenase(Nnt)	Repressed
SH3 and PX domains 2B(Sh3pxd2b)	Repressed
AT rich interactive domain 3A (BRIGHT-like)(Arid3a)	Repressed
reticulon 4 receptor-like 1(Rtn4rl1)	Repressed
thrombospondin 1(Thbs1)	Repressed
deleted in liver cancer 1(Dlc1)	Repressed
kelch-like 13(Klhl13)	Repressed
transmembrane and coiled coil domains 3(Tmcc3)	Repressed
interleukin 7 receptor(Il7r)	Repressed

Gene name (Table 2.3 continued)	Regulation by BCL6
insulin-like growth factor binding protein, acid labile subunit(Igfals)	Repressed
UDP-Gal:betaGlcNAc beta 1,4- galactosyltransferase, polypeptide 1(B4galt1)	Repressed
egl-9 family hypoxia-inducible factor 3(Egln3)	Repressed
transcription factor 7, T cell specific(Tcf7)	Repressed
a disintegrin-like and metallopeptidase (reprolysin type) with thrombospondin type 1 motif, 12(Adamts12)	Repressed
ST3 beta-galactoside alpha-2,3-sialyltransferase 6(St3gal6)	Repressed
leptin(Lep)	Repressed
guanylate binding protein 7(Gbp7)	Repressed
SLIT-ROBO Rho GTPase activating protein 3(Srgap3)	Repressed
signal-induced proliferation-associated 1 like 2(Sipa1l2)	Repressed
predicted gene, 20125(Gm20125)	Repressed
laccase (multicopper oxidoreductase) domain containing 1(Lacc1)	Repressed
a disintegrin-like and metallopeptidase (reprolysin type) with thrombospondin type 1 motif, 2(Adamts2)	Repressed
F-box and leucine-rich repeat protein 7(Fbxl7)	Repressed
FERM domain containing 4B(Frmd4b)	Repressed
immediate early response 5(Ier5)	Repressed
toll-like receptor 8(Tlr8)	Repressed
RIKEN cDNA 4833411C07 gene(4833411C07Rik)	Repressed
acyl-CoA thioesterase 1(Acot1)	Repressed
RIKEN cDNA 9330133O14 gene(9330133O14Rik)	Repressed
ankyrin repeat domain 24(Ankrd24)	Repressed
zinc finger protein 704(Zfp704)	Repressed
hypermethylated in cancer 2(Hic2)	Repressed
ATP-binding cassette, sub-family A (ABC1), member 1(Abca1)	Repressed
dedicator of cytokinesis 9(Dock9)	Repressed
vacuolar protein sorting 37B(Vps37b)	Repressed
salt inducible kinase 1(Sik1)	Repressed
guanine nucleotide binding protein (G protein), alpha inhibiting 1(Gnai1)	Repressed
coiled-coil domain containing 80(Ccdc80)	Repressed
carboxymethylenebutenolidase-like (Pseudomonas)(Cmbl)	Repressed
transferrin receptor(Tfrc)	Repressed
histidine rich carboxyl terminus 1(Hrct1)	Repressed
B cell CLL/lymphoma 11A (zinc finger protein)(Bcl11a)	Repressed
RIKEN cDNA B930025P03 gene(B930025P03Rik)	Repressed
neuronal growth regulator 1(Negr1)	Repressed
chemokine (C-X-C motif) ligand 9(Cxcl9)	Repressed
sushi, von Willebrand factor type A, EGF and pentraxin domain containing 1(Svep1)	Repressed

Gene name (Table 2.3 continued)	Regulation by BCL6
c-mer proto-oncogene tyrosine kinase(Mertk)	Repressed
brain-specific angiogenesis inhibitor 1-associated protein 2(Baiap2)	Repressed
RIKEN cDNA 2310008N11 gene(2310008N11Rik)	Repressed
a disintegrin-like and metallopeptidase (reprolysin type) with thrombospondin type 1 motif, 15(Adamts15)	Repressed
striatin interacting protein 2(Strip2)	Repressed
G protein-coupled receptor kinase 5(Grk5)	Repressed
protein kinase D1(Prkd1)	Repressed
dual specificity phosphatase 10(Dusp10)	Repressed
RIKEN cDNA 3930402G23 gene(3930402G23Rik)	Repressed
lymphocyte antigen 86(Ly86)	Repressed
syntrophin, basic 2(Sntb2)	Repressed
deleted in lymphocytic leukemia, 2(Dleu2)	Repressed
zinc finger and BTB domain containing 5(Zbtb5)	Repressed
RIKEN cDNA A230028O05 gene(A230028O05Rik)	Repressed
ubiquitin specific peptidase 29(Usp29)	Repressed
anoctamin 9(Ano9)	Repressed
transducin (beta)-like 1X-linked receptor 1(Tbl1xr1)	Repressed
guanylate binding protein 3(Gbp3)	Repressed
peroxisome proliferator activator receptor delta(Ppard)	Repressed
coiled-coil domain containing 170(Ccdc170)	Repressed
LPS-induced TN factor(Litaf)	Repressed
integrin alpha 7(Itga7)	Repressed
glutaredoxin(Glrx)	Repressed
deiodinase, iodothyronine type III, opposite strand(Dio3os)	Repressed
G protein-coupled receptor 152(Gpr152)	Repressed
NUAK family, SNF1-like kinase, 2(Nuak2)	Repressed
inhibin beta-B(Inhbb)	Repressed
protein kinase C, delta(Prkcd)	Repressed
cyclin L1(Ccnl1)	Repressed
RIKEN cDNA 0610005C13 gene(0610005C13Rik)	Repressed
jun proto-oncogene(Jun)	Repressed
lymphocyte antigen 6 complex, locus H(Ly6h)	Repressed
arachidonate 5-lipoxygenase activating protein(Alox5ap)	Repressed
atlastin GTPase 2(Atl2)	Repressed
histidine decarboxylase(Hdc)	Repressed
death associated protein kinase 1(Dapk1)	Repressed
neural precursor cell expressed, developmentally down-regulated gene 9(Nedd9)	Repressed
YEATS domain containing 2(Yeats2)	Repressed
SAM and SH3 domain containing 1(Sash1)	Repressed
proviral integration site 3(Pim3)	Repressed

Gene name (Table 2.3 continued)	Regulation by BCL6
CD83 antigen(Cd83)	Repressed
FGGY carbohydrate kinase domain containing(Fggy)	Repressed
lipase, endothelial(Lipg)	Repressed
neuronatin(Nnat)	Repressed
KDM1 lysine (K)-specific demethylase 6B(Kdm6b)	Repressed
carbohydrate (keratan sulfate Gal-6) sulfotransferase 1(Chst1)	Repressed
cAMP responsive element modulator(Crem)	Repressed
slit homolog 3 (Drosophila)(Slit3)	Repressed
homeobox A4(Hoxa4)	Repressed
cysteine rich protein 61(Cyr61)	Repressed
prolactin receptor(Prlr)	Repressed
cyclin D3(Ccnd3)	Repressed
ets variant 3(Etv3)	Repressed
ganglioside-induced differentiation-associated-protein 2(Gdap2)	Repressed
metal response element binding transcription factor 1(Mtf1)	Repressed
RAB13, member RAS oncogene family(Rab13)	Repressed
SH3 domain and tetratricopeptide repeats 1(Sh3tc1)	Repressed
ArfGAP with RhoGAP domain, ankyrin repeat and PH domain 1(Arap1)	Repressed
cardiac mesoderm enhancer-associated non-coding RNA(Carmn)	Repressed
chromodomain helicase DNA binding protein 3(Chd3)	Repressed
insulin-like growth factor 1(Igf1)	Repressed
tweety family member 2(Ttyh2)	Repressed
Kruppel-like factor 2 (lung)(Klf2)	Repressed
SH3 and cysteine rich domain 2(Stac2)	Repressed
nuclear factor of kappa light polypeptide gene enhancer in B cells inhibitor, zeta(Nfkbiz)	Repressed
nocturnin(Noct)	Repressed
zyxin(Zyx)	Repressed
transmembrane protein 159(Tmem159)	Repressed
zinc finger protein 385A(Zfp385a)	Repressed
twist basic helix-loop-helix transcription factor 2(Twist2)	Repressed
RIKEN cDNA 3110043O21 gene(3110043O21Rik)	Repressed
G protein-coupled receptor 156(Gpr156)	Repressed
family with sequence similarity 53, member C(Fam53c)	Repressed
LSM3 homolog, U6 small nuclear RNA and mRNA degradation associated(Lsm3)	Repressed
tumor necrosis factor receptor superfamily, member 10b(Tnfrsf10b)	Repressed
Src-like-adaptor 2(Sla2)	Repressed
phospholipase A2, group IVA (cytosolic, calcium-dependent)(Pla2g4a)	Repressed
leucine rich repeat containing 32(Lrrc32)	Repressed

Gene name (Table 2.3 continued)	Regulation by BCL6
heme oxygenase 1(Hmox1)	Repressed
RAS p21 protein activator 3(Rasa3)	Repressed
transformer 2 alpha homolog (Drosophila)(Tra2a)	Repressed
interferon regulatory factor 2 binding protein 2(Irf2bp2)	Repressed
cysteine-serine-rich nuclear protein 1(Csrnp1)	Repressed
RAS-like, family 11, member B(Rasl11b)	Repressed
histone H4 transcription factor(Hinfp)	Repressed
ubiquitin specific peptidase 18(Usp18)	Repressed
RasGEF domain family, member 1B(Rasgef1b)	Repressed
E26 avian leukemia oncogene 2, 3' domain(Ets2)	Repressed
dihydropyrimidinase-like 3(Dpysl3)	Repressed
acyl-CoA thioesterase 3(Acot3)	Repressed
TRAF-interacting protein with forkhead-associated domain, family member B(Tifab)	Repressed
macrophage expressed gene 1(Mpeg1)	Repressed
transmembrane protein 178(Tmem178)	Repressed
formin homology 2 domain containing 3(Fhod3)	Repressed
hematopoietic cell specific Lyn substrate 1(Hcls1)	Repressed
WD repeat and SOCS box-containing 1(Wsb1)	Repressed
kelch-like 25(Klhl25)	Repressed
WD repeat domain 92(Wdr92)	Repressed
RIKEN cDNA D630024D03 gene(D630024D03Rik)	Repressed
family with sequence similarity 129, member B(Fam129b)	Repressed
v-maf musculoaponeurotic fibrosarcoma oncogene family, protein F (avian)(Maff)	Repressed
insulin receptor substrate 1(Irs1)	Repressed
potassium voltage-gated channel, Isk-related subfamily, gene 4(Kcne4)	Repressed
predicted gene 10790(Gm10790)	Repressed
serum/glucocorticoid regulated kinase 1(Sgk1)	Repressed
PRKC, apoptosis, WT1, regulator(Pawr)	Repressed
basic helix-loop-helix domain containing, class B9(Bhlhb9)	Repressed
nuclear factor of kappa light polypeptide gene enhancer in B cells inhibitor, delta(Nfkbid)	Repressed
urotensin 2 receptor(Uts2r)	Induced
smoothelin-like 2(Smtnl2)	Induced
long non-coding RNA, embryonic stem cells expressed 1(Lncenc1)	Induced
methyltransferase like 15(Mettl15)	Induced
hydroxysteroid dehydrogenase like 2(Hsdl2)	Induced
plexin A1(Plxna1)	Induced
TBC1 domain family, member 4(Tbc1d4)	Induced
antagonist of mitotic exit network 1(Amn1)	Induced

Gene name (Table 2.3 continued)	Regulation by BCL6
Ras association (RalGDS/AF-6) domain family (N-terminal) member 10(Rassf10)	Induced
HRAS-like suppressor family, member 5(Hrasls5)	Induced
protein phosphatase 1, catalytic subunit, beta isoform(Ppp1cb)	Induced
Fraser extracellular matrix complex subunit 1(Fras1)	Induced
interferon, alpha-inducible protein 27(Ifi27)	Induced
neuron navigator 2(Nav2)	Induced
solute carrier family 16 (monocarboxylic acid transporters), member 1(Slc16a1)	Induced
acylphosphatase 2, muscle type(Acyp2)	Induced
inositol 1,4,5-triphosphate receptor 2(Itpr2)	Induced
cDNA sequence BC024139(BC024139)	Induced
tripartite motif-containing 2(Trim2)	Induced
general transcription factor II I repeat domain-containing 1(Gtf2ird1)	Induced
CUGBP, Elav-like family member 2(Celf2)	Induced
cadherin 2(Cdh2)	Induced
epidermal growth factor-containing fibulin-like extracellular matrix protein 1(Efemp1)	Induced
regulator of microtubule dynamics 1(Rmdn1)	Induced
hydroxysteroid (17-beta) dehydrogenase 12(Hsd17b12)	Induced
LYR motif containing 9(Lyrm9)	Induced
RIKEN cDNA A830018L16 gene(A830018L16Rik)	Induced
ST6 (alpha-N-acetyl-neuraminyl-2,3-beta-galactosyl-1,3)-N-acetylgalactosaminide alpha-2,6-sialyltransferase 6(St6galnac6)	Induced
SRY (sex determining region Y)-box 6(Sox6)	Induced
neurotrophic tyrosine kinase, receptor, type 2(Ntrk2)	Induced
doublesex and mab-3 related transcription factor 2(Dmrt2)	Induced
RIKEN cDNA 4833417C18 gene(4833417C18Rik)	Induced
1-acylglycerol-3-phosphate O-acyltransferase 3(Agpat3)	Induced
3-oxoacid CoA transferase 1(Oxct1)	Induced
interleukin 15 receptor, alpha chain(Il15ra)	Induced
serine/threonine kinase 38 like(Stk38l)	Induced
PTC7 protein phosphatase homolog(Pptc7)	Induced
RIKEN cDNA C030037D09 gene(C030037D09Rik)	Induced
tetratricopeptide repeat domain 30B(Ttc30b)	Induced
acyl-CoA thioesterase 11(Acot11)	Induced
RIKEN cDNA 4831440E17 gene(4831440E17Rik)	Induced
carbohydrate (N-acetylgalactosamine 4-0) sulfotransferase 9(Chst9)	Induced
tubulin, gamma 2(Tubg2)	Induced
autophagy related 9B(Atg9b)	Induced
delta-like 1 homolog (Drosophila)(Dlk1)	Induced
Ras association and DIL domains(Radil)	Induced

Gene name (Table 2.3 continued)	Regulation by BCL6
solute carrier family 22 (organic cation transporter), member 2(Slc22a2)	Induced
activating transcription factor 6(Atf6)	Induced
tumor protein p53 pathway corepressor 1(Trp53cor1)	Induced
RIKEN cDNA 1700061I17 gene(1700061I17Rik)	Induced
calreticulin 4(Calr4)	Induced
muskelin 1, intracellular mediator containing kelch motifs, opposite strand(Mkln1os)	Induced
Gm45924	Induced
carbohydrate (N-acetylgalactosamine 4-sulfate 6-O) sulfotransferase 15(Chst15)	Induced
SMAD family member 6(Smad6)	Induced
plasminogen receptor, C-terminal lysine transmembrane protein(Plgrkt)	Induced
G protein-coupled receptor kinase 3(Grk3)	Induced
a disintegrin and metallopeptidase domain 11(Adam11)	Induced
succinate dehydrogenase complex assembly factor 3(Sdhaf3)	Induced
purinergic receptor P2Y, G-protein coupled 1(P2ry1)	Induced
solute carrier family 36 (proton/amino acid symporter), member 2(Slc36a2)	Induced
v-myc avian myelocytomatosis viral related oncogene, neuroblastoma derived(Mycn)	Induced
kelch domain containing 7A(Klhdc7a)	Induced
LIM domain only 1(Lmo1)	Induced
acetyl-Coenzyme A acyltransferase 1B(Acaa1b)	Induced
pleckstrin homology domain containing, family G (with RhoGef domain) member 6(Plekhg6)	Induced
phosphotriesterase related(Pter)	Induced
synaptotagmin XIV(Syt14)	Induced
protein phosphatase 1, regulatory (inhibitor) subunit 3B(Ppp1r3b)	Induced
dehydrogenase/reductase (SDR family) member 9(Dhrs9)	Induced
glycerol-3-phosphate acyltransferase, mitochondrial(Gpam)	Induced
translocating chain-associating membrane protein 2(Tram2)	Induced
coenzyme Q8A(Coq8a)	Induced
zinc finger and SCAN domain containing 2(Zscan2)	Induced
schwannomin interacting protein 1(Schip1)	Induced
multiple EGF-like-domains 9(Megf9)	Induced
transmembrane protein 266(Tmem266)	Induced
metaxin 2(Mtx2)	Induced
transmembrane protein 268(Tmem268)	Induced
EH-domain containing 3(Ehd3)	Induced
lectin, mannose-binding, 1(Lman1)	Induced
inhibitor of DNA binding 2(Id2)	Induced

Gene name (Table 2.3 continued)	Regulation by BCL6
electron transferring flavoprotein, alpha polypeptide(Etfa)	Induced
RIKEN cDNA A530046M15 gene(A530065N20Rik)	Induced
protein phosphatase 2, regulatory subunit B", alpha(Ppp2r3a)	Induced
solute carrier family 7 (cationic amino acid transporter, y+ system), member 8(Slc7a8)	Induced
patatin-like phospholipase domain containing 3(Pnpla3)	Induced
pyruvate dehydrogenase E1 alpha 1(Pdha1)	Induced
leucine-rich repeat-containing G protein-coupled receptor 6(Lgr6)	Induced
zinc finger protein 354C(Zfp354c)	Induced
immunoglobulin superfamily, member 21(Igsf21)	Induced
homeobox C4(Hoxc4)	Induced
sideroflexin 5(Sfxn5)	Induced
protein phosphatase 3, catalytic subunit, gamma isoform(Ppp3cc)	Induced
dematin actin binding protein(Dmtn)	Induced
cerebral dopamine neurotrophic factor(Cdnf)	Induced
predicted gene 2447(Gm2447)	Induced
tumor suppressor candidate 3(Tusc3)	Induced

Table 2.4. List of genes displayed in the "White and brown adipocyte-specific genes" heatmap (Figure 2.11A)

Gene name	Specificity
insulin-like growth factor 1(Igf1)	White adipocyte-specific
coiled-coil domain containing 80(Ccdc80)	White adipocyte-specific
cyclin D2(Ccnd2)	White adipocyte-specific
collagen, type III, alpha 1(Col3a1)	White adipocyte-specific
collagen, type IV, alpha 2(Col4a2)	White adipocyte-specific
doublesex and mab-3 related transcription factor 2(Dmrt2)	White adipocyte-specific
eukaryotic elongation factor-2 kinase(Eef2k)	White adipocyte-specific
endonuclease/exonuclease/phosphatase family domain containing 1(Eepd1)	White adipocyte-specific
growth arrest and DNA-damage-inducible 45 alpha(Gadd45a)	White adipocyte-specific
glutamyl-tRNA(Gln) amidotransferase, subunit B(Gatb)	White adipocyte-specific
insulin-like growth factor 1(Igf1)	White adipocyte-specific
leptin(Lep)	White adipocyte-specific
lysophosphatidylglycerol acyltransferase 1(Lpgat1)	White adipocyte-specific
low density lipoprotein receptor-related protein 1(Lrp1)	White adipocyte-specific
N-myc downstream regulated gene 1(Ndrg1)	White adipocyte-specific
neuronatin(Nnat)	White adipocyte-specific
nuclear receptor interacting protein 1(Nrip1)	White adipocyte-specific

Gene name (Table 2.4 continued)	Specificity
nuclear protein transcription regulator 1(Nupr1)	White adipocyte-specific
phosphatidylinositol 3-kinase, regulatory subunit, polypeptide 1 (p85 alpha)(Pik3r1)	White adipocyte-specific
protein kinase C, delta binding protein(Prkcdbp)	White adipocyte-specific
brain glycogen phosphorylase(Pygb)	White adipocyte-specific
quiescin Q6 sulfhydryl oxidase 1(Qsox1)	White adipocyte-specific
acyl-Coenzyme A dehydrogenase, short chain(Acads)	Brown adipocyte-specific
acyl-Coenzyme A dehydrogenase, very long chain(Acadvl)	Brown adipocyte-specific
acetyl-Coenzyme A acetyltransferase 1(Acat1)	Brown adipocyte-specific
aconitase 2, mitochondrial(Aco2)	Brown adipocyte-specific
acyl-CoA synthetase family member 2(Acsf2)	Brown adipocyte-specific
acyl-CoA synthetase long-chain family member 5(Acsl5)	Brown adipocyte-specific
adenylate cyclase 3(Adcy3)	Brown adipocyte-specific
1-acylglycerol-3-phosphate O-acyltransferase 3(Agpat3)	Brown adipocyte-specific
A kinase (PRKA) anchor protein 1(Akap1)	Brown adipocyte-specific
alpha-methylacyl-CoA racemase(Amacr)	Brown adipocyte-specific
aurora kinase A interacting protein 1(Aurkaip1)	Brown adipocyte-specific
branched chain ketoacid dehydrogenase E1, beta polypeptide(Bckdhb)	Brown adipocyte-specific
basigin(Bsg)	Brown adipocyte-specific
complement component 1, q subcomponent binding protein(C1qbp)	Brown adipocyte-specific
coiled-coil-helix-coiled-coil-helix domain containing 3(Chchd3)	Brown adipocyte-specific
cytokine induced apoptosis inhibitor 1(Ciapin1)	Brown adipocyte-specific
coenzyme Q6 monooxygenase(Coq6)	Brown adipocyte-specific
cytochrome c oxidase assembly protein 10(Cox10)	Brown adipocyte-specific
cytochrome c oxidase subunit Va(Cox5a)	Brown adipocyte-specific
cytochrome c oxidase subunit VIIa 2(Cox7a2)	Brown adipocyte-specific
carnitine palmitoyltransferase 1b, muscle(Cpt1b)	Brown adipocyte-specific
cardiolipin synthase 1(Crls1)	Brown adipocyte-specific
cytochrome c-1(Cyc1)	Brown adipocyte-specific
desmin(Des)	Brown adipocyte-specific
dihydrolipoamide dehydrogenase(Dld)	Brown adipocyte-specific
dihydrolipoamide S-succinyltransferase (E2 component of 2-oxo-glutarate complex)(Dlst)	Brown adipocyte-specific
DnaJ heat shock protein family (Hsp40) member A3(Dnaja3)	Brown adipocyte-specific
DnaJ heat shock protein family (Hsp40) member C11(Dnajc11)	Brown adipocyte-specific
enoyl coenzyme A hydratase 1, peroxisomal(Ech1)	Brown adipocyte-specific
enoyl Coenzyme A hydratase, short chain, 1, mitochondrial(Echs1)	Brown adipocyte-specific
ECSIT signalling integrator(Ecsit)	Brown adipocyte-specific

Gene name (Table 2.4 continued)	Specificity
enoyl-Coenzyme A, hydratase/3-hydroxyacyl Coenzyme A dehydrogenase(Ehhadh)	Brown adipocyte-specific
electron transferring flavoprotein, alpha polypeptide(Etfa)	Brown adipocyte-specific
flavin adenine dinucleotide synthetase 1(Flad1)	Brown adipocyte-specific
glycerol kinase(Gk)	Brown adipocyte-specific
glutaredoxin 5(Glrx5)	Brown adipocyte-specific
glutamic-oxaloacetic transaminase 1, soluble(Got1)	Brown adipocyte-specific
hydroxyacyl-Coenzyme A dehydrogenase/3-ketoacyl-Coenzyme A thiolase/enoyl-Coenzyme A hydratase (trifunctional protein), alpha subunit(Hadha)	Brown adipocyte-specific
holocytochrome c synthetase(Hccs)	Brown adipocyte-specific
heat shock protein 9(Hspa9)	Brown adipocyte-specific
heat shock protein 1 (chaperonin)(Hspd1)	Brown adipocyte-specific
isocitrate dehydrogenase 3 (NAD+) alpha(Idh3a)	Brown adipocyte-specific
isocitrate dehydrogenase 3 (NAD+) beta(Idh3b)	Brown adipocyte-specific
inner membrane protein, mitochondrial(Immt)	Brown adipocyte-specific
potassium channel, subfamily K, member 3(Kcnk3)	Brown adipocyte-specific
LETM1 domain containing 1(Letmd1)	Brown adipocyte-specific
membrane-associated ring finger (C3HC4) 5(March5)	Brown adipocyte-specific
mitochondrial ribosomal protein L15(Mrpl15)	Brown adipocyte-specific
mitochondrial ribosomal protein L34(Mrpl34)	Brown adipocyte-specific
mitochondrial ribosomal protein S18B(Mrps18b)	Brown adipocyte-specific
mitochondrial ribosomal protein S22(Mrps22)	Brown adipocyte-specific
mitochondrial ribosomal protein S5(Mrps5)	Brown adipocyte-specific
mitchondrial ribosomal protein S7(Mrps7)	Brown adipocyte-specific
mitochondrial translational initiation factor 2(Mtif2)	Brown adipocyte-specific
NADH dehydrogenase (ubiquinone) 1 alpha subcomplex, 13(Ndufa13)	Brown adipocyte-specific
NADH dehydrogenase (ubiquinone) 1, alpha/beta subcomplex, 1(Ndufab1)	Brown adipocyte-specific
NADH dehydrogenase (ubiquinone) complex I, assembly factor 5(Ndufaf5)	Brown adipocyte-specific
NADH dehydrogenase (ubiquinone) 1 beta subcomplex, 2(Ndufb2)	Brown adipocyte-specific
NADH dehydrogenase (ubiquinone) 1 beta subcomplex, 7(Ndufb7)	Brown adipocyte-specific
NADH dehydrogenase (ubiquinone) 1 beta subcomplex, 9(Ndufb9)	Brown adipocyte-specific
NADH dehydrogenase (ubiquinone) Fe-S protein 1(Ndufs1)	Brown adipocyte-specific
NADH dehydrogenase (ubiquinone) Fe-S protein 2(Ndufs2)	Brown adipocyte-specific
NADH dehydrogenase (ubiquinone) Fe-S protein 3(Ndufs3)	Brown adipocyte-specific
NADH dehydrogenase (ubiquinone) Fe-S protein 8(Ndufs8)	Brown adipocyte-specific
NADH dehydrogenase (ubiquinone) flavoprotein 1(Ndufv1)	Brown adipocyte-specific

Gene name (Table 2.4 continued)	Specificity
oxoglutarate (alpha-ketoglutarate) dehydrogenase (lipoamide)(Ogdh)	Brown adipocyte-specific
oxidoreductase NAD-binding domain containing 1(Oxnad1)	Brown adipocyte-specific
pantothenate kinase 1(Pank1)	Brown adipocyte-specific
phosphoenolpyruvate carboxykinase 1, cytosolic(Pck1)	Brown adipocyte-specific
pyruvate dehydrogenase E1 alpha 1(Pdha1)	Brown adipocyte-specific
prohibitin 2(Phb2)	Brown adipocyte-specific
polymerase (DNA-directed), delta interacting protein 2(Poldip2)	Brown adipocyte-specific
DNA polymerase N(Poln)	Brown adipocyte-specific
peroxisome proliferative activated receptor, gamma, coactivator 1 beta(Ppargc1b)	Brown adipocyte-specific
peptidylprolyl isomerase F (cyclophilin F)(Ppif)	Brown adipocyte-specific
pentatricopeptide repeat domain 3(Ptcd3)	Brown adipocyte-specific
syndecan 4(Sdc4)	Brown adipocyte-specific
succinate dehydrogenase complex, subunit A, flavoprotein (Fp)(Sdha)	Brown adipocyte-specific
succinate dehydrogenase complex, subunit C, integral membrane protein(Sdhc)	Brown adipocyte-specific
sphingosine phosphate lyase 1(Sgpl1)	Brown adipocyte-specific
solute carrier family 25 (mitochondrial carrier oxoglutarate carrier), member 11(Slc25a11)	Brown adipocyte-specific
solute carrier family 25, member 39(Slc25a39)	Brown adipocyte-specific
superoxide dismutase 2, mitochondrial(Sod2)	Brown adipocyte-specific
succinate-CoA ligase, GDP-forming, alpha subunit(Suclg1)	Brown adipocyte-specific
transforming growth factor beta regulated gene 4(Tbrg4)	Brown adipocyte-specific
thioesterase superfamily member 4(Them4)	Brown adipocyte-specific
translocase of inner mitochondrial membrane 44(Timm44)	Brown adipocyte-specific
translocase of inner mitochondrial membrane 50(Timm50)	Brown adipocyte-specific
uncoupling protein 1 (mitochondrial, proton carrier)(Ucp1)	Brown adipocyte-specific
ubiquinol-cytochrome c reductase complex assembly factor 1(Uqcc1)	Brown adipocyte-specific
ubiquinol-cytochrome c reductase, complex III subunit X(Uqcr10)	Brown adipocyte-specific
ubiquinol-cytochrome c reductase binding protein(Uqcrb)	Brown adipocyte-specific
ubiquinol-cytochrome c reductase core protein 1(Uqcrc1)	Brown adipocyte-specific
von Willebrand factor A domain containing 8(Vwa8)	Brown adipocyte-specific

Table 2.5. List of antibodies used in this study.

Antibody	Manufacturer	Catalog # & RRID #	Clone ID	Lot #
Anti-mouse UCP1	Abcam	Cat# ab10983; RRID:AB_2241462	N/A	GR249119-2
Anti-mouse BCL6	Cell Signaling Technology	Cat# 5650; RRID:AB_10949970	D65C10	4
Anti-mouse HSP90	Cell Signaling Technology	Cat# 4874; RRID:AB_2121214	N/A	4
Total OXPHOS Rodent WB Antibody Cocktail	Abcam	Cat# ab110413; RRID:AB_2629281	N/A	J3798
Anti-mouse MCT1	EMD Millipore	Cat# AB1286, RRID:AB_90565	N/A	2979947
Anti-mouse Ki67 (for staining sections)	Abcam	Cat# ab15580, RRID:AB_443209	N/A	790309
Anti-rabbit IgG, HRP-conjugated (secondary)	Cell Signaling Technology	Cat# 7074, RRID:AB_2099233	N/A	26
Mouse IgG kappa binding protein (m-IgGκ BP) HRP-conjugated (secondary)	Santa Cruz Biotechnology	Cat# sc-516102, RRID:AB_2687626	N/A	E1917
Anti-mouse Lamin B1	Cell Signaling Technology	Cat# 12586, RRID: AB_2650517	D4Q4Z	2
Anti-mouse H3K27ac	Abcam	Cat# ab4729, RRID: AB_2118291	N/A	GR3211959-1
Anti-mouse CD45 APC-Cy7	Biolegend	Cat# 103116, RRID: AB_312981	30-F11	B237400
Anti-mouse CD11b PerCP/Cy5.5	Biolegend	Cat# 101228, RRID: AB_893232	M1/70	B149793
Anti-mouse F4/80 PE/Cy7	Biolegend	Cat# 123114, RRID: AB_893478	BM8	B173257
Anti-mouse CD11c FITC	Biolegend	Cat# 117306, RRID: AB_313775	N418	B168004

Antibody	Manufacturer	Catalog # & RRID #	Clone ID	Lot #
Anti-mouse CD115 PE	Biolegend	Cat# 135505, RRID: AB_1937254	AFS98	B223860
Anti-mouse CD206 APC	Biolegend	Cat# 141708, RRID: AB_10900231	C068C2	B170352
Anti-mouse Ly6G Pacific Blue	Biolegend	Cat# 127612, RRID: AB_2251161	1A8	B154289
Anti-mouse CD3e FITC	Biolegend	Cat# 100306, RRID: AB_312671	145-2C11	B162655
Anti-mouse CD4 Pacific Blue	Biolegend	Cat# 100428, RRID: AB_493647	GK15	B176054
Anti-mouse CD8 PerCP/Cy5.5	Biolegend	Cat# 100734, RRID: AB_2075238	53-6.7	B193838
Anti-mouse CD25 PE	Biolegend	Cat# 102007, RRID: AB_312856	PC61	B127639
Goat anti-Chicken IgY (H+L) Alexa-Fluor 555 (secondary)	Thermo Fisher Scientific	Cat# A-21437, RRID: AB_2535858	N/A	1889319
Goat anti-rabbit IgG Alexa-Fluor-488 (secondary)	Thermo Fisher Scientific	Cat# A-11008, RRID:AB_143165	N/A	1761258
Anti-Phospho-PKA Substrate (RRXS*/T*)	Cell Signaling Technology	Cat# #9624, RRID: AB_331817	100G7E	N/A
Anti-mouse β3-Adrenergic Receptor	Abcam	Cat# ab94506, RRID: AB_10863818	N/A	N/A
Anti-mouse ERRα	Cell Signaling Technology	Cat# 13826S, RRID: AB_2750873	E1G1J	1

Table 2.6. List of primers used in this study.

Gene Name	Primer Type	Forward Primer Sequence	Reverse Primer Sequence
Acot1	RT-qPCR	AACATCACCTTTGGAGGGGAG	TCCCCAACCTCCAAACCATCA
Acot3	RT-qPCR	GCTCAGTCACCCTCAGGTAA	AAGTTTCCGCCGATGTTGGA
Acot4	RT-qPCR	ACATCCAAAGGTAAAAGGCCCA	TCCACTGAATGCAGAGCCATT
Atp5g1	RT-qPCR	AGTTGGTGTGGCTGGATCA	GCTGCTTGAGAGATGGGTTC
Bmf	RT-qPCR	CCCATAAGCCAGGAAGACAA	CTGAAGCTTTCTGGCGATCT
Ucp1	RT-qPCR	AAGCTGTGCGATGTCCATGT	AAGCCACAAACCCTTTGAAAA
36b4	RT-qPCR	AACGGCAGCATTTATAACCC	CGATCTGCAGACACACACTG
Ccdc80	RT-qPCR	CTCCTGCCTTGGATAGCGAC	GAGCTGACCTACTGCTGATTG
Egln3	RT-qPCR	AGGCAATGGTGGCTTGCTATC	GCGTCCCAATTCTTATTCAGGT

Gene Name	**Primer Type**	**Forward Primer Sequence**	**Reverse Primer Sequence**
Ndufv1	Nuclear DNA qPCR	CTTCCCCACTGGCCTCAAG	CCAAAACCCAGTGATCCAGC
Mt-co1	Mitochondrial DNA qPCR	TGCTAGCCGCAGGCATTAC	GGGTGCCCAAAGAATCAGAAC
Esrra	RT-qPCR	GGGGAGCATCGAGTACAGC	AGACGCACACCCTCCTTGA
Esrrg	RT-qPCR	CTATGGGGTTGCATCATGTGAA	CGTCTGCGCTTTGTGATCTC
Esrrb	RT-qPCR	AACCGAATGTCGTCCGAAGAC	GTGGCTGAGGGCATCAATG

Discussion

Brown adipose tissue thermogenesis is an essential component of mammalian adaptation to environmental cold. While short-term changes in environmental temperature are buffered by changes in BAT thermogenic rate, long-term acclimation to warm or cold environments leads to remodeling of BAT thermogenic capacity. For example, chronic exposure to environmental cold results in recruitment of additional thermogenic capacity in brown and beige adipocytes, whereas acclimation to environmental warmth results in a decrease in thermogenic capacity by entry of brown and beige adipocytes into dormancy. While dormant beige adipocytes acquire molecular characteristics of white adipocytes, dormant brown adipocytes maintain their cellular identity and a basal thermogenic capacity (Roh et al., 2018). However, our mechanistic understanding of how dormancy is regulated in brown adipocytes is limited. Here, we have demonstrated that the transcriptional repressor BCL6, while not required for differentiation or cold adaptation of brown adipocytes, is essential for the maintenance of thermogenic capacity during dormancy. The reduced thermogenic competence of BCL6-deficient dormant brown adipocytes is partially attributable to loss of their cellular identity, as revealed by their molecular, metabolic, and morphological shift towards a white adipocyte phenotype. Thus, unlike other transcription factors that act downstream of adrenergic stimuli to activate thermogenesis, BCL6 functions in a parallel pathway to maintain the basal thermogenic capacity in dormant brown adipocytes (Figure 2.14).

During adaptation to cold, BAT cellularity increases to support the higher demand for thermogenesis. This is due to the positive effect of adrenergic signaling on proliferation of brown adipocyte precursors and survival of differentiated brown adipocytes (Lee et al., 2015c; Lindquist and Rehnmark, 1998). However, since the rate of apoptosis is low in dormant BAT of

wild type mice (Hellman and Hellerstrom, 1961; Kotzbeck et al., 2018), additional factors likely promote survival of brown adipocytes in the absence of adrenergic signaling. Three distinct lines of evidence suggest that BCL6 is one of these factors. First, loss of BCL6 resulted in a higher frequency of apoptosis among brown adipocytes, leading to reduction of BAT mass during dormancy. Second, loss of BCL6 resulted in elevated expression of pro-apoptotic genes. And third, BCL6 directly bound near a subset of pro-apoptotic genes, including *Bmf*, *Egln3*, and *Dapk1*, indicating a mechanism of direct repression. Thus, in the absence of adrenergic signals, BCL6 acts in a cell-autonomous manner to promote survival of brown adipocytes.

Several characteristics set BCL6 apart from the "classical" transcriptional regulators of brown adipocyte commitment, differentiation, and activation, such as early b cell factor 2 (EBF2), peroxisome proliferator activated receptor γ (PPARγ), estrogen related receptor α/γ (ERRα/γ), CCAAT/enhancer binding protein (C/EBPβ), and interferon regulated factor 4 (IRF4), (Loft et al., 2017; Wang and Seale, 2016). First, unlike transcription factors that act downstream of adrenergic signals, BCL6 operates in a parallel pathway. As a consequence, it is functionally more important during dormancy when sympathetic input into BAT is largely absent (Figure 2.14). Second, unlike ERRα/γ, BCL6 is dispensable for expression of genes involved in oxidative phosphorylation and electron transport, but similarly required for supporting uncoupled respiration and fatty acid oxidation in the mitochondria (Figure 2.14). Third, BCL6 directly binds to only a small number of genes linked to thermogenic metabolism, such as *Acot1* and *Atp5g1*, where it acts as a transcriptional repressor to sustain thermogenic capacity during dormancy. Fourth, BCL6 positively regulates many thermogenic genes by an indirect mechanism, possibly by activating ERRs. The potential regulation of ERR transcriptional activity by BCL6 is intriguing, because it might represent a point of convergence with the adrenergic signaling

pathway, which is known to induce expression and activity of ERRs (Giguere, 2008). In this scenario, BCL6 might be important for maintaining basal activity of ERRs during dormancy, whereas full activation of ERRα/γ by adrenergic stimuli is necessary for adaptation to environmental cold. In support of this model, the molecular, histological, and physiological phenotypes of mice lacking ERRα/γ or ERRγ in their brown adipocytes partially overlap with those observed in dormant BAT of *Bcl6*$^{f/f}$*Ucp1*^{Cre} mice (Ahmadian et al., 2018; Brown et al., 2018). Although these data suggest convergence of BCL6 and ERRs in expression of thermogenic genes in dormant brown adipocytes, elucidation of the precise mechanisms will require additional investigation in the future.

The chromatin state of differentiated cells is known to be highly stable and can be used to distinguish one differentiated cell type from another (Feil and Fraga, 2012). For example, in response to changes in environmental temperature, brown adipocytes dramatically alter their morphology and gene expression, but maintain a relatively stable chromatin state (Roh et al., 2018). Although this epigenetic state of brown adipocytes is established during differentiation in an EBF2-dependent manner (Shapira et al., 2017), it was not known what factors might be involved in its stable maintenance across different thermal conditions. The data presented here demonstrate that BCL6 contributes to the maintenance of the stable epigenetic landscape of brown adipocytes. BCL6 accomplishes this by simultaneously reinforcing brown-specific enhancers while opposing white-specific enhancers in dormant BAT. Since ~17% of the active enhancers regulated by BCL6 were white-specific, it suggests that BCL6, in part, maintains the cellular identity of brown adipocytes by repressing alternative cellular fates. In support of this hypothesis, profiling of genes comprising the BATLAS, which can be used to assess enrichment of white or brown adipocytes in adipose tissues (Perdikari et al., 2018), revealed a dramatic shift

in the cellular identity of iBAT of *Bcl6*$^{f/f}$*Ucp1*^{Cre} mice. In particular, we found that expression of white adipocytes makers was increased, whereas expression of brown adipocyte selective genes was decreased in iBAT of *Bcl6*$^{f/f}$*Ucp1*^{Cre} mice. Together, these findings demonstrate that the transcriptional repressor BCL6 is critically important for the maintenance of cellular identity of brown adipocytes, but not for their differentiation or thermogenic activation by adrenergic stimuli.

Previous studies have suggested that UCP1 not only provides a defense against environmental cold (Enerback et al., 1997), but also contributes to diet-induced thermogenesis to mitigate the deleterious effects of obesogenic diets (Feldmann et al., 2009). This anti-obesity effect of UCP1 was originally uncovered by housing *Ucp1*$^{-/-}$ mice at thermoneutrality and challenging them with a high fat diet. Since thermoneutral mice do not engage in cold-induced thermogenesis, the increased weight gain observed in *Ucp1*$^{-/-}$ mice was attributed to increased metabolic efficiency stemming from absence of diet-induced thermogenesis (Feldmann et al., 2009). In contrast, we found that while BCL6 was essential for maintenance of thermogenic fitness during transition from thermoneutrality to cold, it was dispensable for diet-induced thermogenesis in mice housed at thermoneutrality. Because a similar disconnect between cold- and diet-induced thermogenesis has been observed in other mouse models, including mice lacking *Prdm16*, *ERRα/γ*, *Cpt2*, and *Hdac3* in their brown adipocytes (Brown et al., 2018; Emmett et al., 2017; Harms et al., 2014; Lee et al., 2016; Lee et al., 2015a), it suggests that increased metabolic efficiency and predisposition to diet-induced obesity might be a unique feature of *Ucp1*$^{-/-}$ mice. In this regard, recent studies demonstrate that, in addition to absence of UCP1, expression and activity of the mitochondrial respiratory chain is severely reduced in BAT of *Ucp1*$^{-/-}$ mice (Kazak et al., 2017; Odegaard et al., 2016). Together, these findings suggest that

the metabolic phenotypes observed in *Ucp1*$^{-/-}$ mice might not accurately reflect the putative functions of BAT in diet-induced thermogenesis, an issue that remains controversial in the literature (Kozak, 2010). Because there is immense clinical interest in therapeutic targeting of BAT for the treatment of obesity and metabolic diseases (Enerback, 2010; Kajimura et al., 2015; Tseng et al., 2010; Vosselman et al., 2013), additional studies will be necessary to validate the functions of BAT in diet-induced thermogenesis in both mice and humans.

In summary, our studies reveal an unanticipated role for the transcriptional repressor BCL6 in the maintenance of thermogenic capacity of brown adipocytes during dormancy. We find that, unlike other transcription factors that control commitment, differentiation, and activation of brown adipocytes, the transcriptional repressor BCL6 is specifically required for the maintenance of thermogenic competence in dormant BAT (Figure 2.14). Regulation by BCL6 involves both direct repression of pro-apoptotic genes and genes that oppose thermogenic metabolism, and indirect activation of thermogenic genes, possibly via activation of ERRs. Thus, the action of BCL6 during dormancy parallels the action of adrenergic signaling during cold adaptation, serving to stabilize thermogenic capacity during temperature transitions.

Acknowledgements

We thank members of the Chawla laboratory discussions and comments, and X. Cui for assistance with mouse husbandry. The authors' work was supported by grants from NIH (DK094641, DK101064) to A.C. and AHA Predoctoral Fellowship (18PRE34080250, 16PRE26960008) to V.K. The authors declare that they have no competing financial interests.

Materials and Methods

Mice. All experiments involving mice were conducted under an approved Institutional Animal Care and Use Committee (IACUC) protocol at University of California, San Francisco (UCSF). All mice were congenic to the C57BL6/J background. Both male and female mice at 8-9 weeks of age (unless otherwise indicated) were used in these studies. C57BL/6J (Stock No. 000664), $Bcl6^{f/f}$ (Stock No. 023727), $Ucp1^{Cre}$ (Stock No. 024670), $Myf5^{Cre}$ (Stock No. 007893), and $Adipoq^{Cre}$ (Stock No. 028020) mice were purchased from Jackson Laboratories and bred in our vivarium. $Bcl6^{f/f}$ mice were backcrossed >10 generations onto the C57BL/6J *Nnt* null background prior to assembly with the various Cre recombinase lines, which were congenic with the C57BL/6J background. For experiments at 22º C (room temperature), mice were housed in cages placed in racks exposed to room air. For experiments at 30º, 10º, or 4º C, mice were housed in cages inside temperature-controlled chambers (Darwin Chambers, Powers Scientific) set to the indicated temperature. All mice had free access to food and water (with the exception of 6 hour fasting prior to glucose and insulin tolerance tests) and experienced a 12-hour light:dark cycle. For all *in vivo* studies, cohorts of greater than or equal to three mice per genotype or treatment were assembled, and experiments were repeated two to three independent times.

Cold tolerance tests. Cold tolerance tests were performed as described previously (Lee et al., 2015b). Briefly, mice were housed within a temperature-controlled chamber (Powers Scientific) set to 10º or 4º C, two mice per cage, with free access to food and water. Mouse core (rectal) temperature was measured hourly using a BAT-12 microprobe thermometer with RET-3

thermocouple (Physitemp). As per IACUC guidelines, ‘‘survival’’ was defined as a core temperature >28º C. The same housing conditions were used for 48-hour cold exposure studies.

Diet-induced thermogenesis. For studies on diet-induced thermogenesis, mice were bred and housed at 30ºC and fed high fat diet (HFD) *ad libitum* starting at 10 weeks of age. HFD consisted of 20% protein, 60% fat, and 20% carbohydrates (Research Diets # D12492i), while normal chow diet consisted of 25% protein, 13% fat, and 62% carbohydrates (Pico Lab #5053). Mice were weighed once per week and maintained on HFD for total duration of 14 weeks. Glucose and insulin tolerance tests were conducted at the start of the 13^{th} and 14^{th} weeks, respectively, and body composition (lean and fat mass) was analyzed by dual-energy x-ray absorptiometry (DEXA, GE Lunar PIXImus) during the 14^{th} week. Mice were sacrificed and adipose tissues isolated after the 14^{th} week. For glucose tolerance test, fasted mice (6 hour fast from 9 a.m. to 3 p.m.) were given an intraperitoneal injection of glucose (1.5 g/kg) and tail blood glucose was measured at 15, 30, 45, 60, and 120 min after injection (Bayer Contour blood glucose meter). For insulin tolerance test, fasted mice (6 hour fast from 9 a.m. to 3 p.m.) were given an intraperitoneal injection of insulin (1 unit/kg, Lilly, Eli and Company #1325240) and blood glucose was measured at 15, 30, 45, and 60 min after injection.

Energy expenditure. A temperature-controlled CLAMS chamber (Columbus Instruments) was used to quantify oxygen consumption, carbon dioxide emission, food and water consumption, and locomotor activity of individual mice. Mice were acclimated to the chamber for 24 hours prior to recording. Mice were given an intraperitoneal injection of norepinephrine (1 mg/kg in

saline, Sigma-Aldrich #N5785), and respiration rate was recorded every 4.5 min. Respiratory exchange ratio (RER) represents the ratio of CO_2 produced and O_2 consumed.

β3-adrenergic receptor signaling. For *in vivo* studies of β3-adrenergic receptor signaling, mice born and raised at 30º C were given an intraperitoneal injection of the β3 agonist CL-316,243 (1 mg/kg in saline, Sigma-Aldrich #C5976). iBAT was isolated 30 minutes after injection and processed for immunoblotting.

Immunoblotting. To prepare whole cell extracts from tissues, frozen tissue samples were placed into 2 mL tubes containing 0.5 mL of modified RIPA buffer (50 mM Tris-Cl, pH 7.5, 150 mM NaCl, 1% Nonidet P-40 substitute, 0.1% SDS, 0.5% sodium deoxycholate, 1 mM EDTA, with 1:200 protease inhibitor cocktail (Sigma-Aldrich #P8340)) and a metal bead, and homogenized in a TissueLyser II (Qiagen) for 120 seconds at 30 Hz. Nuclear extracts from tissues and cultured brown adipocytes were prepared using NE-PER Nuclear and Cytoplasmic Extraction Reagents (Thermo Scientific #78833) according to the manufacturer's instructions. Protein concentration was measured with a Pierce BCA Protein Assay Kit (Thermo Scientific #23225) according to the manufacturer's instructions. Protein (5-30 μg) was diluted in sample buffer (62.5 mM Tris-Cl, pH 6.8, 10% glycerol, 2% SDS, 5% 2-mercaptoethanol, 0.008% bromophenol blue), incubated at 90º C for 5 minutes, separated by SDS–PAGE, and transferred to a 0.45 μm nitrocellulose membrane (Bio-Rad #1620115). The membrane was blocked with 5% nonfat dry milk in PBS containing 0.1% Tween-20 for 30 min, and probed with the primary and HRP-conjugated secondary antibodies diluted in PBS containing 0.1% Tween-20 and 2% BSA (see Table 2.5 for full list of

antibodies). HSP90a/b and Lamin B1 were used as loading controls for whole cell extracts and nuclear extracts, respectively. Immunoblotted proteins were detected on HyBlot CL autoradiography film (Denville Scientific #1159M39) using ProSignal Pico chemiluminescent substrate (Prometheus Protein Biology Products #20-300) and Mini-Medical 90 X-ray Film Processor (AFP Imaging #9992305300).

RNA isolation and quantitative RT-PCR. For RNA isolation from frozen tissues, samples were placed in tubes containing 1 mL of Trisure (Bioline #38032) and a metal bead, and homogenized in a TissueLyser II (Qiagen) for 120 seconds at 30 Hz. Samples were centrifuged and the Trisure supernatant was collected for RNA isolation according to the manufacturer's instructions, with 1-bromo-3-chloropropane used instead of chloroform. RNA concentration was measured with a Nanodrop 2000 spectrophotometer (Thermo Fisher Scientific). 1 μg of RNA was used as starting material for cDNA synthesis with qScript cDNA SuperMix (Quantabio #95048) according to the manufacturer's instructions. qPCR was performed with a Sensifast SYBR No-ROX kit (Bioline #098020) on a CFX384 Real-Time System (Bio-Rad) according to the manufacturer's instructions. The final concentration of primers in each reaction was 400 nM. See Table 2.6 for full list of primers used in this study. Reactions were performed in duplicate, and for each sample the average cycle threshold value (CT) of the reference mRNA (*36b4*) was subtracted from the average CT of the target mRNA to yield the ΔCT value. The relative difference in target mRNA abundance between samples was calculated by the following formula, in which X equals the ratio of target mRNA abundance in sample 1 over target mRNA abundance in sample 2:

$$X=2^{-(\Delta CT[sample1]-\Delta CT[sample2])}$$

Acyl-CoA thioesterase assay. Acyl-CoA thioesterase activity in cytosolic and mitochondrial fractions was measured as described previously with the following modifications (Franklin et al., 2017). 50-70 μg of protein were diluted in assay buffer (50 mM KCl, 10 mM HEPES, 50 μM DTNB) to a final volume of 150 μl in a microwell plate. Baseline absorbance at 405 nm was measured, and 40 μM of palmitoyl-CoA was added. The sample was incubated at 37ºC and absorbance at 405 nm was measured every min for 9 min. A CoA standard curve (0-15 μM) was used to convert change in absorbance to change in CoA concentration. Thioesterase activity was calculated as μmoles CoA/minute/μg of sample protein.

Complex V activity assay. Complex V activity was measured with a MitoCheck Complex V Activity Assay Kit (Cayman Chemical Company #701000) according to the manufacturer's instructions. 5 μg of isolated mitochondria were used per reaction. Activity was measured for 20 min, and non-specific activity was measured in control reactions that received 10 μg/ml oligomycin (Complex V inhibitor, Sigma-Aldrich #O4876). An NADH standard curve (0, 50, 150 μg/mL in assay buffer) was used to convert change in absorbance to change in ATP concentration. Non-specific activity was subtracted and Complex V activity was calculated as μmoles ATP/min/mg of protein.

Quantification of mitochondrial and genomic DNA. Total DNA from iBAT samples was isolated using a DNeasy Blood & Tissue kit (Qiagen #69504) as per the manufacturer's instructions. Samples were treated with RNase cocktail (Invitrogen #AM2286) for 2 min to degrade RNA. Relative abundance of mitochondrial DNA (mtDNA) and nuclear DNA (nucDNA) was

determined by qPCR according to the protocol described above for RT-qPCR, using primers specific for *Ndufvb* (nuclear gene) and *Mt-co1* (mitochondrial gene). Reactions were performed in duplicate, and the mtDNA/nucDNA copy number ratio was calculated using the following formula, in which "CT" is the average cycle threshold value for the amplification of the indicated gene:

$$\text{mtDNA/nucDNA} = 2^{(\text{CT}[\textit{Ndufvb}]-\text{CT}[\textit{Mt-co1}])}$$

Histology, immunofluorescence, and TUNEL. Freshly isolated BAT was fixed in 10% formalin for 24-48 hours at room temperature. Tissues were embedded in paraffin, sectioned at 5 µm thickness, deparaffinized with Histoclear (National Diagnostics #HS-200) and rehydrated through graded concentrations of ethanol in water. Sections were then stained with hematoxylin and eosin, or processed for immunofluorescence or TUNEL. For staining of Ki67 and MCT-1, sections were permeabilized for 8 min at room temperature with 0.1% Triton X–100 and 0.1% sodium citrate, washed in phosphate-buffered saline (PBS), and blocked with PBS containing 2.5% normal donkey serum and 2.5% normal goat serum. Sections were incubated overnight at 4ºC with primary antibodies diluted 1:200 in blocking buffer. See Table 2.5 for full list of antibodies used in this study. Sections were washed with PBS and incubated for 1 hour at room temperature with secondary goat anti-chicken IgY conjugated to Alexa-Fluor-555 (Invitrogen #A-21437) and goat anti-rabbit IgG conjugated to Alexa-Fluor-488 (Invitrogen #A-11008) diluted 1:250 in blocking buffer. Terminal deoxynucleotidyl transferase dUTP nick end labeling (TUNEL) was done with an In Situ Cell Death Detection Kit (Roche #11684795910) as per the manufacturer's instructions. For pretreatment of the tissue sections, the permeabilization solution was used. Sections were then mounted with DAPI Fluoromount-G (SouthernBiotech #0100-20). Immunofluorescence and TUNEL samples were imaged on an EVOS FL Cell Imaging System

(Invitrogen) at 20x magnification and analyzed in ImageJ (NIH). Positive staining for Ki67 or TUNEL was identified as specific signal overlapping DAPI staining. H&E samples were imaged on an EVOS XL Core Configured Microscope (Invitrogen) at 20x magnification, and lipid droplet diameter was measured with ImageJ.

Cultured brown adipocytes. SV40 large T antigen-immortalized mouse BAT preadipocytes were obtained from Dr. Patrick Seale's laboratory. Preadipocytes were grown and differentiated as described previously with minor modifications (Klein et al., 2002). The base media consisted of DMEM (4.5 g/L glucose, Gibco #11995065) supplemented with 10% FBS (heat-inactivated, Gemini Bio-Products #100-106), penicillin/streptomycin, and 20 mM HEPES. Preadipocytes were grown to confluence and given induction cocktail containing 43 nM insulin (Gemini Bio-Products #800-112), 1 nM T3 (Sigma-Aldrich #T2877), 125 nM indomethacin (Sigma-Aldrich #I7378), 500 nM dexamethasone (Sigma-Aldrich #D4902), and 0.5 mM IBMX (Sigma-Aldrich #I5879) for 48 hours. Afterwards, they were maintained with 860 nM insulin and 1 nM T3 and media was changed every 48 hours. Differentiation was considered complete after 6 days of maintenance.

Flow cytometric analysis of stromal vascular fraction of BAT. Freshly isolated BAT was finely minced with scissors and incubated in digest buffer consisting of Ham's F10 (Corning #10070CV) with 15 mg/ml BSA and 1 mg/ml Collagenase Type 1 (Worthington #LS004197) for 30 min at 37ºC with shaking and occasional vortexing. The digested samples were then filtered through a 70 μm strainer and fixed with BD Fixation/Permeabilization Solution (BD

Biosciences). Cells were washed with Perm/Wash buffer (BD Biosciences) and incubated with fluorochrome-conjugated antibodies against surface antigens in Perm/Wash buffer on ice for 15 min. See Table 2.5 for full list of antibodies used in this study. Stained cells were analyzed with a BD FACSVerse flow cytometer. The data was analyzed with FlowJo (FlowJo, LLC). Gates were constructed to identify target populations based on surface marker staining. Immune cells were identified as $CD45^+$. T cells were identified as $CD11b^-$, $CD3\varepsilon^+$ and either $CD4^+$, $CD8^+$, or $CD4^+CD25^+$ (regulatory T cells). Myeloid cell subsets were identified as $F4/80^+$ (macrophages), $F4/80^+CD206^+$ (M2 macrophages), $CD11c^+$ (dendritic cells and some macrophages), $CD115^+$ (monocytes), or $Ly6G^+$ (neutrophils).

Quantification of DNA in adipocyte fraction. Freshly isolated mouse iBAT was minced with a razor blade into small fragments (1-2 mm diameter) and placed into digestion buffer (120 mM NaCl, 4.7 mM KCl, 2.2 mM CaCl2, 10 mM HEPES, 1.2 mM KH2PO4, 1.2 mM MgSO4, 2.5 mM glucose, 4% crude bovine serum albumin, 1 mg/mL Collagenase (Sigma-Aldrich C2139), pH 7.2). The mixture was incubated at 37ºC for 45 minutes while shaking (100 rpm), with brief vortexing every 15 minutes. The mixture was then passed through a 100 µm strainer, washed with additional digestion buffer, and centrifuged at 50 g for 7 minutes at 4ºC. The floating fraction (adipocytes) was carefully collected and washed again with digestion buffer. The floating adipocyte fraction was collected and DNA was isolated using the DNeasy Blood & Tissue Kit (Qiagen), according to the manufacturer's instructions (incubation at 56ºC for 30 minutes). DNA concentrations were measured with a Qubit dsDNA High Sensitivity Assay Kit and a Qubit 2.0 fluorimeter (Thermo Fisher Scientific).

Electron microscopy. Freshly isolated mouse iBAT was cut with scissors into small fragments (1-2 mm diameter). These specimens were incubated in 2.5% (each) Formaldehyde/Glutaraldehyde in 0.1M sodium cacodylate buffer, pH 7.4 (Electron Microscopy Sciences #15949) for 4 hours at room temperature. Afterwards, specimens were stored at 4ºC in the same buffer for up to three weeks and then delivered to the Electron Microscope Lab at UC Berkeley for all subsequent procedures. Specimens were further washed and post-fixed with a sodium cacodylate buffer containing 1% osmium tetroxide and 1.6% potassium ferricyanide. After rinses, specimens were treated with 1.0% uranyl acetate and dehydrated with increasing concentrations of acetone. They were then infiltrated and embedded in resin. 70 nm sections were cut on a Reichert Ultracut E microtome and collected on Maxtaform copper slot grids (2 × 1-mm oval hole) that had been coated with 0.5% Formvar. Sections were post-stained with uranyl acetate and lead citrate. Samples were examined and imaged under a FEI Tecnai 12 Transmission Electron Microscope at 120KV. Mitochondrial cristae interval and cross-sectional area were measured with ImageJ.

Isolation of mitochondria and cytosolic fractions. Mouse iBAT was minced with scissors, placed into a glass Dounce homogenizer (DWK Life Sciences #885300-0002) with 1 mL of isolation buffer (250 mM sucrose, 10 mM HEPES, 1 mM EGTA, 0.3% BSA (fatty-acid free), pH 7.2) and homogenized with 10 strokes of the "B" pestle. The sample was centrifuged at 8,500g for 10 min at 4ºC. The resulting supernatant was kept as the cytosolic fraction and the pellet was resuspended in 1 mL isolation buffer (without BSA). The resuspended sample was then centrifuged at 700g for 10 min at 4ºC, and the resulting supernatant was isolated and centrifuged

at 8,500g for 10 min at 4ºC to pellet the mitochondria. The mitochondria were washed once more in isolation buffer (without BSA), and used for assays or stored as a pellet at -80ºC.

Tissue oxygen consumption. For measurement of BAT oxygen consumption, the freshly isolated tissue was finely minced and the fragments were resuspended in tissue respiration buffer (PBS containing 20 mg/ml BSA, 25 mM glucose, and 1 mM pyruvate). The rate of oxygen consumption was recorded with a Mitocell S200 respirometry system (Strathkelvin Instruments) at 22º C. Data were analyzed with Strathkelvin 782 Oxygen System software (version 4.1).

Mitochondrial oxygen consumption. For measurement of mitochondrial oxygen consumption, freshly isolated mitochondria were washed with Buffer 1 (100 mM KCl, 20 mM K+-TES, 1 mM EDTA, 0.6% fatty-acid-free BSA, pH 7.2), centrifuged, and resuspended in Mitochondrial Respiration Buffer (125 mM sucrose, 20 mM K+-TES, 2 mM MgCl2, 1 mM EDTA, 4 mM KH_2PO_4, 0.1% fatty-acid-free BSA, 3 mM malate, 5 mM L-carnitine, pH 7.2). The rate of oxygen consumption was recorded with a Mitocell S200 respirometry system (Strathkelvin Instruments) at 37º C. Palmitoyl-CoA (30 µM), guanosine diphosphate (GDP, 2 mM), and carbonyl cyanide-4-(trifluoromethoxy)phenylhydrazone (FCCP, 1.4 µM) were sequentially added to the respiration chamber with 45 second intervals. The rate of oxygen consumption after the addition of each reagent was determined with Strathkelvin 782 Oxygen System software (version 4.1). The rates were normalized to mitochondrial protein amount, which was determined by isolation in RIPA buffer and quantification with a Pierce BCA Protein Assay Kit, as described above for immunoblotting.

Thermal imaging of interscapular region. At least 3 days prior to the experiment, mice were anesthetized with Isoflurane and the interscapular skin (above the iBAT) was depilated with Nair to expose the skin surface. On the day of the experiment, the baseline temperature of the interscapular region was recorded with an E60 FLIR infrared camera. Mice were then moved to pre-chilled cages at 4ºC for 15 minutes (one mouse per cage), and the temperature was recorded again.

Chromatin immunoprecipitation (ChIP). Anti-BCL6, anti-H3K27ac, and anti-ERRα chromatin immunoprecipitation was performed in isolated mouse iBAT from 9-week old male *Bcl6*$^{f/f}$ and *Bcl6*$^{f/f}$ *Ucp1*^{Cre} mice bred and housed at 30º C (and also at 22º C for anti-H3K27ac). Fresh or frozen iBAT samples were minced with a razor blade and fixed in 1% formaldehyde in PBS for 20 min at room temperature, followed by addition of 125 mM glycine. The samples were then collected in cell lysis buffer (50 mM Tris-Cl, pH 8.0, 140 mM NaCl, 1 mM EDTA, 10% glycerol, 0.5% Nonidet P-40 substitute, 0.25% Triton X-100, 1:200 protease inhibitor cocktail (Sigma-Aldrich #P8340)) and homogenized in a glass Dounce homogenizer (15 strokes with type "B" pestle). Following centrifugation, the nuclear pellet was resuspended in nuclear lysis buffer (10 mM Tris-Cl, pH 8.0, 1 mM EDTA, 0.5 mM EGTA, 0.2% SDS, 1:200 protease inhibitor cocktail) and incubated for 20 min on ice. Samples were sonicated with an XL-2000 sonicator (QSonica) for 12 rounds of 20 seconds on setting 2, with 60 seconds on ice between rounds, to generate fragments of 150-300 bp. Sonicated samples were centrifuged, and the supernatants were diluted two-fold with Dilution Buffer (16.7 mM Tris-Cl, pH 8.1, 0.01% SDS, 1.1% Triton X-100, 1.2 mM EDTA, 167 mM NaCl, 1:200 protease inhibitor cocktail) and

incubated with either 2 μg of anti-BCL6 antibody (Cell Signaling Technology #5650), 2 μg of anti-H3K27ac antibody (Abcam #ab4729), or 1.5 μg of anti-ERRα antibody (Cell Signaling Technologies #13826S) overnight at 4ºC, then with 50 μl of Protein G Dynabeads for 4 hours at 4ºC. Beads were washed on a magnetic stand twice with Buffer 1 (0.1% SDS, 0.1% sodium deoxycholate, 1% Triton x-100, 0.15 M NaCl, 1 mM EDTA, 20 mM Tris-Cl, pH 8.0), once with Buffer 2 (same as Buffer 1 but with 0.5 M NaCl), once with Buffer 3 (0.25 M LiCl, 0.5% sodium deoxycholate, 0.5% Nonidet P-40 substitute (Fluka #74385), 1 mM EDTA, 20 mM Tris-Cl, pH 8.0), twice with Buffer 4 (1 mM EDTA, 20 mM Tris-Cl, pH 8.0), and then resuspended in elution buffer (50 mm Tris-Cl, pH 8.0, 10 mm EDTA, 1% SDS). Beads in elution buffer were incubated at 65ºC for 10 min, and the supernatant was collected. Elution was repeated a second time and the combined eluates were incubated at 65ºC overnight to reverse crosslinks. Samples were treated with RNAse cocktail (Invitrogen #AM2286, 1 hour at 37ºC), Proteinase K (Promega #V302B, 2 hours at 65ºC), and DNA was isolated with a Qiaquick PCR Purification Kit (Qiagen #28104) according to the manufacturer's instructions. DNA concentrations were measured with a Qubit dsDNA High Sensitivity Assay Kit and a Qubit 2.0 fluorimeter (Thermo Fisher Scientific).

Preparation of libraries for Next Generation Sequencing. For construction of RNA-Seq libraries, a TruSeq Stranded mRNA Library Prep Kit (Illumina #RS-122-2101) was used according to the manufacturer's instructions. 2 μg of total RNA was used as the starting material. PolyA-containing RNA was purified and fragmented, followed by first and second strand cDNA synthesis, adapter ligation, and PCR amplification (15 cycles). A library size of 200-300 bp was verified by agarose gel electrophoresis and library concentration was measured with a Qubit

dsDNA High Sensitivity Assay Kit and a Qubit 2.0 fluorimeter (Thermo Fisher Scientific). For construction of ChIP-Seq libraries, the same kit was used with several modifications. 10 ng of ChIP DNA was used as input and treated with end repair enzymes (Thermo Scientific #K0771) before proceeding to the 3' adenylation and adapter ligation steps. Subsequently, samples were resolved on a 2% agarose gel containing SYBR Gold Stain (Life Technologies # S11494), visualized by ultraviolet illumination, and gel sections containing 250-500 bp fragments were excised and DNA extracted with a Gel DNA Recovery Kit (Zymo Research # D4007). Libraries were then amplified by PCR and quantified as described above.

Next Generation Sequencing. Sequencing was performed with the assistance of the Molecular Core Facility at the San Francisco VA Medical Center. Libraries were pooled (up to 24 per run), denatured with NaOH, diluted to 1.8 pM, and sequenced on a NextSeq 500 Sequencing System (Illumina) with a NextSeq 500/550 High Output v2 kit (75 cycles, Illumina #FC-404-2005) in single-read mode.

Statistical analysis. Data were analyzed using Prism (GraphPad) and are presented as mean±SEM. Unless otherwise noted, all measurements were taken from distinct biological samples. Statistical significance was determined using the unpaired two-tailed Student's t test or Mann-Whitney U test for single variables and two-way ANOVA followed by Bonferroni post-tests for multiple variables. For survival experiments, statistical significance was determined using the Mantel-Cox log-rank test. A p value of <0.05 was considered to be statistically

significant and is listed. Otherwise, p values are presented as *p < 0.05, **p < 0.01, or ***p < 0.001.

RNA-seq analysis. Raw sequence data were pseudoaligned to the mouse transcriptome (mm10, UCSC annotation) using Kallisto (Bray et al., 2016). Differential expression, defined as a fold change ≥1.5 and an adjusted p-value ≤0.05, was determined using DESeq2 (Love et al., 2014). Genes with extremely low expression (average normalized count of 20 or less) were excluded from the analysis. Principal Components Analysis (PCA) plots and heat maps were generated in R (Team, 2008). Venn Diagrams were generated using BioVenn (Hulsen et al., 2008). Gene ontology enrichment analysis was performed using DAVID Bioinformatics Resources 6.8 (Huang da et al., 2009).

ChIP-seq analysis. Raw sequence data were aligned to the mouse genome (mm10) using Bowtie2 (Langmead and Salzberg, 2012). For BCL6 ChIP-Seq, Homer was used to identify and annotate peaks (corresponding to BCL6 binding sites) in pooled BAT samples from *Bcl6*$^{f/f}$ mice (n=5), with pooled BAT samples from *Bcl6*$^{f/f}$ *Ucp1*^{Cre} mice (n=2) serving as a negative control (default settings) (Heinz et al., 2010). For H3K27ac and ERRα ChIP-seq, Homer was used to identify and annotate peaks in 3 and 4 biological replicates per condition, respectively, and DESeq2 was used to compare enrichment at each peak in *Bcl6*$^{f/f}$ and *Bcl6*$^{f/f}$ *Ucp1*^{Cre} BAT samples. Differential H3K27ac and ERRα enrichment was defined as a fold change ≥2 and ≥1.5, respectively (false discovery rate of ≤0.05). Homer was also used for sequence motif enrichment analysis (default settings). DeepTools was used to generate heat maps of differentially abundant

peaks (Ramirez et al., 2016). BigWig files were generated with the bedGraphToBigWig program (Kent et al., 2010) and visualized with the UCSC Genome Browser (Kent et al., 2002).

For analysis of brown and white adipocyte-specific enhancers, the coordinates of previously characterized adipocyte H3K27ac and H3K4me1 peaks were obtained from the laboratory of Dr. Evan Rosen (Roh et al., 2018), and H3K27ac ChIP-seq data for brown and white adipocytes (from 30ºC-adapted mice) were downloaded from Sequence Read Archive (SRA) (#SRP126748). We defined active enhancers as H3K27ac peaks that overlap at least one H3K4me1 peak, as determined by BEDtools (Quinlan and Hall, 2010). Active enhancers were classified as brown or white adipocyte-specific if they had 4-fold or greater enrichment of H3K27ac in the corresponding cell type (relative to the other), as determined by DESeq2 (false discovery rate ≤0.05). The list of brown and white adipocyte-specific enhancers is provided in Dataset S1. Similarly, active enhancers were classified as BCL6-regulated if the difference in H3K27ac enrichment between *Bcl6*$^{f/f}$ and *Bcl6*$^{f/f}$ *Ucp1*^{Cre} samples exceeded 1.5-fold (false discovery rate ≤0.05). Venn Diagrams were generated using BioVenn (Hulsen et al., 2008).

For the initial analysis of ERRα and ERRγ binding sites in BAT (Figure 6 C-E), we downloaded ChIP-Seq data for ERRα in BAT (SRA #SRP077663) and ERRγ in BAT (SRA #SRP063705). Binding sites were identified as described above for BCL6 ChIP-Seq. Overlap between ERRα/ERRγ binding sites and H3K27ac peaks was determined with BEDtools (Quinlan and Hall, 2010).

Data and software availability. The RNA-seq and ChIP-seq data has been deposited at GEO (https://www.ncbi.nlm.nih.gov/geo/) under the accession number GEO: GSE122746.

CHAPTER 3: DISCUSSION

This Chapter will serve as an extension of the Discussion section in Chapter 2, addressing many of the important questions arising from analysis of our research results. It will review the key insights, their significance for the field of thermogenesis, and also propose future directions for investigation.

A unique role for BCL6 in maintenance of thermogenic capacity specifically during dormancy

To our knowledge, we are the first to report a brown adipocyte transcription factor that is specifically required for maintenance of thermogenic capacity during dormancy. This result initially led us to hypothesize that BCL6 is a dormancy-specific factor that is selectively upregulated upon transition from cold to warmth. However, we did not observe a significance difference in BCL6 mRNA or protein abundance between dormant and cold-adapted iBAT, and *in vitro* we did not observe changes in BCL6 protein abundance or binding to target genes in response to adrenergic signaling (data not shown), suggesting that BCL6 action is independent of temperature. This is also supported by the observation that many changes in gene expression that are observed in BCL6-deficient iBAT during dormancy (30º C) are also observed in BCL6-deficient iBAT during cold adaptation (22º C), although usually to a lesser degree. So why do we only observe defective thermogenic capacity after initiation of dormancy? The most plausible explanation for this result is that the adrenergic signaling pathway, which is constantly active in the setting of cold adaptation, is sufficient to compensate for the loss of BCL6. The strong induction of thermogenic capacity as a result of chronic adrenergic signaling overcomes the smaller influence of BCL6 deletion, resulting in a competent thermogenic response in the BCL6 knockout at 22ºC. Only after removal of adrenergic signaling, by housing at 30ºC, does the role of BCL6 become essential.

Regulation of brown adipocyte survival by BCL6

The influence of BCL6 on thermogenic capacity can be divided into two distinct categories: regulation of brown adipocyte survival and regulation of thermogenic gene expression. The positive effect of BCL6 on cell survival has been observed in other cell types, including germinal center B cells, in which BCL6 represses pro-apoptotic genes like *TP53*, *ATR*, and *CHEK1* (Basso et al., 2010; Ci et al., 2009). Thus, the observation of reduced brown adipocyte abundance and elevated apoptosis in BCL6-deficient dormant BAT was not particularly surprising. However, the mechanisms by which BCL6 regulates cell survival in brown adipocytes and germinal center B cells appear to be distinct. For example, in BCL6-deficient iBAT we did not observe altered expression of *Tp53, Atr, Chek1, Bcl2,* and other apoptosis-related genes that are known to be regulated by BCL6 in germinal center B cells (data not shown). Instead, we saw upregulation of other pro-apoptotic genes, including *Bmf, Egln3, Dapkl, and Wdr92,* which are directly bound by BCL6. This leads us to conclude that BCL6 regulates cell survival by different mechanisms in a cell type-dependent manner. While our evidence points to direct repression of *Bmf, Egln3,* and *Dapk1* by BCL6, we have not definitively tested this idea. In future studies, this prediction may be tested by mutating the BCL6 binding sites near these genes and determining if these mutations disrupt the ability of BCL6 to regulate the expression of the genes.

The observation that BCL6 is required for brown adipocyte survival only in the dormant state, but not the cold-adapted state, is consistent with the earlier proposition that cold-induced adrenergic signaling compensates for the loss of BCL6. Adrenergic signaling is known to positively regulate brown adipocyte abundance by multiple mechanisms, including enhancement of cell survival (Lindquist and Rehnmark, 1998) and stimulation of precursor proliferation and

differentiation (Lee et al., 2015c). Presumably the stimulation of these pathways in response to cold is sufficient to overcome the negative impact of BCL6 ablation on cell survival. Interestingly, the absence of BCL6 in dormant iBAT leads to only a partial reduction in iBAT size, even after 8 weeks of housing at 30ºC. This indicates that BCL6 is not absolutely required for brown adipocyte survival even after prolonged absence of adrenergic signaling. This may be a consequence of heterogeneity in the brown adipocyte population with respect to sensitivity to apoptosis. Those brown adipocytes which are more sensitive to apoptotic stimuli, perhaps because they have reduced access to circulating pro-survival factors like insulin (Guerra et al., 2001), may be the ones lost in the absence of BCL6, while the rest are able to survive. The existence of such heterogeneity in the brown adipocyte population has not been previously demonstrated, and may be an interesting topic to explore with the aid of single-cell transcriptome profiling technology.

Elevated inflammatory response signature in BCL6-deficient iBAT

Analysis of gene expression changes in BCL6-deficient iBAT revealed significant upregulation of genes linked to inflammation and immune cell function. Previous studies had observed increased inflammation in models of BAT dysfunction, including *Ucp1* global knockout and BAT-specific *Cpt2* knockout mice (Gonzalez-Hurtado et al., 2018; Kazak et al., 2017). It is possible that this inflammatory response is induced by damage-associated molecules from dying brown adipocytes. However, the exact nature of this inflammation is unclear. Abundance of various immune cell populations in iBAT was unchanged in $Bcl6^{f/f}Ucp1^{Cre}$ mice. These findings suggest that the increase in inflammatory gene expression is not a reflection of elevated immune cell composition due to recruitment, but rather due to activation of tissue-

resident immune populations. The implications of this inflammatory response for the function of brown adipocytes in the *Bcl6*$^{f/f}$*Ucp1*^{Cre} mice are unclear. While the influence of immune cells on nutrient homeostasis and browning in white adipose tissue has been extensively studied (van den Berg et al., 2017), the role of immune cells in brown adipose tissue is less well understood.

BCL6 maintains the distinctive thermogenic properties of BAT mitochondria during dormancy

The profound thermogenic defect in the dormant BAT of *Bcl6*$^{f/f}$*Ucp1*^{Cre} mice raised the possibility that BCL6 is essential for maintenance of mitochondria, which are the engines of thermogenesis (Cannon and Nedergaard, 2004). Unexpectedly, the mitochondrial density, as reflected by the ratio of mitochondrial and genomic DNA, was not significantly reduced. Furthermore, the structure of the mitochondria, including the average cross-sectional area and cristae interval as determined by electron microscopy, was unchanged in the absence of BCL6. The abundance of electron transport complexes I-IV was also not significantly altered. These findings indicated that BCL6 is not required for maintaining the abundance and core structural features of mitochondria. In contrast, loss of BCL6 had a striking effect on two distinctive characteristics of thermogenic mitochondria: ATP synthase was upregulated, while UCP1 was downregulated. This represented a reversal of the normally low abundance of ATP synthase and high abundance of UCP1 that distinguishes the uncoupled mitochondria of brown and beige adipocytes from mitochondria in other cell types (Cannon and Nedergaard, 2004), consistent with the notion that BCL6 is required for maintenance of brown adipocyte identity. The greater degree of UCP1 downregulation during dormancy is likely to be a key reason for the greater thermogenic defect in the dormant *Bcl6*$^{f/f}$*Ucp1*^{Cre} BAT. Most likely this is due to the ability of cold-induced adrenergic signaling to largely compensate for the absence of BCL6 in the

regulation of *Ucp1*. In contrast, the ability of BCL6 to repress ATP synthase appears to be temperature-independent, presumably because adrenergic signaling does not regulate ATP synthase.

The molecular mechanisms by which BCL6 regulates these two complexes appear to be distinct. In the case of ATP synthase, BCL6 directly represses *Atp5g1*, which encodes the ATP synthase subunit that is rate-limiting for assembly of the full complex (Houstek et al., 1995), through multiple binding sites located near the gene's promoter. In the case of *Ucp1*, the absence of nearby BCL6 binding sites suggests an indirect mechanism of regulation. One possibility is that BCL6 directly represses a second gene which encodes a factor that subsequently represses *Ucp1*. Of the likely direct targets of BCL6 in BAT (Table 2.3), potential candidates for this hypothetical second gene include *Prkd1*, *Thbs1*, and *Nnat* which are all repressed by BCL6 and have been previously shown to repress *Ucp1* and other thermogenic genes (Gburcik et al., 2013; Inoue et al., 2013; Löffler et al., 2018). To test such a mechanism, we could potentially generate a double knockout of *Bcl6* and one these candidates genes; if our hypothesis is correct, then co-deletion of one or more of the candidate genes would restore *Ucp1* expression in the dormant BAT of the double knockout. A similar mechanism may potentially be responsible for the indirect regulation of most fatty acid β-oxidation genes by BCL6, which also do not have nearby BCL6 binding sites. The observation that estrogen-related receptor alpha and gamma (ERRα/γ) binding is enriched among the hypoacetylated chromatin sites in $Bcl6^{f/f}Ucp1^{Cre}$ BAT, including those near *Ucp1* and β-oxidation genes, suggest that they are likely operating downstream of BCL6 as part of this indirect mechanism. Since we do not observe changes in ERRα/γ expression or recruitment of ERRα to the vast majority of its binding sites in $Bcl6^{f/f}Ucp1^{Cre}$ BAT, the indirect regulation of ERRα/γ by BCL6 is perhaps occurring at the level of post-translational

modifications and/or interactions with co-activators like PGC-1α. How exactly BCL6 regulates the expression of *Ucp1* and β-oxidation genes remains a key question for future studies.

Regulation of fatty acid metabolism by BCL6 in dormant BAT

A previous study in white adipocytes had demonstrated that BCL6 negatively regulates lipogenesis while positively regulating fatty acid oxidation (Senagolage et al., 2018). We observed a similar function in brown adipocytes, as demonstrated by the increased lipid content in iBAT of $Bcl6^{f/f}Ucp1^{Cre}$ mice. RNA-seq analysis confirmed that the majority of fatty acid β-oxidation genes were downregulated in BAT of $Bcl6^{f/f}Ucp1^{Cre}$ mice. Furthermore, we found that BCL6 regulates fatty acid activation and trafficking by controlling expression of acyl-CoA thioesterase (ACOT) genes, in part through direct repression of a cluster of ACOT genes containing *Acot1, Acot3,* and *Acot4*. These observations highlight how BCL6 regulates fatty acid metabolism at multiple levels to support brown adipocyte thermogenic capacity.

BCL6 maintains brown adipocyte identity by regulating cell type-specific enhancers

One of the key characteristics that distinguishes brown and beige adipocytes is that brown adipocytes mostly maintain their thermogenic characteristics during dormancy, whereas beige adipocytes undergo dramatic loss of thermogenic characteristics, becoming almost indistinguishable from white adipocytes (Roh et al., 2018). Thus, the loss of thermogenic characteristics during dormancy in BAT of $Bcl6^{f/f}Ucp1^{Cre}$ mice suggested a switch to a beige-like condition. Consistent with this notion, dormant BAT of $Bcl6^{f/f}Ucp1^{Cre}$ mice exhibited upregulation of white-specific genes and downregulation of brown-specific genes. A similar trend was observed in the H3K27 acetylation profiles of brown and white adipocyte-specific

enhancers. These findings indicate that BCL6 reinforces brown adipocyte identity during dormancy by acting on adipocyte-specific enhancers, mitigating the strong influence of temperature that is evident in the beige adipocyte lineage. The selective requirement of BCL6 during dormancy distinguishes it from other factors that are required for maintenance of brown adipocyte identity even in the cold-adapted state, such as ZFP516, LSD1 (Sambeat et al., 2016), and PRDM16/PRDM3 (Harms et al., 2014), suggesting that BCL6 operates in a distinct pathway.

Additional remaining unanswered questions

Is lack of BCL6 in beige adipocytes a contributing factor to their inability to maintain thermogenic capacity during dormancy?

While the functions of BCL6 are highly cell type-dependent, a general characteristic of BCL6 is that it inhibits transitions to alternative cell states (Table 1.1). For example, in a germinal center B cell, BCL6 inhibits differentiation to a plasma B cell state (Basso et al., 2010). In accordance with this general trend, we found that BCL6 opposes the loss of brown adipocyte thermogenic characteristics during dormancy. In contrast, beige adipocytes undergo dramatic loss of thermogenic characteristics during dormancy, becoming almost indistinguishable from white adipocytes (Roh et al., 2018). Intriguingly, we observed much lower BCL6 abundance in inguinal WAT, which contains a mixture of beige and white adipocytes, in comparison to iBAT and gWAT, which contain only brown and white adipocytes, respectively (Figure 2.2). Based on this observation, we hypothesize that low BCL6 expression is a contributing factor to the instability of thermogenic capacity in dormant beige adipocytes. This hypothesis is supported by

the observation that BCL6 abundance is much higher in inguinal WAT at 3 weeks of age, a stage at which the resident adipocytes have much more stable thermogenic capacity (Melissa Kinnebrew, unpublished data). If this hypothesis is correct, then ectopic expression of BCL6 in adult beige adipocytes would confer greater stability to their thermogenic capacity, increasing their resemblance to brown adipocytes.

Does BCL6 play a role in the developmental trajectory of human brown adipose tissue?

In humans, brown adipose tissue undergoes dramatic changes over the course of postnatal development. During infancy, BAT is abundant and contains cells that seem to resemble mouse brown adipocytes (Lidell et al., 2013). By adulthood, BAT quantity is greatly reduced and the cells resemble either brown or beige adipocytes of mice, depending on the anatomical location (Cypess et al., 2013; Sharp et al., 2012). The greater abundance and stability of BAT during infancy correlates with the greater demand for BAT thermogenesis during this stage of development. Infants experience greater heat loss due to a higher body surface to volume ratio and reduced insulation, and also lack the muscle shivering capacity present in adults (Lidell, 2019). As a result, they are thought to be more dependent on BAT thermogenesis than adults. From this perspective, the decline of BAT during adulthood may reflect a switch to an alternative mode of thermoregulation.

A great deal of interest in human BAT stems from its potential to increase energy expenditure for the treatment of obesity (Lee et al., 2013). With this goal in mind, some researchers are exploring strategies to amplify human BAT (Tharp and Stahl, 2015). Surprisingly, very little is known about why human BAT declines during development in the first place. Understanding the various factors influencing this trajectory would be highly

beneficial for developing strategies to regenerate BAT in adults. Similar transitions have been observed in other organisms. In mice, as mentioned previously, the thermogenic adipocytes of inguinal WAT appear to resemble brown adipocytes at 3 weeks of age, and later transition to the standard beige-like state by 8 weeks of age (Melissa Kinnebrew, unpublished data). In sheep, perirenal adipose tissue contains brown-like adipocytes at birth, which then become white-like adipocytes by 8 weeks of age (Basse et al., 2015). Interestingly, during both of these transitions that feature loss of brown-like characteristics, BCL6 is highly downregulated (Melissa Kinnebrew, unpublished data; Basse et al., 2015). These observations raise the possibility that BCL6 is also downregulated in human BAT during the transition from infancy to adulthood. If this is the case, then downregulation of BCL6 may be an essential step in the transition from brown adipocyte characteristics to beige or white adipocyte characteristics. Perhaps preventing the downregulation of BCL6 during these transitions would be sufficient to preserve brown-like thermogenic characteristics.

What are the extracellular signals that control the expression and/or activity of BCL6 in brown adipocytes?

Despite the importance of BCL6 during transition from warmth to cold, the abundance of BCL6 is not regulated by temperature (Figure 2.2E). It remains unclear which extracellular signals, if any, control the expression and/or activity of BCL6 in mature brown adipocytes. In mouse hepatocytes, BCL6 was shown to be regulated by growth hormone signaling (Meyer et al., 2009), resulting in much higher expression in males due to the pulsatile pattern of growth hormone secretion in males, in contrast to the more continuous secretion pattern in females (Meyer et al., 2009). In mouse iBAT, BCL6 protein abundance was similar in males and females

(data not shown), suggesting that this mechanism of regulation by growth hormone does not occur in brown adipocytes. The high degree of variability in BCL6 protein abundance among BAT samples of the same condition (Figure 2.2A, E) suggests that BCL6 may be regulated by an extracellular signal that is highly dynamic. Identification of signals that control BCL6 expression or activity may lead to new opportunities for manipulation of brown adipocyte thermogenic capacity. This will be an important question to pursue in future studies.

REFERENCES:

Ahmadian, M., Liu, S., Reilly, S.M., Hah, N., Fan, W., Yoshihara, E., Jha, P., De Magalhaes Filho, C.D., Jacinto, S., Gomez, A.V., *et al.* (2018). ERRγ Preserves Brown Fat Innate Thermogenic Activity. Cell Rep *22*, 2849-2859.

Angilletta, M.J., Cooper, B.S., Schuler, M.S., and Boyles, J.G. (2010). The evolution of thermal physiology in endotherms. Front Biosci (Elite Ed) *2*, 861-881.

Anunciado-Koza, R., Ukropec, J., Koza, R.A., and Kozak, L.P. (2008). Inactivation of UCP1 and the glycerol phosphate cycle synergistically increases energy expenditure to resist diet-induced obesity. J Biol Chem *283*, 27688-27697.

Arch, J.R. (2011). Challenges in β(3)-Adrenoceptor Agonist Drug Development. Ther Adv Endocrinol Metab *2*, 59-64.

Audet-Walsh, É., and Giguére, V. (2015). The multiple universes of estrogen-related receptor α and γ in metabolic control and related diseases. Acta Pharmacol Sin *36*, 51-61.

Barish, G.D., Yu, R.T., Karunasiri, M., Ocampo, C.B., Dixon, J., Benner, C., Dent, A.L., Tangirala, R.K., and Evans, R.M. (2010). Bcl-6 and NF-kappaB cistromes mediate opposing regulation of the innate immune response. Genes & development *24*, 2760-2765.

Barish, G.D., Yu, R.T., Karunasiri, M.S., Becerra, D., Kim, J., Tseng, T.W., Tai, L.J., Leblanc, M., Diehl, C., Cerchietti, L., *et al.* (2012). The Bcl6-SMRT/NCoR cistrome represses inflammation to attenuate atherosclerosis. Cell Metab *15*, 554-562.

Basse, A.L., Dixen, K., Yadav, R., Tygesen, M.P., Qvortrup, K., Kristiansen, K., Quistorff, B., Gupta, R., Wang, J., and Hansen, J.B. (2015). Global gene expression profiling of brown

to white adipose tissue transformation in sheep reveals novel transcriptional components linked to adipose remodeling. BMC Genomics *16*, 215.

Basso, K., and Dalla-Favera, R. (2012). Roles of BCL6 in normal and transformed germinal center B cells. Immunol Rev *247*, 172-183.

Basso, K., Saito, M., Sumazin, P., Margolin, A.A., Wang, K., Lim, W.K., Kitagawa, Y., Schneider, C., Alvarez, M.J., Califano, A., *et al.* (2010). Integrated biochemical and computational approach identifies BCL6 direct target genes controlling multiple pathways in normal germinal center B cells. Blood *115*, 975-984.

Bereshchenko, O.R., Gu, W., and Dalla-Favera, R. (2002). Acetylation inactivates the transcriptional repressor BCL6. Nat Genet *32*, 606-613.

Berrahmouni, N., and Burgess, N. (2019). Northern Africa. In Deserts and xeric shrublands (World Wildlife Fund).

Betz, M.J., and Enerbäck, S. (2015). Human Brown Adipose Tissue: What We Have Learned So Far. Diabetes *64*, 2352-2360.

Blondin, D.P., Labbé, S.M., Tingelstad, H.C., Noll, C., Kunach, M., Phoenix, S., Guérin, B., Turcotte, E.E., Carpentier, A.C., Richard, D., *et al.* (2014). Increased brown adipose tissue oxidative capacity in cold-acclimated humans. J Clin Endocrinol Metab *99*, E438-446.

Bovell, D. (2015). The human eccrine sweat gland: Structure, function, and disorders. Journal of Local and Global Health Science.

Bray, N.L., Pimentel, H., Melsted, P., and Pachter, L. (2016). Near-optimal probabilistic RNA-seq quantification. Nat Biotechnol *34*, 525-527.

Brown, D.A., and London, E. (1998). Structure and origin of ordered lipid domains in biological membranes. J Membr Biol *164*, 103-114.

Brown, E.L., Hazen, B.C., Eury, E., Wattez, J.S., Gantner, M.L., Albert, V., Chau, S., Sanchez-Alavez, M., Conti, B., and Kralli, A. (2018). Estrogen-Related Receptors Mediate the Adaptive Response of Brown Adipose Tissue to Adrenergic Stimulation. iScience *2*, 221-237.

Cannon, B., and Nedergaard, J. (2004). Brown adipose tissue: function and physiological significance. Physiol Rev *84*, 277-359.

Cannon, B., and Nedergaard, J. (2011). Nonshivering thermogenesis and its adequate measurement in metabolic studies. J Exp Biol *214*, 242-253.

Cao, W., Daniel, K.W., Robidoux, J., Puigserver, P., Medvedev, A.V., Bai, X., Floering, L.M., Spiegelman, B.M., and Collins, S. (2004). p38 mitogen-activated protein kinase is the central regulator of cyclic AMP-dependent transcription of the brown fat uncoupling protein 1 gene. Mol Cell Biol *24*, 3057-3067.

Cao, W., Medvedev, A.V., Daniel, K.W., and Collins, S. (2001). beta-Adrenergic activation of p38 MAP kinase in adipocytes: cAMP induction of the uncoupling protein 1 (UCP1) gene requires p38 MAP kinase. J Biol Chem *276*, 27077-27082.

Cardenas, M.G., Oswald, E., Yu, W., Xue, F., MacKerell, A.D., and Melnick, A.M. (2017). The Expanding Role of the BCL6 Oncoprotein as a Cancer Therapeutic Target. Clin Cancer Res *23*, 885-893.

Carmen, G.Y., and Víctor, S.M. (2006). Signalling mechanisms regulating lipolysis. Cell Signal *18*, 401-408.

Cerchietti, L.C., Lopes, E.C., Yang, S.N., Hatzi, K., Bunting, K.L., Tsikitas, L.A., Mallik, A., Robles, A.I., Walling, J., Varticovski, L., *et al.* (2009). A purine scaffold Hsp90 inhibitor destabilizes BCL-6 and has specific antitumor activity in BCL-6-dependent B cell lymphomas. Nat Med *15*, 1369-1376.

Choi, Y.S., Eto, D., Yang, J.A., Lao, C., and Crotty, S. (2013). Cutting edge: STAT1 is required for IL-6-mediated Bcl6 induction for early follicular helper cell differentiation. J Immunol *190*, 3049-3053.

Chouchani, E.T., Kazak, L., Jedrychowski, M.P., Lu, G.Z., Erickson, B.K., Szpyt, J., Pierce, K.A., Laznik-Bogoslavski, D., Vetrivelan, R., Clish, C.B., *et al.* (2016). Mitochondrial ROS regulate thermogenic energy expenditure and sulfenylation of UCP1. Nature *532*, 112-116.

Ci, W., Polo, J.M., Cerchietti, L., Shaknovich, R., Wang, L., Yang, S.N., Ye, K., Farinha, P., Horsman, D.E., Gascoyne, R.D., *et al.* (2009). The BCL6 transcriptional program features repression of multiple oncogenes in primary B cells and is deregulated in DLBCL. Blood *113*, 5536-5548.

Clarke, A., and Fraser, K.P.P. (2004). Why does metabolism scale with temperature? Functional Ecology *18*, 243-251.

Cypess, A.M., Lehman, S., Williams, G., Tal, I., Rodman, D., Goldfine, A.B., Kuo, F.C., Palmer, E.L., Tseng, Y.H., Doria, A., *et al.* (2009). Identification and importance of brown adipose tissue in adult humans. N Engl J Med *360*, 1509-1517.

Cypess, A.M., White, A.P., Vernochet, C., Schulz, T.J., Xue, R., Sass, C.A., Huang, T.L., Roberts-Toler, C., Weiner, L.S., Sze, C., *et al.* (2013). Anatomical localization, gene

expression profiling and functional characterization of adult human neck brown fat. Nat Med *19*, 635-639.

de Jesus, L.A., Carvalho, S.D., Ribeiro, M.O., Schneider, M., Kim, S.W., Harney, J.W., Larsen, P.R., and Bianco, A.C. (2001). The type 2 iodothyronine deiodinase is essential for adaptive thermogenesis in brown adipose tissue. J Clin Invest *108*, 1379-1385.

Delcuve, G.P., Khan, D.H., and Davie, J.R. (2012). Roles of histone deacetylases in epigenetic regulation: emerging paradigms from studies with inhibitors. Clin Epigenetics *4*, 5.

Dempersmier, J., Sambeat, A., Gulyaeva, O., Paul, S.M., Hudak, C.S., Raposo, H.F., Kwan, H.Y., Kang, C., Wong, R.H., and Sul, H.S. (2015). Cold-inducible Zfp516 activates UCP1 transcription to promote browning of white fat and development of brown fat. Mol Cell *57*, 235-246.

Dent, A.L., Shaffer, A.L., Yu, X., Allman, D., and Staudt, L.M. (1997). Control of inflammation, cytokine expression, and germinal center formation by BCL-6. Science *276*, 589-592.

Dhaka, A., Murray, A.N., Mathur, J., Earley, T.J., Petrus, M.J., and Patapoutian, A. (2007). TRPM8 is required for cold sensation in mice. Neuron *54*, 371-378.

Duan, S., Cermak, L., Pagan, J.K., Rossi, M., Martinengo, C., di Celle, P.F., Chapuy, B., Shipp, M., Chiarle, R., and Pagano, M. (2012). FBXO11 targets BCL6 for degradation and is inactivated in diffuse large B-cell lymphomas. Nature *481*, 90-93.

Duy, C., Hurtz, C., Shojaee, S., Cerchietti, L., Geng, H., Swaminathan, S., Klemm, L., Kweon, S.M., Nahar, R., Braig, M., *et al.* (2011). BCL6 enables Ph+ acute lymphoblastic leukaemia cells to survive BCR-ABL1 kinase inhibition. Nature *473*, 384-388.

Ellis, J.M., Bowman, C.E., and Wolfgang, M.J. (2015). Metabolic and tissue-specific regulation of acyl-CoA metabolism. PLoS One *10*, e0116587.

Emmett, M.J., Lim, H.W., Jager, J., Richter, H.J., Adlanmerini, M., Peed, L.C., Briggs, E.R., Steger, D.J., Ma, T., Sims, C.A., *et al.* (2017). Histone deacetylase 3 prepares brown adipose tissue for acute thermogenic challenge. Nature *546*, 544-548.

Enerback, S. (2010). Human brown adipose tissue. Cell Metab *11*, 248-252.

Enerback, S., Jacobsson, A., Simpson, E.M., Guerra, C., Yamashita, H., Harper, M.E., and Kozak, L.P. (1997). Mice lacking mitochondrial uncoupling protein are cold-sensitive but not obese. Nature *387*, 90-94.

Fedorenko, A., Lishko, P.V., and Kirichok, Y. (2012). Mechanism of fatty-acid-dependent UCP1 uncoupling in brown fat mitochondria. Cell *151*, 400-413.

Feil, R., and Fraga, M.F. (2012). Epigenetics and the environment: emerging patterns and implications. Nature reviews Genetics *13*, 97-109.

Feldmann, H.M., Golozoubova, V., Cannon, B., and Nedergaard, J. (2009). UCP1 ablation induces obesity and abolishes diet-induced thermogenesis in mice exempt from thermal stress by living at thermoneutrality. Cell Metab *9*, 203-209.

Franklin, M.P., Sathyanarayan, A., and Mashek, D.G. (2017). Acyl-CoA Thioesterase 1 (ACOT1) Regulates PPARalpha to Couple Fatty Acid Flux With Oxidative Capacity During Fasting. Diabetes *66*, 2112-2123.

FRY, F.E., and HART, J.S. (1948). The relation of temperature to oxygen consumption in the goldfish. Biol Bull *94*, 66-77.

Gantner, M.L., Hazen, B.C., Eury, E., Brown, E.L., and Kralli, A. (2016). Complementary Roles of Estrogen-Related Receptors in Brown Adipocyte Thermogenic Function. Endocrinology *157*, 4770-4781.

Gburcik, V., Cleasby, M.E., and Timmons, J.A. (2013). Loss of neuronatin promotes "browning" of primary mouse adipocytes while reducing Glut1-mediated glucose disposal. Am J Physiol Endocrinol Metab *304*, E885-894.

Giguere, V. (2008). Transcriptional control of energy homeostasis by the estrogen-related receptors. Endocrine reviews *29*, 677-696.

Goldberg, M.B., Langman, V.A., and Taylor, C.R. (1981). Panting in dogs: paths of air flow in response to heat and exercise. Respir Physiol *43*, 327-338.

Golozoubova, V., Cannon, B., and Nedergaard, J. (2006). UCP1 is essential for adaptive adrenergic nonshivering thermogenesis. American journal of physiology Endocrinology and metabolism *291*, E350-357.

Gonzalez-Hurtado, E., Lee, J., Choi, J., and Wolfgang, M.J. (2018). Fatty acid oxidation is required for active and quiescent brown adipose tissue maintenance and thermogenic programing. Mol Metab *7*, 45-56.

Granneman, J.G., Burnazi, M., Zhu, Z., and Schwamb, L.A. (2003). White adipose tissue contributes to UCP1-independent thermogenesis. American journal of physiology Endocrinology and metabolism *285*, E1230-1236.

Grimpo, K., Völker, M.N., Heppe, E.N., Braun, S., Heverhagen, J.T., and Heldmaier, G. (2014). Brown adipose tissue dynamics in wild-type and UCP1-knockout mice: in vivo insights with magnetic resonance. J Lipid Res *55*, 398-409.

Guerra, C., Navarro, P., Valverde, A.M., Arribas, M., Brüning, J., Kozak, L.P., Kahn, C.R., and Benito, M. (2001). Brown adipose tissue-specific insulin receptor knockout shows diabetic phenotype without insulin resistance. J Clin Invest *108*, 1205-1213.

Guo, M., Xu, Y., and Gruebele, M. (2012). Temperature dependence of protein folding kinetics in living cells. Proc Natl Acad Sci U S A *109*, 17863-17867.

Harkness, J. (1997). Essentials of Pet Rodents (Lakewood, CO: AAHA Press).

Harms, M., and Seale, P. (2013). Brown and beige fat: development, function and therapeutic potential. Nat Med *19*, 1252-1263.

Harms, M.J., Ishibashi, J., Wang, W., Lim, H.W., Goyama, S., Sato, T., Kurokawa, M., Won, K.J., and Seale, P. (2014). Prdm16 is required for the maintenance of brown adipocyte identity and function in adult mice. Cell Metab *19*, 593-604.

Hatzi, K., Nance, J.P., Kroenke, M.A., Bothwell, M., Haddad, E.K., Melnick, A., and Crotty, S. (2015). BCL6 orchestrates Tfh cell differentiation via multiple distinct mechanisms. J Exp Med *212*, 539-553.

Heinz, S., Benner, C., Spann, N., Bertolino, E., Lin, Y.C., Laslo, P., Cheng, J.X., Murre, C., Singh, H., and Glass, C.K. (2010). Simple combinations of lineage-determining transcription factors prime cis-regulatory elements required for macrophage and B cell identities. Molecular cell *38*, 576-589.

Hellman, B., and Hellerstrom, C. (1961). Cell renewal in the white and brown fat tissue of the rat. Acta Pathol Microbiol Scand *51*, 347-353.

Ho, K.Y., Veldhuis, J.D., Johnson, M.L., Furlanetto, R., Evans, W.S., Alberti, K.G., and Thorner, M.O. (1988). Fasting enhances growth hormone secretion and amplifies the complex rhythms of growth hormone secretion in man. J Clin Invest *81*, 968-975.

Houstek, J., Andersson, U., Tvrdik, P., Nedergaard, J., and Cannon, B. (1995). The expression of subunit c correlates with and thus may limit the biosynthesis of the mitochondrial F0F1-ATPase in brown adipose tissue. J Biol Chem *270*, 7689-7694.

Houten, S.M., and Wanders, R.J. (2010). A general introduction to the biochemistry of mitochondrial fatty acid β-oxidation. J Inherit Metab Dis *33*, 469-477.

Hu, X., Zhou, Y., Yang, Y., Peng, J., Song, T., Xu, T., Wei, H., and Jiang, S. (2016). Identification of zinc finger protein Bcl6 as a novel regulator of early adipose commitment. Open Biol *6*.

Huang da, W., Sherman, B.T., and Lempicki, R.A. (2009). Systematic and integrative analysis of large gene lists using DAVID bioinformatics resources. Nature protocols *4*, 44-57.

Hulsen, T., de Vlieg, J., and Alkema, W. (2008). BioVenn - a web application for the comparison and visualization of biological lists using area-proportional Venn diagrams. BMC Genomics *9*, 488.

Ichii, H., Sakamoto, A., Arima, M., Hatano, M., Kuroda, Y., and Tokuhisa, T. (2007). Bcl6 is essential for the generation of long-term memory CD4+ T cells. Int Immunol *19*, 427-433.

Ichii, H., Sakamoto, A., Hatano, M., Okada, S., Toyama, H., Taki, S., Arima, M., Kuroda, Y., and Tokuhisa, T. (2002). Role for Bcl-6 in the generation and maintenance of memory CD8+ T cells. Nat Immunol *3*, 558-563.

Ichii, H., Sakamoto, A., Kuroda, Y., and Tokuhisa, T. (2004). Bcl6 acts as an amplifier for the generation and proliferative capacity of central memory CD8+ T cells. J Immunol *173*, 883-891.

Iida, S., Chen, W., Nakadai, T., Ohkuma, Y., and Roeder, R.G. (2015). PRDM16 enhances nuclear receptor-dependent transcription of the brown fat-specific Ucp1 gene through interactions with Mediator subunit MED1. Genes Dev *29*, 308-321.

Ikeda, K., Kang, Q., Yoneshiro, T., Camporez, J.P., Maki, H., Homma, M., Shinoda, K., Chen, Y., Lu, X., Maretich, P., *et al.* (2017). UCP1-independent signaling involving SERCA2b-mediated calcium cycling regulates beige fat thermogenesis and systemic glucose homeostasis. Nat Med *23*, 1454-1465.

Ikeda, K., Maretich, P., and Kajimura, S. (2018). The Common and Distinct Features of Brown and Beige Adipocytes. Trends Endocrinol Metab *29*, 191-200.

Inoue, M., Jiang, Y., Barnes, R.H., Tokunaga, M., Martinez-Santibañez, G., Geletka, L., Lumeng, C.N., Buchner, D.A., and Chun, T.H. (2013). Thrombospondin 1 mediates high-fat diet-induced muscle fibrosis and insulin resistance in male mice. Endocrinology *154*, 4548-4559.

Jespersen, N.Z., Feizi, A., Andersen, E.S., Heywood, S., Hattel, H.B., Daugaard, S., Peijs, L., Bagi, P., Feldt-Rasmussen, B., Schultz, H.S., *et al.* (2019). Heterogeneity in the perirenal region of humans suggests presence of dormant brown adipose tissue that contains brown fat precursor cells. Mol Metab *24*, 30-43.

Johnston, R.J., Poholek, A.C., DiToro, D., Yusuf, I., Eto, D., Barnett, B., Dent, A.L., Craft, J., and Crotty, S. (2009). Bcl6 and Blimp-1 are reciprocal and antagonistic regulators of T follicular helper cell differentiation. Science *325*, 1006-1010.

Kajimura, S., Spiegelman, B.M., and Seale, P. (2015). Brown and Beige Fat: Physiological Roles beyond Heat Generation. Cell Metab *22*, 546-559.

Kazak, L., Chouchani, E.T., Jedrychowski, M.P., Erickson, B.K., Shinoda, K., Cohen, P., Vetrivelan, R., Lu, G.Z., Laznik-Bogoslavski, D., Hasenfuss, S.C., *et al.* (2015). A creatine-driven substrate cycle enhances energy expenditure and thermogenesis in beige fat. Cell *163*, 643-655.

Kazak, L., Chouchani, E.T., Stavrovskaya, I.G., Lu, G.Z., Jedrychowski, M.P., Egan, D.F., Kumari, M., Kong, X., Erickson, B.K., Szpyt, J., *et al.* (2017). UCP1 deficiency causes brown fat respiratory chain depletion and sensitizes mitochondria to calcium overload-induced dysfunction. Proc Natl Acad Sci U S A *114*, 7981-7986.

Kent, W.J., Sugnet, C.W., Furey, T.S., Roskin, K.M., Pringle, T.H., Zahler, A.M., and Haussler, D. (2002). The human genome browser at UCSC. Genome Res *12*, 996-1006.

Kent, W.J., Zweig, A.S., Barber, G., Hinrichs, A.S., and Karolchik, D. (2010). BigWig and BigBed: enabling browsing of large distributed datasets. Bioinformatics *26*, 2204-2207.

Kiefer, M.C., Van Sluys, M., and Rocha, C.F.D. (2007). Thermoregulatory behaviour in Tropidurus torquatas (Squamata, Tropiduridae) from Brazilian coastal populations: an estimate of passive and active thermoregulation in lizards. Acta Zoologica *88*, 81-87.

Klein, J., Fasshauer, M., Klein, H.H., Benito, M., and Kahn, C.R. (2002). Novel adipocyte lines from brown fat: a model system for the study of differentiation, energy metabolism, and insulin action. Bioessays *24*, 382-388.

Kong, X., Banks, A., Liu, T., Kazak, L., Rao, R.R., Cohen, P., Wang, X., Yu, S., Lo, J.C., Tseng, Y.H., *et al.* (2014). IRF4 is a key thermogenic transcriptional partner of PGC-1α. Cell *158*, 69-83.

Kotas, M.E., and Medzhitov, R. (2015). Homeostasis, inflammation, and disease susceptibility. Cell *160*, 816-827.

Kotzbeck, P., Giordano, A., Mondini, E., Murano, I., Severi, I., Venema, W., Cecchini, M.P., Kershaw, E.E., Barbatelli, G., Haemmerle, G., *et al.* (2018). Brown adipose tissue whitening leads to brown adipocyte death and adipose tissue inflammation. Journal of lipid research *59*, 784-794.

Kozak, L.P. (2010). Brown fat and the myth of diet-induced thermogenesis. Cell Metab *11*, 263-267.

Kramarova, T.V., Shabalina, I.G., Andersson, U., Westerberg, R., Carlberg, I., Houstek, J., Nedergaard, J., and Cannon, B. (2008). Mitochondrial ATP synthase levels in brown adipose tissue are governed by the c-Fo subunit P1 isoform. FASEB journal : official publication of the Federation of American Societies for Experimental Biology *22*, 55-63.

Langmead, B., and Salzberg, S.L. (2012). Fast gapped-read alignment with Bowtie 2. Nature methods *9*, 357-359.

LaPensee, C.R., Lin, G., Dent, A.L., and Schwartz, J. (2014). Deficiency of the transcriptional repressor B cell lymphoma 6 (Bcl6) is accompanied by dysregulated lipid metabolism. PLoS One *9*, e97090.

Lee, C.H., Chawla, A., Urbiztondo, N., Liao, D., Boisvert, W.A., and Evans, R.M. (2003). Transcriptional repression of atherogenic inflammation: modulation by PPARdelta. Science *302*, 453-457.

Lee, C.H., Melchers, M., Wang, H., Torrey, T.A., Slota, R., Qi, C.F., Kim, J.Y., Lugar, P., Kong, H.J., Farrington, L., *et al.* (2006). Regulation of the germinal center gene program by interferon (IFN) regulatory factor 8/IFN consensus sequence-binding protein. J Exp Med *203*, 63-72.

Lee, J., Choi, J., Aja, S., Scafidi, S., and Wolfgang, M.J. (2016). Loss of Adipose Fatty Acid Oxidation Does Not Potentiate Obesity at Thermoneutrality. Cell Rep *14*, 1308-1316.

Lee, J., Ellis, J.M., and Wolfgang, M.J. (2015a). Adipose fatty acid oxidation is required for thermogenesis and potentiates oxidative stress-induced inflammation. Cell reports *10*, 266-279.

Lee, M.W., Odegaard, J.I., Mukundan, L., Qiu, Y., Molofsky, A.B., Nussbaum, J.C., Yun, K., Locksley, R.M., and Chawla, A. (2015b). Activated type 2 innate lymphoid cells regulate beige fat biogenesis. Cell *160*, 74-87.

Lee, P., and Greenfield, J.R. (2015). Non-pharmacological and pharmacological strategies of brown adipose tissue recruitment in humans. Mol Cell Endocrinol *418 Pt 2*, 184-190.

Lee, P., Swarbrick, M.M., and Ho, K.K. (2013). Brown adipose tissue in adult humans: a metabolic renaissance. Endocr Rev *34*, 413-438.

Lee, Y.H., Petkova, A.P., Konkar, A.A., and Granneman, J.G. (2015c). Cellular origins of cold-induced brown adipocytes in adult mice. FASEB J *29*, 286-299.

Lichtenbelt, W., Kingma, B., van der Lans, A., and Schellen, L. (2014). Cold exposure--an approach to increasing energy expenditure in humans. Trends Endocrinol Metab *25*, 165-167.

Lidell, M., Betz, M., Leinhard, O., Heglind, M., Elander, L., Slawik, M., Mussack, T., Nilsson, D., Romu, T., Nuutila, P., *et al.* (2013). Evidence for two types of brown adipose tissue in humans. Nature Medicine *19*, 631-634.

Lidell, M.E. (2019). Brown Adipose Tissue in Human Infants. Handb Exp Pharmacol *251*, 107-123.

Lindquist, J.M., and Rehnmark, S. (1998). Ambient temperature regulation of apoptosis in brown adipose tissue. Erk1/2 promotes norepinephrine-dependent cell survival. J Biol Chem *273*, 30147-30156.

Liu, X., Lu, H., Chen, T., Nallaparaju, K.C., Yan, X., Tanaka, S., Ichiyama, K., Zhang, X., Zhang, L., Wen, X., *et al.* (2016). Genome-wide Analysis Identifies Bcl6-Controlled

Regulatory Networks during T Follicular Helper Cell Differentiation. Cell Rep *14*, 1735-1747.

Loft, A., Forss, I., and Mandrup, S. (2017). Genome-Wide Insights into the Development and Function of Thermogenic Adipocytes. Trends Endocrinol Metab *28*, 104-120.

Long, J.Z., Svensson, K.J., Bateman, L.A., Lin, H., Kamenecka, T., Lokurkar, I.A., Lou, J., Rao, R.R., Chang, M.R., Jedrychowski, M.P., *et al.* (2016). The Secreted Enzyme PM20D1 Regulates Lipidated Amino Acid Uncouplers of Mitochondria. Cell *166*, 424-435.

Love, M.I., Huber, W., and Anders, S. (2014). Moderated estimation of fold change and dispersion for RNA-seq data with DESeq2. Genome Biol *15*, 550.

Lowell, B.B., and Spiegelman, B.M. (2000). Towards a molecular understanding of adaptive thermogenesis. Nature *404*, 652-660.

Löffler, M.C., Mayer, A.E., Trujillo Viera, J., Loza Valdes, A., El-Merahbi, R., Ade, C.P., Karwen, T., Schmitz, W., Slotta, A., Erk, M., *et al.* (2018). Protein kinase D1 deletion in adipocytes enhances energy dissipation and protects against adiposity. EMBO J *37*.

Macher, G., Koehler, M., Rupprecht, A., Kreiter, J., Hinterdorfer, P., and Pohl, E.E. (2018). Inhibition of mitochondrial UCP1 and UCP3 by purine nucleotides and phosphate. Biochim Biophys Acta Biomembr *1860*, 664-672.

Marlatt, K.L., Chen, K.Y., and Ravussin, E. (2018). Is activation of human brown adipose tissue a viable target for weight management? Am J Physiol Regul Integr Comp Physiol *315*, R479-R483.

Meyer, R.D., Laz, E.V., Su, T., and Waxman, D.J. (2009). Male-specific hepatic Bcl6: growth hormone-induced block of transcription elongation in females and binding to target genes inversely coordinated with STAT5. Mol Endocrinol *23*, 1914-1926.

Moon, T.W., and Hochlachka, P.W. (1971). Temperature and enzyme activity in poikilotherms. Isocitrate dehydrogenases in rainbow-trout liver. Biochem J *123*, 695-705.

Morrison, S.F., and Nakamura, K. (2018). Central Mechanisms for Thermoregulation. Annu Rev Physiol.

Mullur, R., Liu, Y.Y., and Brent, G.A. (2014). Thyroid hormone regulation of metabolism. Physiol Rev *94*, 355-382.

Nakayamada, S., Poholek, A.C., Lu, K.T., Takahashi, H., Kato, M., Iwata, S., Hirahara, K., Cannons, J.L., Schwartzberg, P.L., Vahedi, G., *et al.* (2014). Type I IFN induces binding of STAT1 to Bcl6: divergent roles of STAT family transcription factors in the T follicular helper cell genetic program. J Immunol *192*, 2156-2166.

Nedergaard, J., Wang, Y., and Cannon, B. (2018). Cell proliferation and apoptosis inhibition: essential processes for recruitment of the full thermogenic capacity of brown adipose tissue. Biochim Biophys Acta Mol Cell Biol Lipids.

Niu, H., Cattoretti, G., and Dalla-Favera, R. (2003). BCL6 controls the expression of the B7-1/CD80 costimulatory receptor in germinal center B cells. J Exp Med *198*, 211-221.

Niu, H., Ye, B.H., and Dalla-Favera, R. (1998). Antigen receptor signaling induces MAP kinase-mediated phosphorylation and degradation of the BCL-6 transcription factor. Genes Dev *12*, 1953-1961.

Nurieva, R.I., Chung, Y., Martinez, G.J., Yang, X.O., Tanaka, S., Matskevitch, T.D., Wang, Y.H., and Dong, C. (2009). Bcl6 mediates the development of T follicular helper cells. Science *325*, 1001-1005.

Odegaard, J.I., Lee, M.W., Sogawa, Y., Bertholet, A.M., Locksley, R.M., Weinberg, D.E., Kirichok, Y., Deo, R.C., and Chawla, A. (2016). Perinatal Licensing of Thermogenesis by IL-33 and ST2. Cell *166*, 841-854.

Oestreich, K.J., Mohn, S.E., and Weinmann, A.S. (2012). Molecular mechanisms that control the expression and activity of Bcl-6 in TH1 cells to regulate flexibility with a TFH-like gene profile. Nat Immunol *13*, 405-411.

Ohno, H., Shinoda, K., Ohyama, K., Sharp, L.Z., and Kajimura, S. (2013). EHMT1 controls brown adipose cell fate and thermogenesis through the PRDM16 complex. Nature *504*, 163-167.

Okada, K., LeClair, K.B., Zhang, Y., Li, Y., Ozdemir, C., Krisko, T.I., Hagen, S.J., Betensky, R.A., Banks, A.S., and Cohen, D.E. (2016). Thioesterase superfamily member 1 suppresses cold thermogenesis by limiting the oxidation of lipid droplet-derived fatty acids in brown adipose tissue. Mol Metab *5*, 340-351.

Orava, J., Nuutila, P., Noponen, T., Parkkola, R., Viljanen, T., Enerbäck, S., Rissanen, A., Pietiläinen, K.H., and Virtanen, K.A. (2013). Blunted metabolic responses to cold and insulin stimulation in brown adipose tissue of obese humans. Obesity (Silver Spring) *21*, 2279-2287.

Pasqualucci, L., Migliazza, A., Basso, K., Houldsworth, J., Chaganti, R.S., and Dalla-Favera, R. (2003). Mutations of the BCL6 proto-oncogene disrupt its negative autoregulation in diffuse large B-cell lymphoma. Blood *101*, 2914-2923.

Perdikari, A., Leparc, G.G., Balaz, M., Pires, N.D., Lidell, M.E., Sun, W., Fernandez-Albert, F., Muller, S., Akchiche, N., Dong, H., *et al.* (2018). BATLAS: Deconvoluting Brown Adipose Tissue. Cell reports *25*, 784-797 e784.

Periasamy, M., Herrera, J.L., and Reis, F.C.G. (2017). Skeletal Muscle Thermogenesis and Its Role in Whole Body Energy Metabolism. Diabetes Metab J *41*, 327-336.

Phan, R.T., and Dalla-Favera, R. (2004). The BCL6 proto-oncogene suppresses p53 expression in germinal-centre B cells. Nature *432*, 635-639.

Phan, R.T., Saito, M., Kitagawa, Y., Means, A.R., and Dalla-Favera, R. (2007). Genotoxic stress regulates expression of the proto-oncogene Bcl6 in germinal center B cells. Nat Immunol *8*, 1132-1139.

Pixley, F.J., Xiong, Y., Yu, R.Y., Sahai, E.A., Stanley, E.R., and Ye, B.H. (2005). BCL6 suppresses RhoA activity to alter macrophage morphology and motility. J Cell Sci *118*, 1873-1883.

Pérez-Schindler, J., Summermatter, S., Salatino, S., Zorzato, F., Beer, M., Balwierz, P.J., van Nimwegen, E., Feige, J.N., Auwerx, J., and Handschin, C. (2012). The corepressor NCoR1 antagonizes PGC-1α and estrogen-related receptor α in the regulation of skeletal muscle function and oxidative metabolism. Mol Cell Biol *32*, 4913-4924.

Quinlan, A.R., and Hall, I.M. (2010). BEDTools: a flexible suite of utilities for comparing genomic features. Bioinformatics *26*, 841-842.

Rabelo, R., Schifman, A., Rubio, A., Sheng, X., and Silva, J.E. (1995). Delineation of thyroid hormone-responsive sequences within a critical enhancer in the rat uncoupling protein gene. Endocrinology *136*, 1003-1013.

Rajakumari, S., Wu, J., Ishibashi, J., Lim, H.W., Giang, A.H., Won, K.J., Reed, R.R., and Seale, P. (2013). EBF2 determines and maintains brown adipocyte identity. Cell Metab *17*, 562-574.

Ramirez, F., Ryan, D.P., Gruning, B., Bhardwaj, V., Kilpert, F., Richter, A.S., Heyne, S., Dundar, F., and Manke, T. (2016). deepTools2: a next generation web server for deep-sequencing data analysis. Nucleic Acids Res *44*, W160-165.

Ranuncolo, S.M., Polo, J.M., Dierov, J., Singer, M., Kuo, T., Greally, J., Green, R., Carroll, M., and Melnick, A. (2007). Bcl-6 mediates the germinal center B cell phenotype and lymphomagenesis through transcriptional repression of the DNA-damage sensor ATR. Nat Immunol *8*, 705-714.

Read, K.A., Powell, M.D., Baker, C.E., Sreekumar, B.K., Ringel-Scaia, V.M., Bachus, H., Martin, R.E., Cooley, I.D., Allen, I.C., Ballesteros-Tato, A., *et al.* (2017). Integrated STAT3 and Ikaros Zinc Finger Transcription Factor Activities Regulate Bcl-6 Expression in CD4. J Immunol *199*, 2377-2387.

Roh, H.C., Tsai, L.T.Y., Shao, M., Tenen, D., Shen, Y., Kumari, M., Lyubetskaya, A., Jacobs, C., Dawes, B., Gupta, R.K., *et al.* (2018). Warming Induces Significant Reprogramming of Beige, but Not Brown, Adipocyte Cellular Identity. Cell Metab *27*, 1121-1137.e1125.

Rosen, E.D., and MacDougald, O.A. (2006). Adipocyte differentiation from the inside out. Nat Rev Mol Cell Biol *7*, 885-896.

Rothwell, N.J., and Stock, M.J. (1979). A role for brown adipose tissue in diet-induced thermogenesis. Nature *281*, 31-35.

Saely, C.H., Geiger, K., and Drexel, H. (2012). Brown versus white adipose tissue: a mini-review. Gerontology *58*, 15-23.

Saito, M., Novak, U., Piovan, E., Basso, K., Sumazin, P., Schneider, C., Crespo, M., Shen, Q., Bhagat, G., Califano, A., *et al.* (2009). BCL6 suppression of BCL2 via Miz1 and its

disruption in diffuse large B cell lymphoma. Proc Natl Acad Sci U S A *106*, 11294-11299.

Sambeat, A., Gulyaeva, O., Dempersmier, J., Tharp, K.M., Stahl, A., Paul, S.M., and Sul, H.S. (2016). LSD1 Interacts with Zfp516 to Promote UCP1 Transcription and Brown Fat Program. Cell Rep *15*, 2536-2549.

Sanchez-Gurmaches, J., and Guertin, D.A. (2014). Adipocyte lineages: tracing back the origins of fat. Biochim Biophys Acta *1842*, 340-351.

Sanchez-Gurmaches, J., Hung, C.M., and Guertin, D.A. (2016). Emerging Complexities in Adipocyte Origins and Identity. Trends Cell Biol *26*, 313-326.

Seale, P. (2015). Transcriptional Regulatory Circuits Controlling Brown Fat Development and Activation. Diabetes *64*, 2369-2375.

Seale, P., Bjork, B., Yang, W., Kajimura, S., Chin, S., Kuang, S., Scimè, A., Devarakonda, S., Conroe, H.M., Erdjument-Bromage, H., *et al.* (2008). PRDM16 controls a brown fat/skeletal muscle switch. Nature *454*, 961-967.

Senagolage, M.D., Sommars, M.A., Ramachandran, K., Futtner, C.R., Omura, Y., Allred, A.L., Wang, J., Yang, C., Procissi, D., Evans, R.M., *et al.* (2018). Loss of Transcriptional Repression by BCL6 Confers Insulin Sensitivity in the Setting of Obesity. Cell Rep *25*, 3283-3298.e3286.

Shabalina, I.G., Petrovic, N., de Jong, J.M., Kalinovich, A.V., Cannon, B., and Nedergaard, J. (2013). UCP1 in brite/beige adipose tissue mitochondria is functionally thermogenic. Cell Rep *5*, 1196-1203.

Shaffer, A.L., Lin, K.I., Kuo, T.C., Yu, X., Hurt, E.M., Rosenwald, A., Giltnane, J.M., Yang, L., Zhao, H., Calame, K., *et al.* (2002). Blimp-1 orchestrates plasma cell differentiation by extinguishing the mature B cell gene expression program. Immunity *17*, 51-62.

Shaffer, A.L., Yu, X., He, Y., Boldrick, J., Chan, E.P., and Staudt, L.M. (2000). BCL-6 represses genes that function in lymphocyte differentiation, inflammation, and cell cycle control. Immunity *13*, 199-212.

Shapira, S.N., Lim, H.W., Rajakumari, S., Sakers, A.P., Ishibashi, J., Harms, M.J., Won, K.J., and Seale, P. (2017). EBF2 transcriptionally regulates brown adipogenesis via the histone reader DPF3 and the BAF chromatin remodeling complex. Genes & development *31*, 660-673.

Sharma, S., and Black, S.M. (2009). CARNITINE HOMEOSTASIS, MITOCHONDRIAL FUNCTION, AND CARDIOVASCULAR DISEASE. Drug Discov Today Dis Mech *6*, e31-e39.

Sharp, L.Z., Shinoda, K., Ohno, H., Scheel, D.W., Tomoda, E., Ruiz, L., Hu, H., Wang, L., Pavlova, Z., Gilsanz, V., *et al.* (2012). Human BAT possesses molecular signatures that resemble beige/brite cells. PLoS One *7*, e49452.

Sidossis, L., and Kajimura, S. (2015). Brown and beige fat in humans: thermogenic adipocytes that control energy and glucose homeostasis. J Clin Invest *125*, 478-486.

Somero, G.N., and Hochachka, P.W. (1969). Isoenzymes and short-term temperature compensation in poikilotherms: activation of lactate dehydrogenase isoenzymes by temperature decreases. Nature *223*, 194-195.

Sommars, M.A., Ramachandran, K., Senagolage, M.D., Futtner, C.R., Germain, D.M., Allred, A.L., Omura, Y., Bederman, I.R., and Barish, G.D. (2019). Dynamic repression by BCL6 controls the genome-wide liver response to fasting and steatosis. Elife *8*.

Tansey, E.A., and Johnson, C.D. (2015). Recent advances in thermoregulation. Adv Physiol Educ *39*, 139-148.

Team, R.D.C. (2008). R: A language and environment for statistical computing.

(Vienna, Austria: R Foundation for Statistical Computing).

Terrien, J., Perret, M., and Aujard, F. (2011). Behavioral thermoregulation in mammals: a review. Front Biosci (Landmark Ed) *16*, 1428-1444.

Than, A.A. (2011). Effect of Temperatures on the Growth of Escherichia Coli from Water. Universities Research Journal *4*, 163-171.

Tharp, K.M., and Stahl, A. (2015). Bioengineering Beige Adipose Tissue Therapeutics. Front Endocrinol (Lausanne) *6*, 164.

Tillander, V., Alexson, S.E.H., and Cohen, D.E. (2017). Deactivating Fatty Acids: Acyl-CoA Thioesterase-Mediated Control of Lipid Metabolism. Trends Endocrinol Metab *28*, 473-484.

Toney, L.M., Cattoretti, G., Graf, J.A., Merghoub, T., Pandolfi, P.P., Dalla-Favera, R., Ye, B.H., and Dent, A.L. (2000). BCL-6 regulates chemokine gene transcription in macrophages. Nat Immunol *1*, 214-220.

Tseng, Y.H., Cypess, A.M., and Kahn, C.R. (2010). Cellular bioenergetics as a target for obesity therapy. Nature reviews Drug discovery *9*, 465-482.

Tunyaplin, C., Shaffer, A.L., Angelin-Duclos, C.D., Yu, X., Staudt, L.M., and Calame, K.L. (2004). Direct repression of prdm1 by Bcl-6 inhibits plasmacytic differentiation. J Immunol *173*, 1158-1165.

Tzschentke, B., and Rumpf, M. (2011). Embryonic development of endothermy. Respir Physiol Neurobiol *178*, 97-107.

van den Berg, S.M., van Dam, A.D., Rensen, P.C., de Winther, M.P., and Lutgens, E. (2017). Immune Modulation of Brown(ing) Adipose Tissue in Obesity. Endocr Rev *38*, 46-68.

van Marken Lichtenbelt, W.D., Vanhommerig, J.W., Smulders, N.M., Drossaerts, J.M., Kemerink, G.J., Bouvy, N.D., Schrauwen, P., and Teule, G.J. (2009). Cold-activated brown adipose tissue in healthy men. N Engl J Med *360*, 1500-1508.

Villena, J.A., and Kralli, A. (2008). ERRalpha: a metabolic function for the oldest orphan. Trends Endocrinol Metab *19*, 269-276.

Vosselman, M.J., van Marken Lichtenbelt, W.D., and Schrauwen, P. (2013). Energy dissipation in brown adipose tissue: from mice to men. Molecular and cellular endocrinology *379*, 43-50.

Wagner, S.D., Ahearne, M., and Ko Ferrigno, P. (2011). The role of BCL6 in lymphomas and routes to therapy. Br J Haematol *152*, 3-12.

Walker, S.R., Liu, S., Xiang, M., Nicolais, M., Hatzi, K., Giannopoulou, E., Elemento, O., Cerchietti, L., Melnick, A., and Frank, D.A. (2015). The transcriptional modulator BCL6 as a molecular target for breast cancer therapy. Oncogene *34*, 1073-1082.

Walker, S.R., Nelson, E.A., and Frank, D.A. (2007). STAT5 represses BCL6 expression by binding to a regulatory region frequently mutated in lymphomas. Oncogene *26*, 224-233.

Walker, S.R., Nelson, E.A., Yeh, J.E., Pinello, L., Yuan, G.C., and Frank, D.A. (2013). STAT5 outcompetes STAT3 to regulate the expression of the oncogenic transcriptional modulator BCL6. Mol Cell Biol *33*, 2879-2890.

Wang, W., Kissig, M., Rajakumari, S., Huang, L., Lim, H.W., Won, K.J., and Seale, P. (2014). Ebf2 is a selective marker of brown and beige adipogenic precursor cells. Proc Natl Acad Sci U S A *111*, 14466-14471.

Wang, W., and Seale, P. (2016). Control of brown and beige fat development. Nature reviews Molecular cell biology *17*, 691-702.

Wei, F., Zaprazna, K., Wang, J., and Atchison, M.L. (2009). PU.1 can recruit BCL6 to DNA to repress gene expression in germinal center B cells. Mol Cell Biol *29*, 4612-4622.

Wei, W., Schwaid, A.G., Wang, X., Chen, S., Chu, Q., Saghatelian, A., and Wan, Y. (2016). Ligand Activation of ERRα by Cholesterol Mediates Statin and Bisphosphonate Effects. Cell Metab *23*, 479-491.

White, M.G., Luca, L.E., Nonner, D., Saleh, O., Hu, B., Barrett, E.F., and Barrett, J.N. (2007). Cellular mechanisms of neuronal damage from hyperthermia. Prog Brain Res *162*, 347-371.

Wilson, D.F. (2017). Oxidative phosphorylation: regulation and role in cellular and tissue metabolism. J Physiol *595*, 7023-7038.

Wodtke, E. (1981). Temperature adaptation of biological membranes. The effects of acclimation temperature on the unsaturation of the main neutral and charged phospholipids in mitochondrial membranes of the carp (Cyprinus carpio L.). Biochim Biophys Acta *640*, 698-709.

Wu, T., Ji, Y., Moseman, E.A., Xu, H.C., Manglani, M., Kirby, M., Anderson, S.M., Handon, R., Kenyon, E., Elkahloun, A., *et al.* (2016). The TCF1-Bcl6 axis counteracts type I interferon to repress exhaustion and maintain T cell stemness. Sci Immunol *1*.

Xu, L., Chen, Y., Dutra-Clarke, M., Mayakonda, A., Hazawa, M., Savinoff, S.E., Doan, N., Said, J.W., Yong, W.H., Watkins, A., *et al.* (2017). BCL6 promotes glioma and serves as a therapeutic target. Proc Natl Acad Sci U S A *114*, 3981-3986.

Ye, B.H., Cattoretti, G., Shen, Q., Zhang, J., Hawe, N., de Waard, R., Leung, C., Nouri-Shirazi, M., Orazi, A., Chaganti, R.S., *et al.* (1997). The BCL-6 proto-oncogene controls germinal-centre formation and Th2-type inflammation. Nature genetics *16*, 161-170.

Yoshida, K., Sakamoto, A., Yamashita, K., Arguni, E., Horigome, S., Arima, M., Hatano, M., Seki, N., Ichikawa, T., and Tokuhisa, T. (2006). Bcl6 controls granzyme B expression in effector CD8+ T cells. Eur J Immunol *36*, 3146-3156.

Yu, R.Y., Wang, X., Pixley, F.J., Yu, J.J., Dent, A.L., Broxmeyer, H.E., Stanley, E.R., and Ye, B.H. (2005). BCL-6 negatively regulates macrophage proliferation by suppressing autocrine IL-6 production. Blood *105*, 1777-1784.

Zeng, X., Jedrychowski, M.P., Chen, Y., Serag, S., Lavery, G.G., Gygi, S.P., and Spiegelman, B.M. (2016). Lysine-specific demethylase 1 promotes brown adipose tissue thermogenesis via repressing glucocorticoid activation. Genes Dev *30*, 1822-1836.

Zhang, Y., Laz, E.V., and Waxman, D.J. (2012). Dynamic, sex-differential STAT5 and BCL6 binding to sex-biased, growth hormone-regulated genes in adult mouse liver. Mol Cell Biol *32*, 880-896.

Zhao, X.Y., Li, S., Wang, G.X., Yu, Q., and Lin, J.D. (2014). A long noncoding RNA transcriptional regulatory circuit drives thermogenic adipocyte differentiation. Mol Cell *55*, 372-382.

Publishing Agreement

It is the policy of the University to encourage the distribution of all theses, dissertations, and manuscripts. Copies of all UCSF theses, dissertations, and manuscripts will be routed to the library via the Graduate Division. The library will make all theses, dissertations, and manuscripts accessible to the public and will preserve these to the best of their abilities, in perpetuity.

Please sign the following statement:

I hereby grant permission to the Graduate Division of the University of California, San Francisco to release copies of my thesis, dissertation, or manuscript to the Campus Library to provide access and preservation, in whole or in part, in perpetuity.

Vasiliy Kutyavin
Author Signature

06/12/2019
Date